IN2DREAMS

Contract No. 777596

INtelligent solutions 2ward the Development of Railway Energy and Asset Management Systems in Europe

D2.3 Ground to OSS communication platform

DUE DATE OF DELIVERABLE: 31/08/2019

ACTUAL SUBMISSION DATE: 09/12/2019

Leader/Responsible of this Deliverable: UNIBRI - Markos Anastasopoulos

Reviewed: Y

Document status		
Revision	Date	Description
1	29/11/2019	First issue
2	09/12/2019	Final version after TMT approval and quality check

Project funded from the European Union's Horizon 2020 research and innovation programme		
Dissemination Level		
PU	Public	X
CO	Confidential, restricted under conditions set out in Model Grant Agreement	
CI	Classified, information as referred to in Commission Decision 2001/844/EC	

List of Contributions by Partner
University of Bristol
IASA
DotVision

Start date of project: 01/09/2017 Duration: 26 Months

Executive Summary

The main objective of WP2 in IN2DREAMS is to provide a communication platform that will be able to interconnect a growing number of devices (metering devices, sensors and smartphones) located either on-board of trains or at the trackside with the Open Data Management (ODM) platform.

The objective of this deliverable, in the scope of Task 2.3 of WP2, is to describe the architectural and functional definitions as well as specifications and implementation for:

i) the overall IN2DREAMS ground to OSS communication,
ii) the integrated optical and computing infrastructure design and evaluation,
iii) the wireless backhaul technologies (wireless and optical) with emphasis on Free Space Optics and mmWave links
iv) the wireless access technologies (optical wireless and wireless connections) including a 5G access network that has been deployed at UNIVBRIS testbed facilities.

Emphasis is given in supporting an environmentally friendly, energy efficient solution. For this reason, several optimization models have been developed aiming at reducing the energy consumption of the overall solution. Global optimization of the integrated and converged infrastructure is targeted with the objective to increase functionality, capacity, and flexibility and decrease the capital and operational costs.

In addition to the architectural design, operational considerations concentrating on the requirements for the provisioning of end-to-end services are also applied. The overall solution has been implemented and tested in a realistic environment considering all technology domains adopting software defined networking and network function virtualization principles

Abbreviations and Acronyms

Abbreviation	Description
BBU	Base Band Units
CAPEX	Capital Expenditures (CAPEX)
CBM	Condition-Based Maintenance
CBTC	Communications Based Train Control
CDPI	Control to Data-Plane Interface
C-RAN	Cloud-RAN
DC	Data Centres
DMP	Data Management Platform
EMU	Electric Multiple Unit
EU	European Union
FH	Front Haul
FSO	Free Space Optics
GA	Grant Agreement
GPP	General-Purpose Processors
H2020	Horizon 2020 framework programme
HH	Half-Hour
ICT	Information and Communication Technology
ILP	Integer Linear Programming
IoT	Internet of Things
LPF	Low Pass Filter
LTE	Long-Term Evolution
MIMO	Multiple-Input Multiple-Output
MQTT	Message Queuing Telemetry Transport
MZM	Mach-Zehnder Modulator

Abbreviation	Description
M2M	Machine-to-Machine
NFV	Network Function Virtualization
NFVI	Network Function Virtualization Infrastructures
OCC	Operations and Control Centre
ODL	OpenDayLight
ODM	Open Data Management
OMS	Outage Management System
OPEX	Operating Expense
PNF	Physical Network Functions
PTP	Precision Time Protocol
QoS	Quality of Service
REST	Representational State Transfer
RH	Radio Heads
SDD	Spectral Direct Decoding
SDN	Software Defined Networking
TEA	Techno Economic Assessment
ToU	Time-of-Use
VNF	Virtual Network Functions
VOQ	Virtual Output Queues
JU	Shift2Rail Joint Undertaking
WDM	Wavelength Division Multiplex

Table of Contents

List of Figures

List of Tables

1 Introduction

Information and Communication Technology (ICT) platforms for future railway systems are expected to support a wide range of applications with highly variable performance attributes covering both operational and end-user service requirements. These platforms are expected to offer services ranging from delay sensitive video to infotainment services, and from best effort applications to ultra-reliable ones such as M2M (Machine-to-Machine) communications. An important consideration in the design of these platforms is the very high mobility of train transportation systems beyond 2020 that in many cases may exceed 500 km/h. In addition to high mobility scenarios, connectivity for zero to low mobility cases (interconnecting devices at stations and substations) must be also supported. Other applications, such as remote maintenance of rolling stock and remote processing will have central role in future railway platforms [5G Vision].

In response to these challenges, we propose an advanced communication platform enabling connectivity between a variety of monitoring devices and computational resources through a heterogeneous network infrastructure integrating wired and wireless network technologies. This infrastructure offering enhanced throughput, safety and security features is able to support the needs for rail signalling systems (on-board and ground) and M2M communications. It can be also used to support Mission Critical (MC) services defined in the Future Railway Mobile Communication System (FRMCS) including voice and data connectivity as shown in Figure 1.

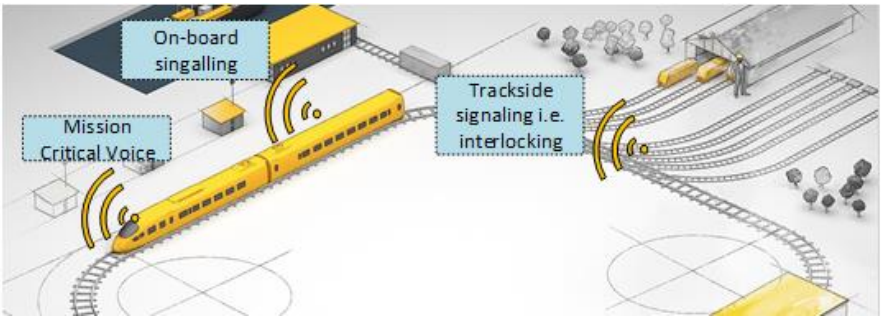

Figure 1: Rail critical services: operational voice, On-board and ground signaling.

To achieve this, IN2DREAMS takes advantage of core 5G network technologies such as SDN and NFV to support the current and future needs of railway and public transport operators. Based on SDN/NFV solutions, costly, legacy network components that are available in railway network infrastructures can be removed, dramatically improving operational efficiency and powering new services and business models.
The IN2DREAMS solution aims at providing a full SDN/NFV compliant network technology that allows railway operators and rolling stock manufacturers to modernize their infrastructures at the right time. By replacing elements of proprietary infrastructure with open-standards-based and virtualized infrastructure, it becomes possible to lower service delivery costs, bring new services to market faster, and adopt new technologies.
In the following subsections, the ground-to-occ technologies considered in IN2DREAMS tested either at real operational environments or in lab are presented. Emphasis is given on the following segments:

- The Free Space Optics (FSO) technology used to interconnect the trackside elements,
- The wired optical network used to provide backbone connectivity
- The control plane solution used the management of the overall infrastructure that is also responsible for the creation of the associated slices allocated to the specific services.

An overall view of the scenario considered in the In2Dreams project along with and Key Technology Components is shown in Figure 2

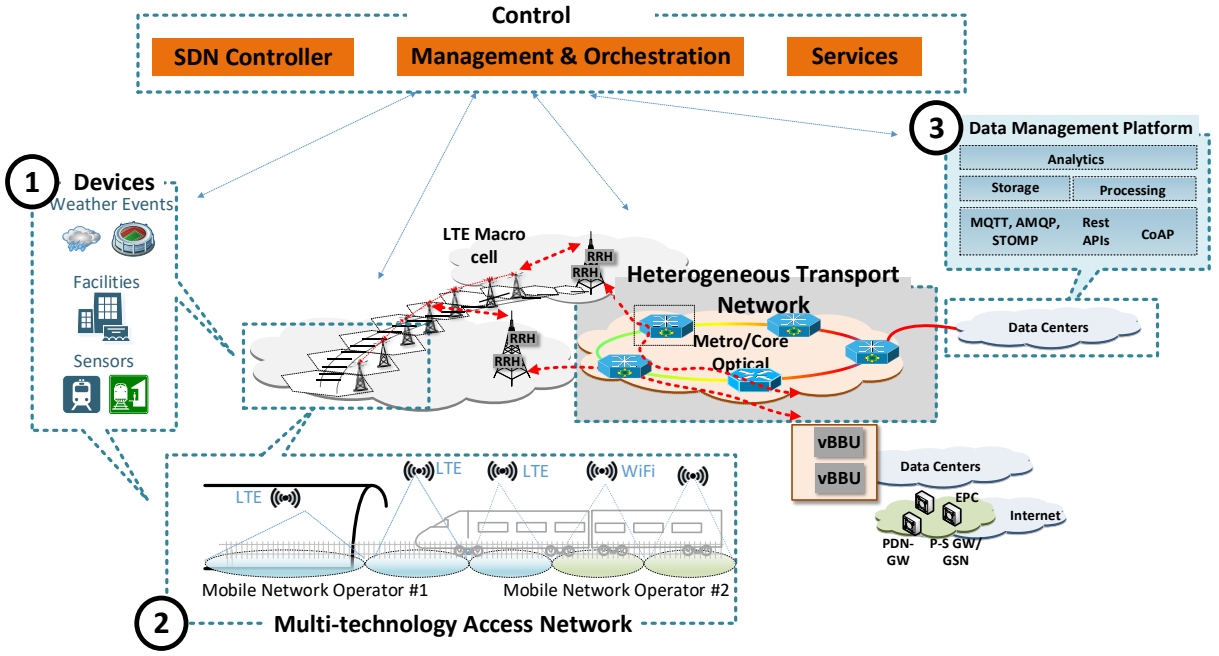

Figure 2: Converged Heterogeneous Network and Compute Infrastructures supporting railway services: Use case where data are collected from various devices (1) are transmitted over a 5G network (2) to the cloud based data management platform (3).

2 Data plane technologies

2.1 Optical Wireless communications system

The last few years, Free Space Optics (FSO) technology is an ideal solution for modern networks desiring maximum signal/data security and speed and can fully cover modern communication network requirements between train busses and train stations. An FSO system is a point to point technology that uses a narrow laser beam through the air to send data and offers full duplex 2.5Gbps Gigabit Ethernet throughput. The main advantages of such technology are the high data rates they can achieve and the relatively low installation and operational cost. Furthermore, FSO systems are license free so they are ideal for locations where radio interference and congestion make installation of radio frequency alternatives impossible. Their successful presence in demanding applications and networks such as High Frequency Stock Trading and real-time Military Theatre of Operations, can guarantee high performance, reliability and security for train network applications. FSO systems are also deployed in locations where radio frequency interference of transmissions could present a safety hazard such as in airports and critical public infrastructure facilities. Optical communications are virtually impossible to intercept and are not susceptible to RF interference of eavesdropping. They are inherently highly secure for data and digital video transmission. Although such systems where used for fixed transmitters and receivers, due to modern tracking techniques they can also be used between mobile transceivers, so links between train busses and train stations or even between mobile trans-receivers, e.g. trains can be deployed. So, FSO

systems will provide communication networks with high performance, availability and security that will meet the modern and future requirements of rail environments.

2.1.1 General Technical Specifications

FSO systems use low power laser beams up to 200mW for distances up to 5km depending on the atmospheric conditions of the area. More specifically a typical FSO system can deploy links of ~5km with attenuation 3dB/km, ~1.5km at 10dB/km and ~1km at 17dB/km.

The wavelengths that are usually used by FSO links are 1550nm and 850nm. Such wavelengths have the advantage of relatively low absorption due to atmosphere and the same wavelengths are also used in optical fibre communications so it is easy to match with all optical components an FSO link with an optical fibre link without need of converting the wavelength of the signal. The wavelength of 850nm is also used by IR LED so the information can be loaded and transmitted in IR LED system that operates in such frequencies. The transverse radius of the beamwidth at the receiver is not more than 1m, so multiple laser beams can be used in a small area without any interference. This narrow beamwidth offers high security as it is difficult to intervene to the beam without distorting it and at the same time being perceived. Such system also offers very low latency, less than 20ns. The power consumption of a typical FSO system is less than 50W and such a low consumption is vital for mobile communications link e.g. between trains. Additionally, the operating temperature lies between -40ºC and 70 ºC, so they can be applied in almost every European city.

Table 1: Technical parameter values of an FSO system

Technical parameters	Typical Values
Wavelength	1550nm / 850nm
Beam Power	~200mW
Latency	<20ns
Power Consumption	<50Watts
Operating Temperature	-40ºC and 70 ºC
Bit Error Rate (BER)	~10^{-10}

FSO systems have multi-protocol support and are compatible with IEEE 1588 precision time protocol (PtP). Another important feature of FSO systems is the clock and data recovery (CDR) for daisy chaining and also offer cascadable back-to-back operation for extended links. A typical FSO system uses the protocols presented in the Table 2.

Table 2: Protocols used by FSO systems [1]-[3] Protocol	Data Rate
Fast Ethernet	125Mbps, full duplex
OC-3/STM-1	155 Mbps, full duplex
Gigabit Ethernet	1.25 Gbps, full duplex
OC-12/STM-4	622 Mbps, full duplex

The element management and control, contains a network or USB management interface and modern systems also contain an embedded SNMP card. The software that is installed with the FSO system can monitor and in some cases control critical parameters such as received signal strength, power supply voltages, laser currents, power and temperatures, clock recovery/sync status and network interface signal status.

2.1.1.1 Advantages

High Performance, reliability and availability

FSO systems are already commercially used for sending up to 1.25Gbps of data, voice and video simultaneously through the air and in the near future will be capable of speeds of 10Gbps using wavelength division multiplex (WDM), a widely used multiplex technique in optical communications. OFDM can also be used, a technique with high impact in communications. FSO systems can cover distances up to 4Km maintaining the high performance. This distance can be extended in case of use of either amplify and forward (AF) or decode and forward (DF), relays. Due to the high bit rate they can achieve it is easily feasible to reduce it for increased availability in case external factor degrade the quality of the channel. Concerning the availability of an FSO system, they are able to reach the five 9's (99.999%).

Low Cost

Another important factor of FSO systems is the very low cost that offers fast and high return of investment (ROI). The low cost is also resulting from the low power that needs, up to a 100mW for a distance of 3Km providing high performance and reliability. Furthermore FSO technology is spectrum license free and can be deployed behind windows, eliminating the need for costly rooftop rights. The cost for an FSO system (transmitter-receiver) is between 10.000€ and 25.000€.

High security

The installation of an FSO system in a railway network will offer high level of communication security. Due to the narrow beamwidth of the laser beam, the intruder will have to expose himself or his equipment in order to intercept a portion of the transmitted power without bringing down the link. Furthermore, if an amount of the signal power is intercepted, the power at the receiver will significantly change of will be distorted. The most vulnerable area of potential interception in an FSO system is behind the transceiver. Because the incident beam of light has a larger cross-section that the lens of the receiver, the laser beam continuous to propagate behind is for some distance. An intruder could conceivably mount an unauthorised receiver in this area. This way can be solved by placing a blocking shield behind the transceiver. Except of high level security of the physical layer, FSO systems use special encryption schemes as the Fastlane KG-189, Taclane KG-75/175 (NSA Type 1) and all the AES and Triple DES encryption systems.

Safety

Safety in FSO systems can be a concern because the technology uses lasers for transmission. The proper use and safety of lasers have been discussed for more than 3 decades. The major concern involve the eye exposure to light beams so strict international standards have been set for safety. Nowadays all lasers of FSO systems are Class 1M that are safe for the naked eye. Furthermore all FSO systems comply with the following standards [29], [30]:

- International Laser Standard IEC 60825-1/A2:2001
- European Standard EN 60825-1/A2:2000, DIN VDE 0837-1A/2
- IEC/EN 60825-7:1998
- DIN V VDE V 0837-7:1999
- US user Standard ANSI Z 136.1, CDRH 21DRF

2.1.1.2 Challenges and enhancement techniques

The primary challenge to FSO based communications is dense fog due to the size of water droplets. Rain and snow have little effect of FSO technology. A solution to counter fog when deploying FSO systems is to install relay nodes between the transmitter and the receiver, known as multihop technique. These relay nodes can be AF nodes or DF. AF offers a simple and low delay solution while DF nodes are more effective and reliable[4], [5]. FSO installations in extremely foggy cities such as San Francisco have successfully achieved carrier-class reliability.

Another factor that degrades the performance of an FSO system is the misalignment due to building sway. The movement of buildings can upset receiver and transmitter alignment. A solution is the use of divergent beam to maintain connectivity. When combined with tracking, multiple beam FSO systems provide even greater performance and enhanced installation simplicity.

Finally, turbulence is another factor that affects the reliability and availability of the system. Heated air rising from the earth or man-made devices such as heating ducts, create temperature and pressure variations among different air pockets. This causes fluctuations in signal irradiance at the receiver, the so-called scintillation effect (i.e. similar with the fading channels in RF). Such fluctuations are very fast and intense and can't be predicted. So theoretically this phenomenon is investigated statistically. In order to reduce the impact of turbulence, the signal can be sent multiple times, a technique known as diversity. Most of the times, diversity is realising in space, in time or in wavelength. In the spatial diversity scheme, the FSO system uses multiple transmitters and/or receivers at different places that send and receive copies of the same signal, resulting to a decreased probability of error [6], [7]. In time diversity schemes, there is only one transmitter – receiver pair, but each piece of the information signal is retransmitted at different time slots. Finally, the wavelength diversity system uses a composite transmitter and the signal is transmitted at the same time at different wavelengths towards a number of wavelength-selected receivers.

A technique that can always be used in order to enhance the performance of an FSO system is OFDM-FSO Transmission Link Incorporating OSSB and OTSB Schemes. By introducing the OFDM scheme, an effort has been made to probe the impact of the environment conditions and to design a high speed and long reach FSO system free from fading. It is concluded that hybrid OFDM-FSO system performs better in diverse channel conditions and upon comparing both OSSB and OTSB schemes OSSB performs better than OTSB at high data rate as it has more immunity against fading due to weather conditions.

Another enhancing technique is the SAC OCDMA Based FSO System [8], [9]. Spectral Amplitude Coding Optical Code Division Multiple Access technique is used in FSO system by the researchers. This multiplexing scheme has several advantages like flexibility of channel allocation, asynchronously operative ability, privacy enhancement, and network capacity increment. KS (Khazani-Syed) codes are used with SDD (spectral direct decoding) technique. An optical external modulator (OEM) is used to modulate the code sequence with data. The data is an independent unipolar digital signal. Mach-Zehnder Modulator

(MZM) is used and combination of modulated code sequences is transmitted through the FSO link and these sequences are separated by an optical splitter at the receiver end. The overlapping chips are discarded to avoid the interference at receiver end and decoder will only filter the non-overlapping chips. Optical band pass filters serve the purpose of encoders and decoders. A low pass filter (LPF) is used to recover the original data. The performance of this system with SDD technique is analysed along with FSO system using intensity modulation with direct detection technique. SDD technique performs better and the link distance is increased.

Table 3: Performance of a commercial FSO system [3], [4]

Weather	Data Rate	Link Distance
Clear	2Gbps	10km
	5Gbps	6km
Low Haze	2Gbps	5.4km
	5Gbps	3.4km
Low Fog	2Gbps	1.35km
	5Gbps	1km

Another factor that decreases the performance of an FSO system is the optical noise of the sunlight at the receiver's input that deteriorates the signal to noise ratio (SNR) of the optical link. A very significant effect that increases the noise of an FSO system is the background optical noise with the main source being the sunlight radiation that is difficult to be avoided. A robust technique for reducing the effect of background noise is the application of optical filters at the receiver's photodiode in order to decrease the wavelength range received that is not used for data transmission. The SNR improvement, due to the VO2 optical bandpass filter, has already been estimated theoretically and verified experimentally. It works by reflecting unwanted wavelengths. In comparison to interference filters, VO2 is a simple layer and this makes fabrication of VO2 filter simpler and economically viable [10]-[13].

2.1.2 System Analysis

2.1.2.1 FSO network for ground to ground communication

The railway network from Redhill to Leigh (26Km) can be fully covered using roughly 10 FSO transceivers. These FSO systems can be placed in the train stations between Redhill and Leigh (Nutfield, Godstone, Edenbridge, Penshurst). Due to the high humidity of the area, the distance between the FSO nodes could be shorter, so a few more nodes will be required. This FSO network will provide fast, reliable and secure data flow between all the train stations.

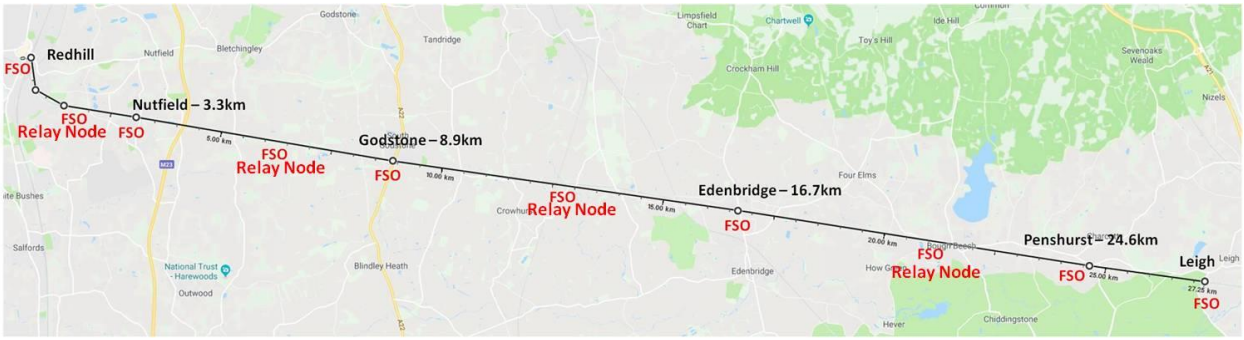

Figure 3: Communication coverage of railway network between Redhill and Leigh using FSO systems

Figure 4: Satellite View of the Area

According to the satellite view, the area is flat and the railway network has almost no turns. So it will be easy to deploy an FSO system that require line of sight. In addition, the high density of trees could cause high attenuation in RF communications due to high absorption of the water in such frequencies, so the LoS optical wireless communications could provide the best solution in this area. The FSO transceivers and relay nodes can be easily installed and powered along the rail network in the already existing communication network of the area. The height of the trees is only a few meters so it is feasible to deploy the FSO network above them.

Figure 5: Existing power and communication network

Furthermore, it is important to notice the presence of an airport in less than 1km near the rail network.

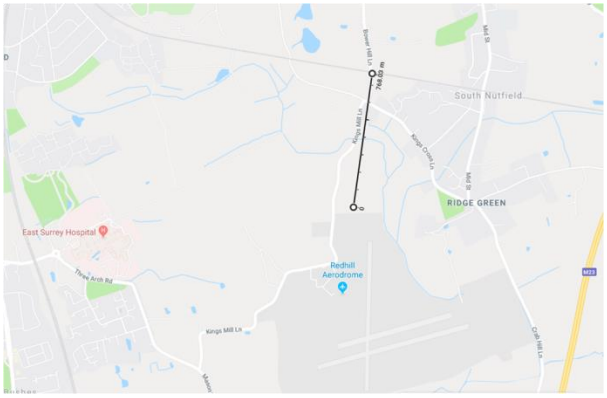

Figure 6: Redhill Airport

Therefore, in this area it is preferred not to use other RF communication systems apart from these of the airport for security reasons to avoid possible interference. As long as the distance between the stations is more than 5km, more FSO transceivers or relay nodes can be placed between these stations, applying a multi-hop technique. The relay nodes can be either Amplify and Forward (AF) of Decode and Forward (DF). In case of AF nodes, the signal is just amplified and retransmitted to the next FSO system. This technique has low cost and low complexity but also has low performance as the noise is also amplified with the signal. On the other hand, DF nodes, have significantly better performance as the signal is firstly decoded and then retransmitted but their complexity add more delay to the system.

While the train passes through a tunnel, the RF signal becomes very weak or in some cases can't even penetrate. So, the communication may be interrupted without using multiple antennas in the tunnel. Optical communications may solve this problem by using the already existing tunnel lighting as visible light communication (VLC) transceivers communicating with the respective lights of the train. Therefore, in a long tunnel there is no need for placing FSO transceivers inside, only in the entrance and in the exit, creating a cascaded FSO-VLC system. The signal conversion between the FSO and the VLC system has low complexity and delay. Furthermore, the optical signal of the FSO transceiver can be easily converted to drive internal WiFi or LiFi systems of the train. So, when the train passes through tunnels there will be no reduction of the quality of service if the FSO transceiver is placed in the tunnel.

2.1.3 Validation and Experimental Data

2.1.3.1 General characteristics of the experimental FSO link

Several FSO experimental links have been deployed in order to verify the high performance and the security they can offer in a communication system. Concerning Ground-to-Ground wireless optical communications, a commercial FSO system has been installed for research purposes in the city of Piraeus.

Figure 7: 3D view of the link

An extensive study of weather parameters of the area is required before installing the FSO system. So, a comparison between the weather conditions of the last 10 years between the Redhill and the city of Piraeus where the experiment was held will be provided.

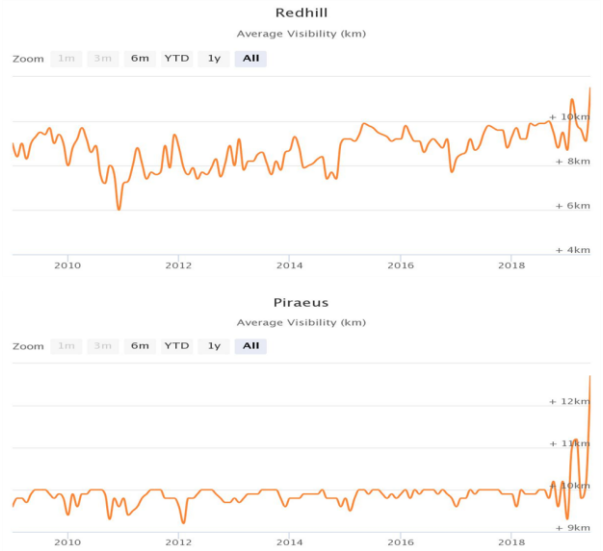

Figure 8: Visibility in Redhill and Piraeus

According to the above information, the weather conditions between these two areas are not very different. More specifically the visibility which is the most important factor in optical communications is almost always above 8km while the distance between FSO transceivers and relay nodes are in not greater than 5km. So, the FSO system can be a very robust solution for the communication between the train stations in the Redhill. But except of the impact of the weather conditions in the attenuation and turbulence that degrade the performance of the system, the presence of pointing errors mostly due to wind and earthquakes should be further investigated. In the next figure, a wind speed comparison is also made

Figure 9: Wind speed in Redhill and Piraeus

According to the results, the wind speed in the area of Redhill is about the same as the one in the area of Piraeus where the experiments were held. As long as visibility and wind speed are not very different between these two areas, the results that will be presented will validate the efficiency of an FSO system in the area of Redhill. The most important technical specifications of the link are presented in the following table:

Table 4: Technical Specifications of FSO system

Parameter	Values
Data Protocol	Fast Ethernet, ATM, OC3, STM1, E3, T3, OC1/STM0 &Open Protocol
Distance	3km
Bit Error Rate	Less than 10^{-12} (unfaded)
Wavelength	830-860nm
Maximum Bit Rate	100Mbps
Output Power	100mW - 3 Laser beams
Total Power Consumption	22W
Beam Divergence	2mrad
Receiver Field of View	5 mrad
Sensitivity	-46dBm
Operating Temperature	-20°C to 50°C
Eye Safety Class	1M
Total Weight (with accessories)	25kg
Management	SNMP protocol -Built in

The FSO devices with their panel and software interface are presented in the following figures:

Figure 10: FSO Transceivers

Figure 11: FSO Panel

Figure 12: FSO Software Interface

The main factor that degrades the performance of the FSO system is the various atmospheric and weather phenomena. So, an extensive investigation has been conducted in order to estimate the effect of such phenomena on the performance of the system.

2.1.3.2 Measurement Setup

Using the management interface of the FSO head of the system, the parameter of received signal strength indication (RSSI) can be monitored. This parameter is the voltage output of the head in miliwatts and is proportional to the optical power of the received signal. The data of the RSSI are stored in the internal memory of the system and can be easily extracted in editable files.

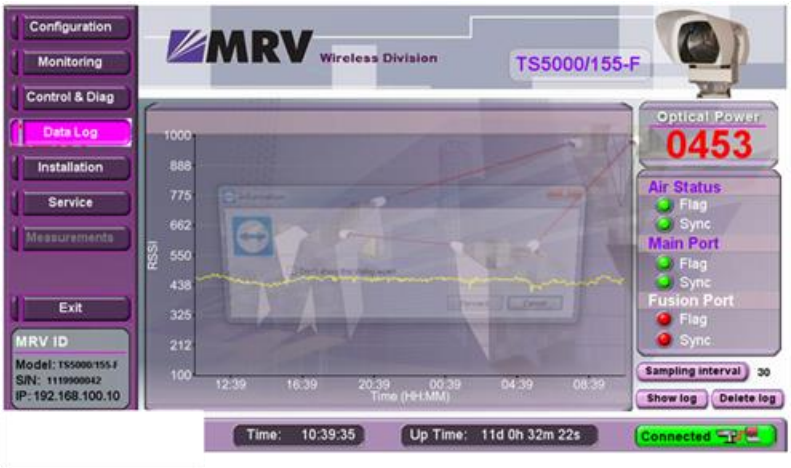

Figure 13: Management Interface

Near the FSO system, a weather station has been installed in order to receive various atmospheric and weather metrics. More specifically, the station measures temperature, relative humidity, atmospheric pressure, dew point temperature, rain rate, solar radiation and wind speed every minute. All this data can be extracted in editable files. Finally, the bit rate of the system is estimated using appropriate software (i.e Jperf).

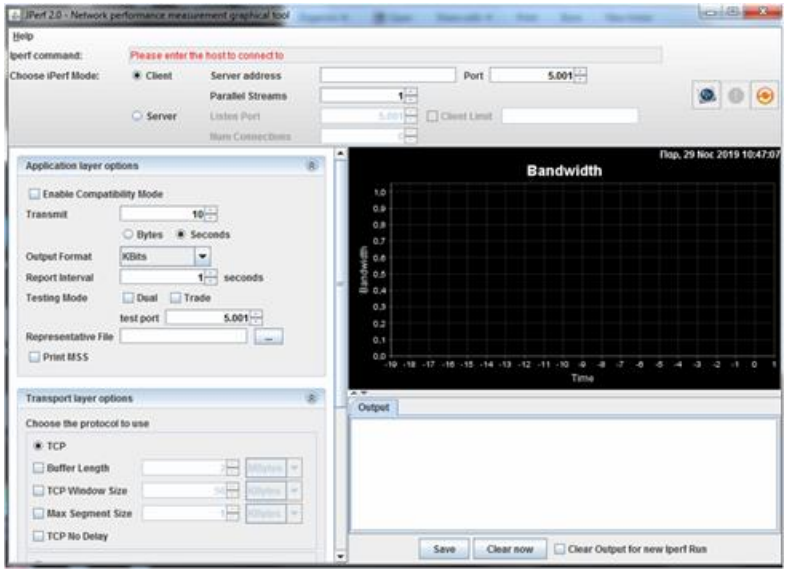

Figure 14: Jperf Interface

In the link described above, the bit rate and the RSSI of the link is measured daily for more than 4 years except of a few months that the link is shut down for maintenance. The initial goal of the study is to investigate how various weather conditions affect the RSSI of the system. For the distance of 3Km the maximum RSSI that can be achieved is 500 according to the manufacturer's manual.

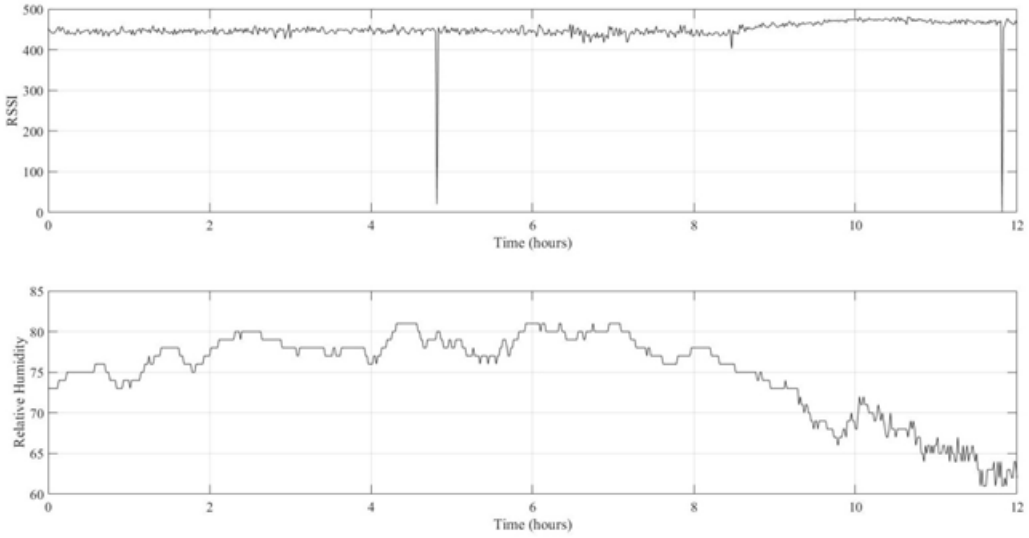

Figure 15: RSSI and Relative Humidity

In **Figure 15** the RSSI is presented for a night with high relative humidity. The mean value of the RSSI until 7 o'clock in the morning, that the relative humidity was high, was calculated at 445 and between 7 and 12 o'clock that the relative humidity was reduced due to the sunlight, was calculated at 458. So the relative humidity slightly decreased the RSSI value by 2.8%.

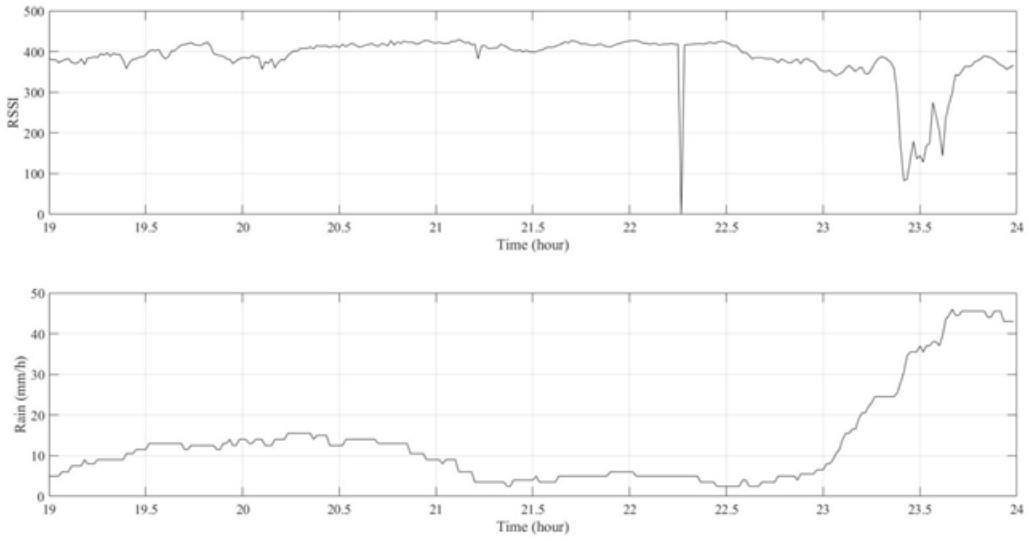

Figure 16: RSSI in a rainy day

In **Figure 16**, the RSSI is presented in a day with various rain intensities. In case of light or moderate rain (<7.6mm/h) the optical power at the receiver has weak fluctuations and the mean value of the RSSI is above 400. For heavy rain (7.6mm/h<rain<40mm/h) the optical power is significantly affected with the

RSSI falling below 400 and finally for violent rain intensity (>40mm/h) the link performance deteriorates and the probability of outage is very high. According to weather statistics in Redhill, violent storms are rare and their duration is only for a few minutes.

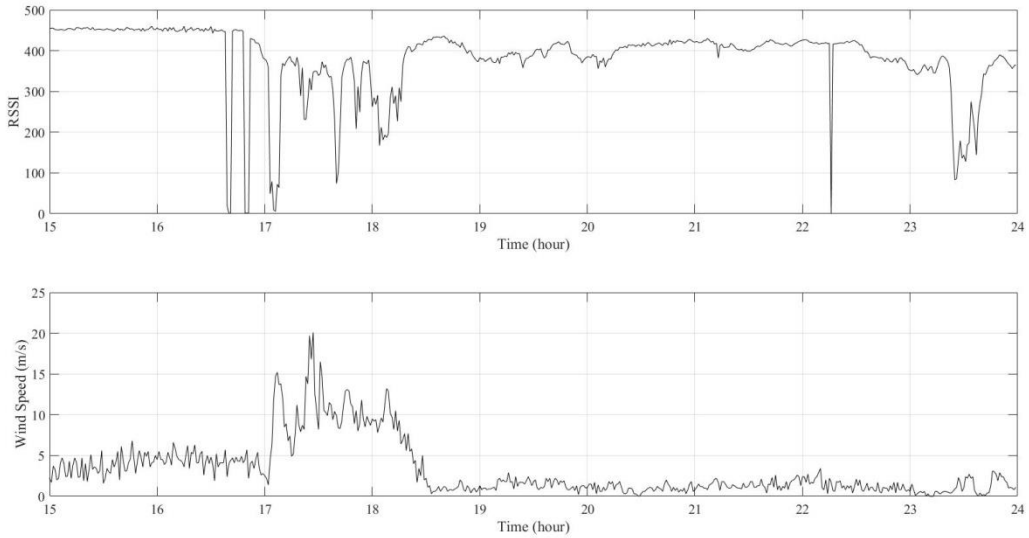

Figure 17: RSSI in various wind speed cases

In **Figure 17**, the RSSI is presented in case of high wind speed. Between 5 and 6 o'clock an incident of strong gale occurred. The high pointing errors deteriorated the performance of the system increasing the probability of link outage.

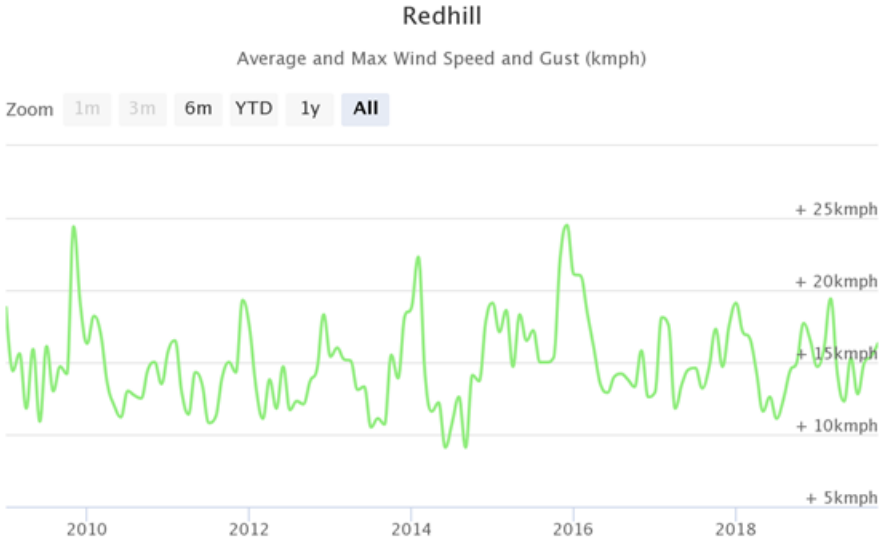

Figure 18: Wind Speed in Redhill

According to average and max wind speed in Redhill, only cases up to moderate breeze (up to 25km/h or 7m/s) have been recorded during the last 10 years. So, pointing error due to wind are expected to be negligible. Furthermore, except of the optical power, the maximum bit rate was also measured in various weather conditions. The results are presented in the next figures:

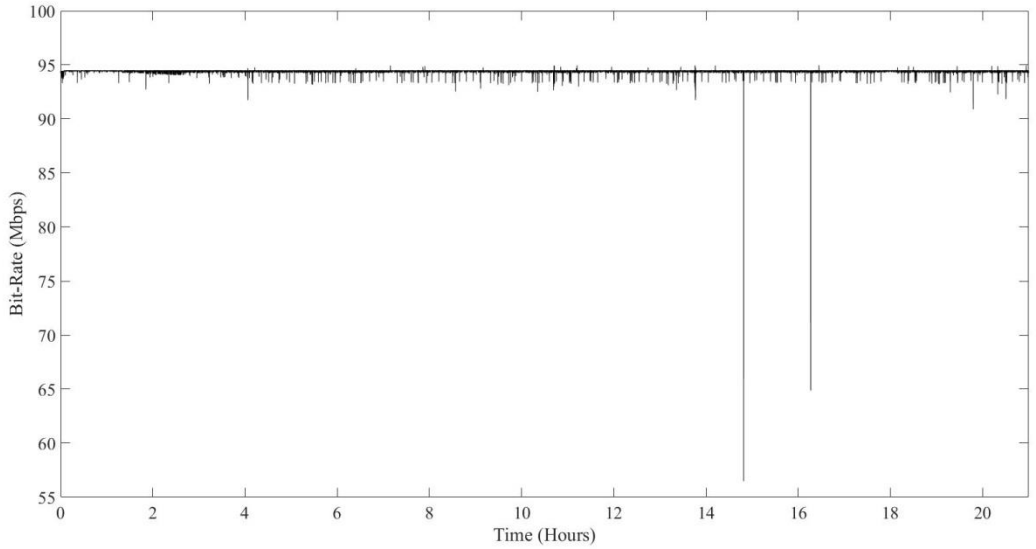

Figure 19: Bit rate per second of 18 March 2018

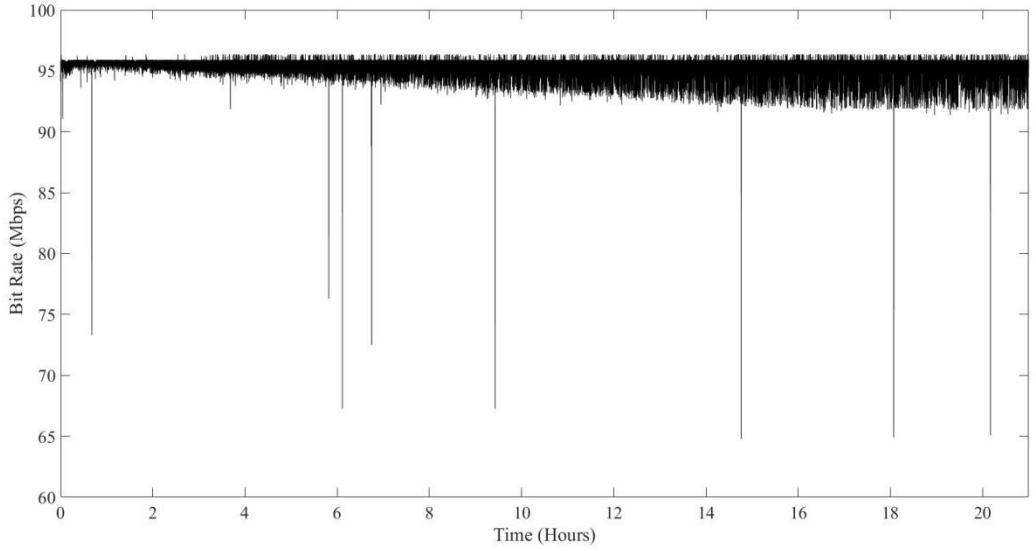

Figure 20: Bit rate per second of 15 June 2018

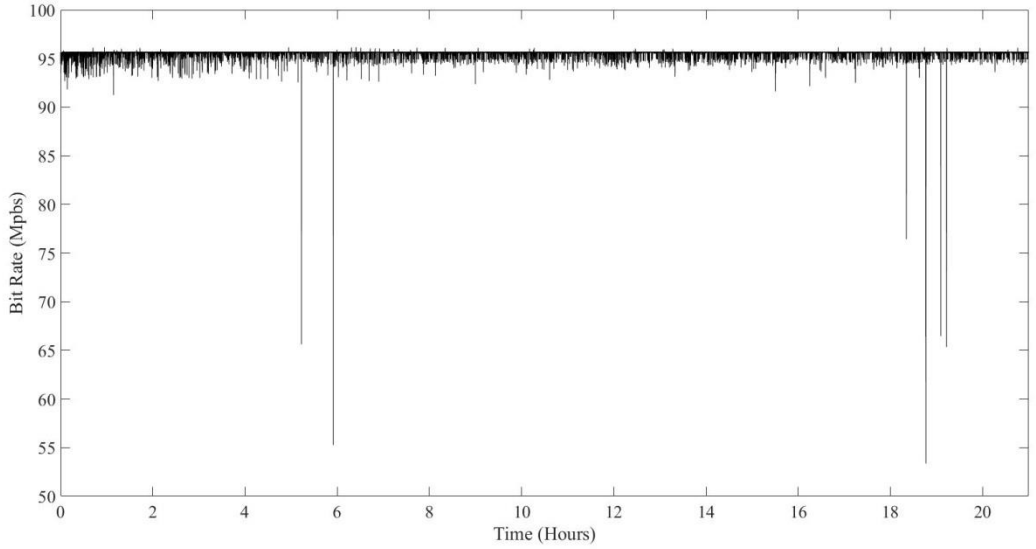

Figure 21: Bit Rate per second of 16 December 2018

As we can see the link presents a high performance as the bit rate remains high with only a few low spikes that are caused because mostly because of obstacles that pass through the beam fast enough in order not to cause a link outage. In order to investigate how the performance of the system is affected by weather conditions daily data of bit rate per second (bps) are collected for more than two years. In the following tables, the bit rate of the link is presented in an hour of clear day and in cases of heavy rain and fog.

Table 5: Bit-rate in case of a Clear Day

Bit-rate in a Clear Day	
Number of Data	3600
Mean value	96.681Mbps
Standard Deviation	1.74Mbps

Table 6: Bit-rate in case of Rain

Bit-rate in a Rainy Day - 4.83mm/h	
Number of Data	3600
Mean value	94.575Mbps
Standard Deviation	4.023Mbps

Table 7: Bit-rate in case of Fog

Bit-rate in a Foggy Day - Visibility 3Km	
Number of Data	3600
Mean value	84.223Mbps
Standard Deviation	3.4Mbps

It is clear that the performance of the system is slightly affected even in case of fog that mostly affects optical communications. So FSO links can be used in areas with extreme weather conditions providing high quality services. Similar results from experiments all around the world have also been published [17]-[20].

Except of the investigation of the bit rate, the experimental link has also been used in order to verify various theoretical statistical models that are used in order to model a turbulent channel. Atmospheric turbulence is an atmospheric phenomenon that degrades the performance of systems and can only be

investigated through statistical models. So the verification of these theoretical models is very important in order to deploy an FSO link with specific characteristics.

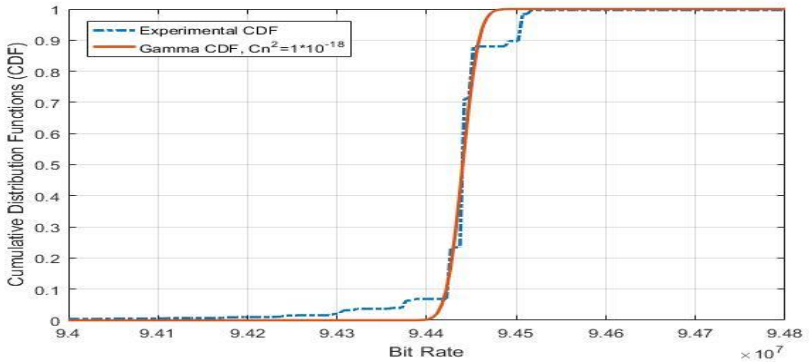

Figure 22: CDF of Gamma distribution verification, [21]

In **Figure 22** the Gamma distribution which is suitable to model weak turbulence conditions, is verified using experimental data and is proved to be very accurate. According to the above experimental results, the FSO link that is presented in Figure (20), is feasible to be deployed offering high performance and robust communications between Redhill and Leigh. The optical wireless network will offer high bit-rate and availability even under extreme weather conditions that is the main reason that degrade the performance of an FSO link. It is also important that the network can be designed with high precision using various theoretical models as long as their accuracy has been experimentally verified, decreasing the risk of failure.

2.1.4 Hybrid FSO/RF/mmw

In order to maximise the link's performance for all weather conditions an RF system or millimetre wave (mmw) can be used in parallel in order to deploy a hybrid FSO/RF link [22][23]. Almost all FSO systems are designed to combine the best features of both laser light and RF waves to form a single wireless communication link between the transceivers. By leveraging both technologies, a five 9s availability can be provided under any weather conditions. The main characteristics of such a hybrid link, based on the are FSO system that was used in Piraeus for experimental validation, are presented in the following table:

Protocol	10BaseTX (IEEE 802.11b or 802.11a or 802.11g)
Frequency	2.4GHz or 5.5GHz ISM band
Output power	-4 to 24dBm
Sensitivity	-85dBm

Such links have already been studied theoretically and the extracted results are very promising for areas where a single FSO links may have decreased performance due to the atmospheric and weather conditions.

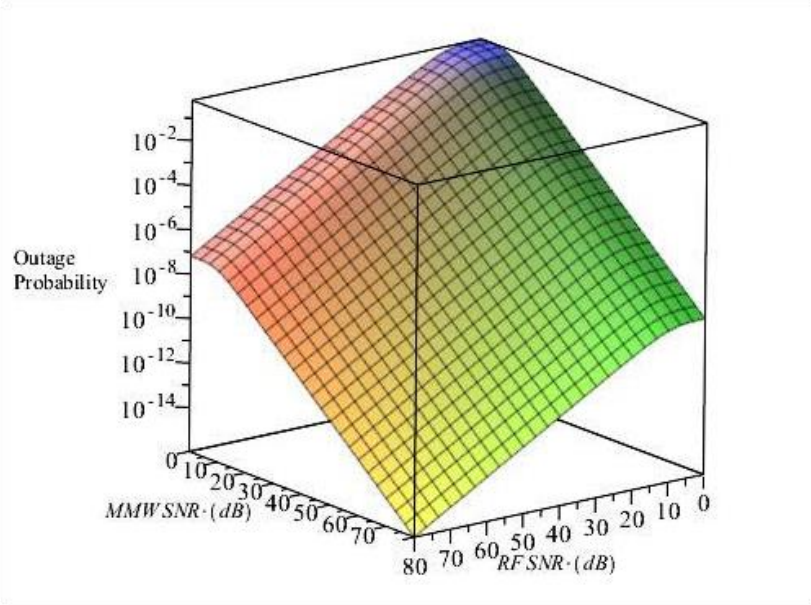

Figure 23: Outage Probability in FSO/RF/MMW system

In **Figure 23**, the outage probability for a hybrid system is presented and it is clear that despite the inadequate performance of the FSO link, the hybrid system manages to operate better and the availability of the overall system appears to be higher than the availability of each separate subsystem.

2.2 Terrestrial Optical Network Technology development

The Cloud-Radio Access Network (C-RAN) concept has been proposed to address the inefficiencies of traditional RAN systems and support services requiring very low latency, high reliability, density and mobility. Through its pooling and coordination gains, C-RAN can address the increased capital and operational costs, as well as the limited scalability and flexibility of traditional RAN. An example is shown in Figure 24 where C-RAN can be used to interconnect the Remote Units (RUs) with the virtual Basband Units (vBBUs). This enables efficient coordination of RUs allowing the creation of super cells thus reducing the frequency of handovers to address the high mobility requirements

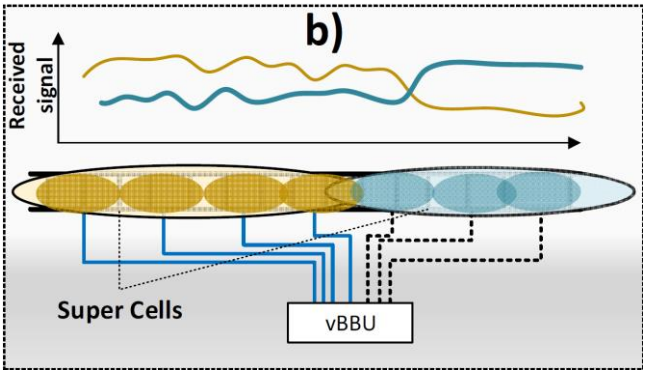

Figure 24: Adoption of C-RAN in railway system

However, C-RAN requires tremendous transport bandwidth and impose strict latency and synchronisation constraints [34]-[35]. To address the need for a flexible transport network offering the required capacity levels we have proposed the Time Shared Optical Network (TSON) solution. TSON offers a high capacity optical transport network that can support high levels of granularity as it adopts a frame based approach [34]. The transport capacity problem is further exaggerated under survivable C-RAN deployments (see i.e. [36]-[41]) which is a very important topic in mission critical infrastructures (i.e. railways where high level

of availability needs to be ensured). In many protection schemes, the optical network capacity is duplicated in size [41] to make possible realistic survivable C-RAN deployments.

A typical example of systems offering protection to any kind of failures (either at the optical transport or the compute domain where BBUs are hosted) is shown in **Figure 25** a). Specifically, in case of failure of the main paths interconnecting the RUs with the BBUs (i.e. paths 1-6, 3-5), FH flows are routed to their destination through a set of secondary (protection) paths (1-2-4-5, 3-2-4-6). A similar approach is taken for the C-RAN protection against BBU failures [39]. It is clear that under this scenario, multiple FH flows need to be transferred over a set of links introducing even higher transport bandwidth requirements.

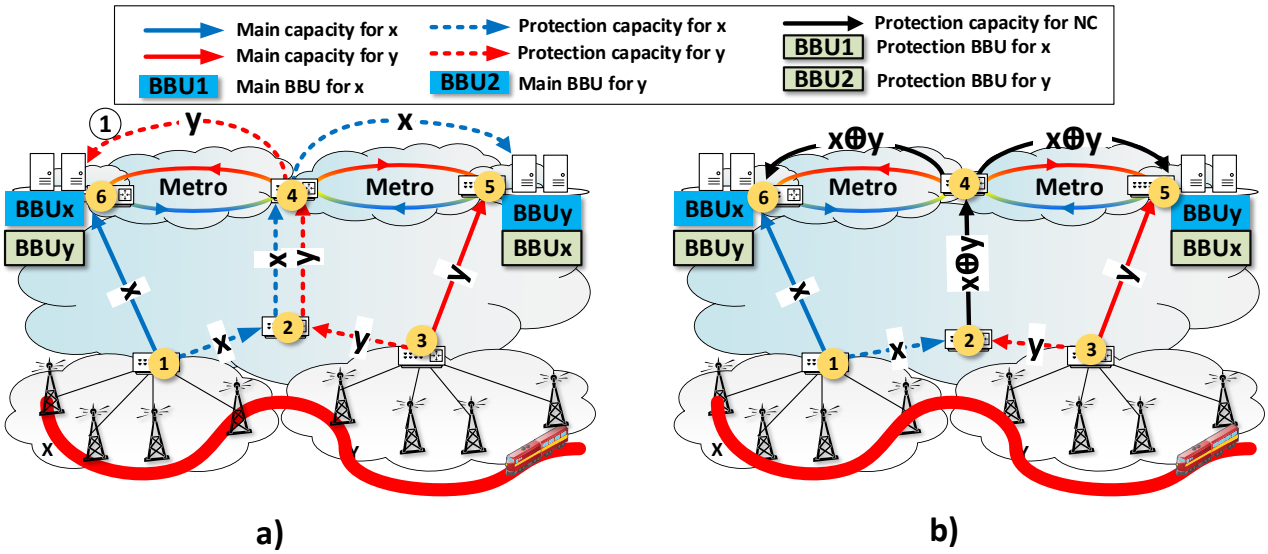

Figure 25: Protection of a C-RAN network from failures of compute and/or network elements. a) In the traditional approach, working and protection capacity for regions x, y are establishes over common links causing bottleneck b) Protection of C-RAN adoting NC. FH flows from regions x, y are multiplexed ($x \oplus y$) at ingress edge node and replicated at the reducing bandwidth requirmens by half.

To address this issue the concept of Network Coding (NC) [43] is proposed with the aim offer resilient FH services by multiplexing FH flows and therefore reducing the volume of the transmitted I/Q streams. Using NC, different FH traffic streams with the same source and destination nodes are routed through the network following diverse paths. These can be protected through their modulo-two sum that is generated at the source node and forwarded to the common destination node. This allows reconstruction of each one of the two initial streams at the destination node, in case of the occurrence of a failure along one of the two paths that the initial two streams are traversing. This approach offers 1+1 protection capabilities without having to transfer separately the working and protection copies of the two FH streams across the optical transport network. This reduces the overall protection bandwidth requirement by half (see link 2-4 in in **Figure 25** b). Through this approach, simultaneous protection against optical network and/or compute elements can be achieved.

Although NC has been extensively used to protect networks against link failures, its application in resilient FH networks has not been proposed before. This can be attributed mainly to the overhead that the application of the modulo-two sum and the replication operations of NC introduce in practical systems that may degrade the performance of C-RANs. At the same time, the operation of the decoding process at the edge imposes significant buffering requirements due to the high data rate of FH streams. To quantify the benefits of the proposed approach at a network level and further improve performance, an optimisation framework is proposed. The proposed scheme focuses on optimally placing the NC-enabled edge nodes to minimise the overall deployment cost and protect the system from possible network or

compute element failures. The performance of the proposed scheme is experimentally validated over the Bristol city testbed considering the requirements imposed by an operating open source LTE platform.

2.2.1 Implementation Aspects

To apply NC in 5G operational environments, two main practical aspects should be resolved: 1) implementation of the modulo-two sum and the replication operations at the FH line rate and, 2) synchronisation between flows reaching decode nodes (flows $x, x \oplus y$ and flows $y, x \oplus y$ of **Figure 25** b). In the following subsections, the implementation details together with experimental demonstration of an NC-enabled optical edge node is presented.

2.2.1.1 NC operations implementation at TSON

TSON [46][47] is a multi-wavelength fully bi-directional synchronous, and flexible active optical transport network technology. Its network implementation consists of Field Programmable Gate Array (FPGA) optoelectronics platforms integrated with advanced optical components to enable high performance processing and transparent switching and transport. TSON provides a multiple protocol programable interface that meets 5G Key Performance Indicators (KPIs) such as high bandwidth and sub-millisecond end-to-end latency [47]. Although natively TSON allows handling Ethernet frames, its configuration can support a broad range of framing structures and communication protocols including CPRI, either natively or through their packaged versions.

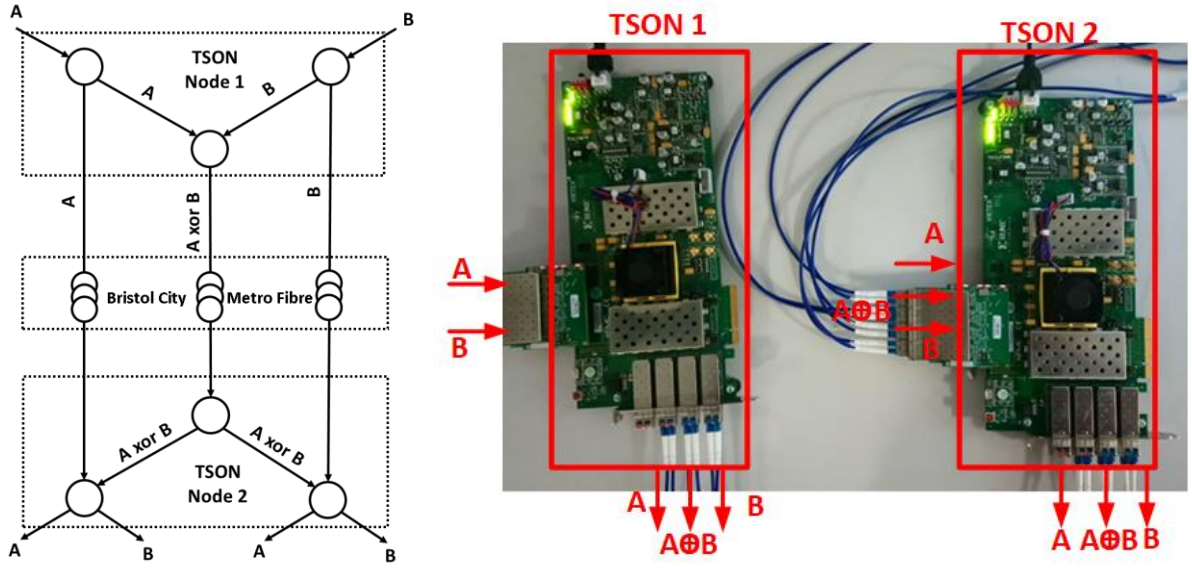

a) b)

Figure 26: TSON Implementation architecture for evaluation concept, b) TSON edge node setup for the experimental implementation

Figure 26 shows the TSON architecture implemented to solve this problem. The ingress TSON node is responsible for traffic coding and mapping. Its ports consist of two clients: X and Y. The output ingress node contains three different wavelengths that can be configured on the fly using Software Defined Networking (SDN) to address different programmable parameters. The egress edge nodes include the reverse functionality and ports. For the implementation of our experimental configuration we have employed two Xilinx VC709 evaluation boards. These contain 4XSFP/SFP+ cages. FM-S18 modules are used to expand the number of SFP+ cages as more than 4X10Gbs ports are required for the experiment. The FM-S18 is an FPGA Mezzanine Card (FMC) module that provides up to eight SFP/SFP+ module interfaces directly into Multi-Gigabit Transceivers of the FPGA. Figure 26 shows the implementation architecture for the evaluation of the proposed concept with two TSON nodes. Each TSON node emulates three source nodes of a butterfly network, with the aim to create a proof of concept experiment and

showcase the concept of linear network coding. TSON node 1 receives two different traffic streams (A and B) and sends the streams A, B, and their modulo 2 sum (XOR) of both traffic streams to TSON node 2. TSON node 2 receives the three traffic streams and transmits each traffic stream A and B simultaneously to two destinations of TSON node 2.

2.2.1.2 Synchronisation of Network Coded flows

To reduce buffering requirements during the coding/decoding phase of the FH flows, high synchronisation accuracy across the network is needed. An early TSON prototype with local synchronisation capabilities is described in [44]. To address the system wide strict synchronisation requirements of the NC implementation, a subsystem relying on separate developed time stamper has been developed. **Figure 27** shows the Subsystem architecture for the NC-enabled TSON nodes. The time stamper unit is located between the MAC and PCS/PMA IP cores, uses the Timer Syns clock and follows the IEEE 1588 protocol. In addition, the time stamper considers the physical layer delay for stamping.

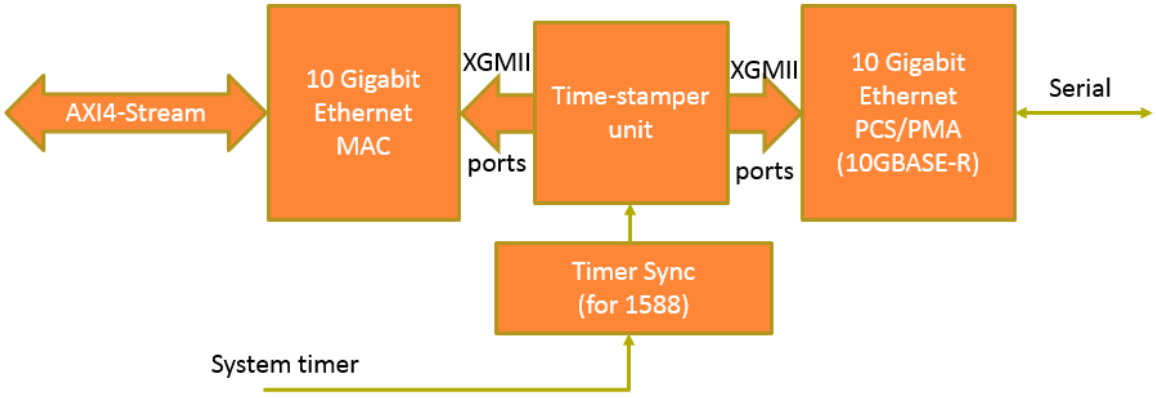

Figure 27: Synchronisation subsystem for the NC implementation

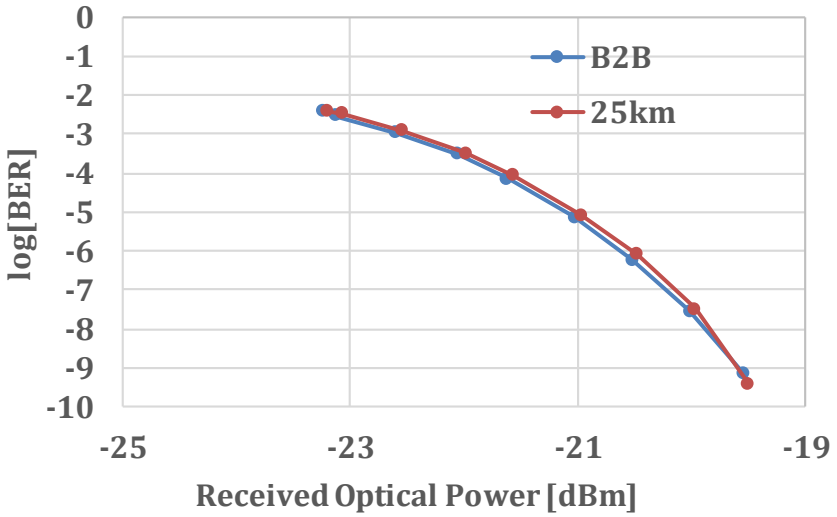

Figure 28: BER measurements

2.2.1.3 Subsystem experimental validation

Two different scenarios are considered for experimental evaluation of the subsystems responsible for the NC- operations, including the modulo-two sum and synchronisation accuracy. The first scenario includes both FPGAs connected back-to-back with short fibre lengths. In the second scenario, the proposed technologies are evaluated over the Bristol City test-bed Fibre with 25km of standard single-mode fibre

(SSMF). An Anritsu traffic analyser generates two Ethernet traffic streams to the TSON edge node 1 at 9Gbps. The traffic is received from the TSON node 2. The performance parameters under consideration include Bit Error Rate (BER) and latency. Latency is defined as the time difference between the arrival of a frame at the analyser, and its departure from the analyser.

Figure 28 shows the BER measurements as a function of received optical power for the different scenarios under consideration. The BER curves show that the penalty observed for the case of 25km of SSMF transmission over the Bristol City Infrastructure compared to the back-to-back (B2B) performance is less than 1dB. Table 8 displays the end-to-end latency for the transmitted flows. The TSON nodes latency for the 25km transmission is less than 2% of total latency.

Table 8: End-to-end flow latency

latency	**μs**
B2B	1.979
25km	125.4

2.2.2 Optimal 5G Network design with resilience considerations

In the previous section, the implementation details of NC-enabled TSON nodes have been described. In this section, the problem of optical placement of these nodes to support resilient operation of C-RANs in a railway environment is provided.

2.2.2.1 Traditional Optimisation framework

This section provides a description of the modelling framework used to identify the optical network resources for the interconnection of the RUs with the compute resources where the BBU are hosted. Taking into account both FH network and BBU processing demands, let $\mathcal{P}_r$ be the set of paths interconnecting RU $r \in \mathcal{R}$ with server s where BBUs are hosted with $\in \mathcal{P}_r$. Now let x_{rp} be the rate at which FH demand originating from r flows through path p. The following demand constraints should be satisfied:

$$\sum_{s \in \mathcal{S}} \sum_{p \in P_r} \alpha_{rs} x_{rp} = h_r, \qquad \forall r \in \mathcal{R} \qquad \text{Eq. 1}$$

where α_{rs} is a binary coefficient taking values equal to 1 if RU $r \in \mathcal{R}$ is supported by server s.

In order to protect the planned network from a possible server failure hosting the BBU, a backup mechanism is introduced. This mechanism ensures that in case of failure of the primary server s, FH flows are routed to an alternative server s' $(s' \neq s)$ through the candidate path p' $(p' \in \mathcal{P}_r)$ with corresponding flow $x_{rp'}$. To formulate this requirement the binary coefficient $\alpha_{rss'}$ is introduced to indicate whether FH flow originating from RU r is assigned to servers s, s' or not. This coefficient equals to 1, if BBU of RU r is processed at server s or in case of its failure on server s'; 0 otherwise. In order to protect the operation of an RU from a possible server s failure, the following FH flow protection constraints should be satisfied:

$$\sum_{\substack{s,s' \in \mathcal{S} \\ s' \neq s}} \sum_{p' \in P_r} \alpha_{rss'} x_{rp'} = h_r, \forall r \in \mathcal{R}, s \in \mathcal{S} \qquad \text{Eq. 2}$$

Summing all FH flows over the optical network link e $(e \in \mathcal{E})$, the necessary link e capacity, denoted as u_e, is determined. Apart from server failures, optical network link failures are also addressed by

forwarding FH flows to their destination via alternative paths. In order to protect the network from a possible link failure, a mechanism routing flows through alternative paths is introduced. Now, let $\mathcal{Q}_{rp}$ be the set of paths that can be used to protect a path $p \in \mathcal{P}_r$ from a possible failure, y_{rq} the rate at which FH demand originating from r flows through path $q_p \in \mathcal{Q}_{rp}$ protecting main path $p \in \mathcal{P}_r$ (with p, q being disjoint) and $u'_e = \mathcal{C}_e - u_e$ the remaining link e capacity. Adopting the same rationale as in the previous equations, path-protection constraints are introduced.

So far, the proposed model ensures that the network capacity is adequate to support the transmission of the FH flows to the servers where BBUs are hosted. However, once the information arrives at its destination, server s should have adequate capacity to support of BBU processing. To evaluate this capacity, h_r is mapped from a network type of requirement to a computing resource through the introduction of parameter $\mathcal{M}_{rs}$. This parameter specifies the computational requirements (usually in Instructions Per Second - IPS) to support FH flow r on server s.

To evaluate this parameter, an extensive benchmarking campaign utilising OpenAirInterface (OAI) has been carried out. OAI is an open source software-based implementation of the LTE architecture for 5G experimentation and prototyping that encompasses the full protocol stack both in the E-UTRAN and the Evolved Packet Core (EPC) that runs in a commodity x86-based Linux Personal Computer or data centre. In this system, the transceiver functionality is realised via a software radio frontend (such as the Ettus USRP B210). The combination of the open-source software and the inexpensive hardware involved, makes OAI a very attractive platform for experimentation and research towards the forthcoming 5th Generation. The platform comprises two components: i) openairinterface5g which implements the E-UTRAN, that is, eNodeB and UE and, ii) openair-cn which implements the Core Network, that is, the MME HSS, S-GW and P-GW. Based on OAI, the parameters $\mathcal{M}_{rs}$ for various wireless access network configurations has been evaluated.

Besides the working capacity, a spare set of resources should be reserved at each server s for protection purposes. As already mentioned, the primary objective of the proposed scheme is to minimise the total power consumption of the resulting network configuration. Let k_e being the cost of the capacity of link e of the optical network and PC_s the power consumed at server s. The following cost function should be minimized:

$$\boldsymbol{min}\mathcal{O}(\boldsymbol{p},\boldsymbol{x}) = \sum_{e\in\mathcal{E}_o} \boldsymbol{k}_e(\boldsymbol{u}_e(\boldsymbol{x}) + \boldsymbol{u'}_e(\boldsymbol{x})) + \sum_{s\in\mathcal{S}} \boldsymbol{PC}_s(\boldsymbol{v}_s(\boldsymbol{x}) + \boldsymbol{v'}_s(\boldsymbol{x})) \qquad \text{Eq. 3}$$

subject to the constraints mentioned above

2.2.2.2 Extension: Integration of NC

In the previous section, a modelling framework enabling resilient operation of the C-RAN system by protecting it from possible optical network and/or compute failure has been proposed. To address the very high bandwidth requirements that are imposed by this approach, an alternative formulation employing NC is proposed. To demonstrate the potential of NC in resilient C-RAN networks let us consider the simple 5G topology of. Adopting the traditional approach, multiple source-destination paths must be established double-sizing the necessary network bandwidth is some parts of the optical network. This may act as bottleneck considering that in FH networks this capacity may be extremely high. The adoption of NC, however, resolves this issue as it multiplexes FH streams originating from the two RUs. At the edge, FH streams are replicated (nodes 1, 3) and transmitted through disjoint paths 1-2, 1-3. Then, at node 2 instead of forwarding protection FH flows from regions x and y, the modulo-two sum $x \oplus y$ is transmitted over links 2-4, 4-6 and 4-5. At the egress nodes where BBUs are connected, the operations $x \oplus (x \oplus y)$ and $y \oplus (x \oplus y)$, are performed for BBU1 and BBU2, respectively, recovering FH flows y and x, respectively. Thus, by enabling encoding and decoding processes at the edge, throughput in survivable C-RAN architectures can be increased by a factor of 2.

An architectural decision in NC-enabled C-RANs is associated with the placement of the modulo-two sum and replication operations at the edge nodes. To optimise the operation of resilient NC-enabled C-RANs, a suitable set of constraints enabling NC is introduced. Let $\mathcal{N}_1$, $\mathcal{N}_2$, be the set of nodes where the modulo sum and replication operations are performed. To keep the analysis tractable, we assume that RUs are located in regions, x, y, as shown in **Figure 30** b), however, it can be easily extended to multiple nodes. Now, let $\mathcal{R}_x$, $\mathcal{R}_y$ be the set of RUs belonging to regions x, y, respectively with $\mathcal{R} = \mathcal{R}_x \cup \mathcal{R}_y$ and δ_{n1} a binary variable taking value equal to 1 if the protection flows of RUs originating from regions x, y are multiplexed at node $n_1 \in \mathcal{N}_1$. The following flow constraints should be satisfied:

$$\sum_{n_1 \in \mathcal{N}_1} \sum_{q \in \mathcal{Q}_{rn_1}} \delta_{n1} y_{rq} = h_z, \quad \forall r \in \mathcal{R}_z, z = x, y \qquad \text{Eq. 4}$$

$$\sum_{r \in \mathcal{R}_x} \sum_{\substack{k \in \mathcal{R}_y \\ k \neq r}} \sum_{n_1 \in \mathcal{N}_1} \delta_{n1} = 1 \qquad \text{Eq. 5}$$

where $\mathcal{Q}_{rn_1}$ denotes the set of paths interconnecting an RU r with node n_1. Eq. 5 indicates that the encoding process of all RUs will be performed at a single node. The encoded multiplexed stream $y_{n1} = y_{rq} \oplus y_{kq}$ is then forwarded to node $n_2 \in \mathcal{N}_2$ where the replication operation is performed. Flows are transmitted over candidate paths $q \in \mathcal{Q}_{n1n2}$ interconnecting nodes n_1 and n_2 with capacity z_q, $q \in \mathcal{Q}_{n1n2}$. The replicated flows are then routed to the locations where BBU are hosted over the shorted available paths. Finally, taking the summation of all FH flows over the optical network link e, the necessary protection capacity at e, u'_e, is determined. Finally, the NC-enabled C-RAN network is optimised by minimising the cost function Eq. 3 subject to the constraints mentioned above.

2.2.2.3 Network level evaluation

To evaluate the performance of the overall system, the processing requirements of the virtualised BBUs, and, consequently parameter $\mathcal{M}_{rs}$, are determined. To achieve this, an extensive set of experiments has been carried out using OAI. Performance analysis includes CPU Utilisation and instructions' measurement for different data rates as well as the application profiling. The measurements where performed with the use of the top command, which monitors the running processes in Linux systems and perf which is a collection of tools for system profiling. More specifically, the OAI profiling was done with the record command, which summarises where CPU time is spent. Measurements were performed in the idle mode (LTE device phone not connected) and while downloading with different data rates (100Kbps, 200Kbps, 500Kbps, 1Mbps and 2Mbps). The results are given in **Figure 29**. The measurement was performed with the perf stat command. As we can see, the instructions are clearly increasing in proportion to the data rate.

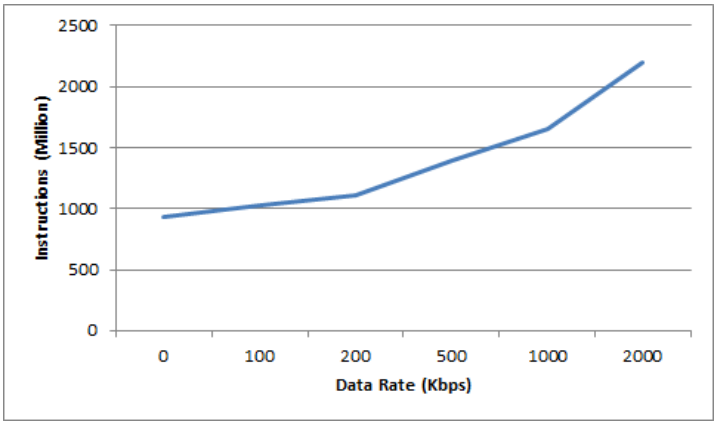

Figure 29: TSON. Total instructions per second for OAI as a function of access data rate

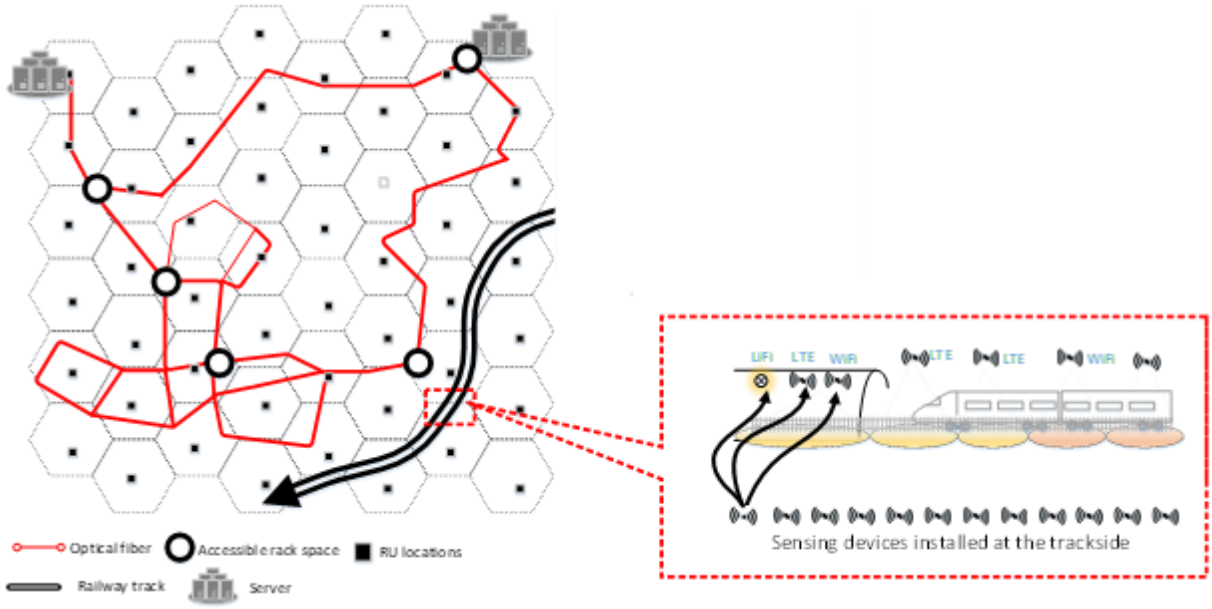

a)

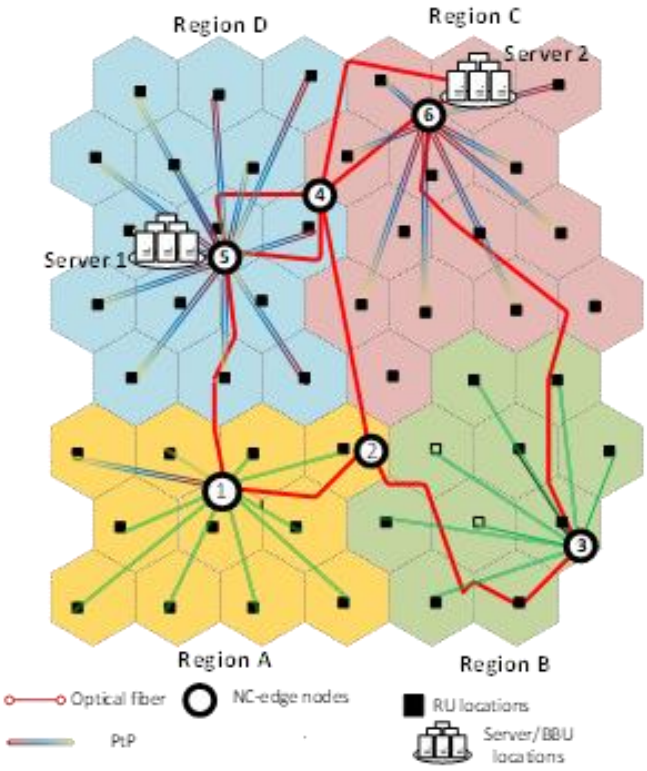

Figure 30: a) Bristol is Open Topology physical topology shown also the location of the rail line b) Modified Bristol city topology with NC enabled nodes.

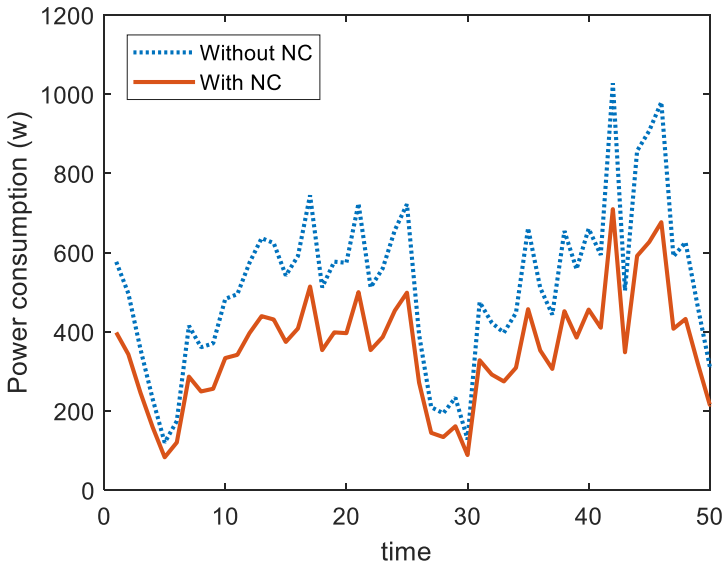

Figure 31 Bristol City Optical Network Power Consumption for the provisioning of Resilient C-RAN services.

Once BBU requirements have been determined, the performance of the overall system with and without NC considerations is examined for the Bristol City topology shown in **Figure 31**. In this topology, RUs are attached to the edge node through point to point links. For this topology, BBU processing for Regions A and D will be provided by Server 1 whereas BBU processing for Regions B and C by Server 2. At the same time, the main FH connectivity will be provided through links 1-5 and 3-6 for regions A, B, respectively. Protection of FH flows will be provided through paths 1-2-4-6 for Region A, 3-2-4-5 for region B, 5-4-6 for region D and 6-4-5 for region C. The encoding (replication) processes for regions A, B will be performed at node 2 (4), while for Regions C and D decoding and replication operations will be both formed at node 4.

2.3 Scalable Service Chaining in MEC-assisted 5G Networks

We consider a 5G network supporting railway operations as shown in **Figure 32**. This network is modelled as an undirected graph $G(N, E)$ where N is the set of nodes and E the set of links. In this network, vBBU SCs generated by a set $\mathcal{R}$ of R RUs are supported by a set of heterogeneous compute resources, located both at the edge (MEC) and at the metro/core (Central Cloud). Connectivity between these two endpoints is provided through a multi-technology transport network comprising point-to-point microwave links and optical network technologies. For the wireless transport we consider links operating in the Sub-6 GHz and 60GHz frequency bands, while for the optical transport, WDM network platforms [1] combining both active and passive optical elements. Active frame based WDM optical networks offer very low latency, transparent synchronisation and service differentiation at the edge while WDM-PONs are used for the interconnection of the RUs with the metro/core optical network and the BBUs. Now, let Σ_{r1}, Σ_{r2} be the processing requirements of the lower and upper-layer functions, respectively, of RU $r \in \mathcal{R}$. As shown in **Figure 32**., Σ_{r1} includes BBU functions ranging from "RF-to-basedband" conversion up to "receive processing" whereas Σ_{r2} includes the "decoding" and "MAC" functions. Let also S be the set of all servers (MEC, central cloud) and S^t be the set of MEC and central cloud servers hosting BBU functions at stage $t, t = 1,2$ of the optimisation process with $S^1 \cup S^2 \subseteq S$.

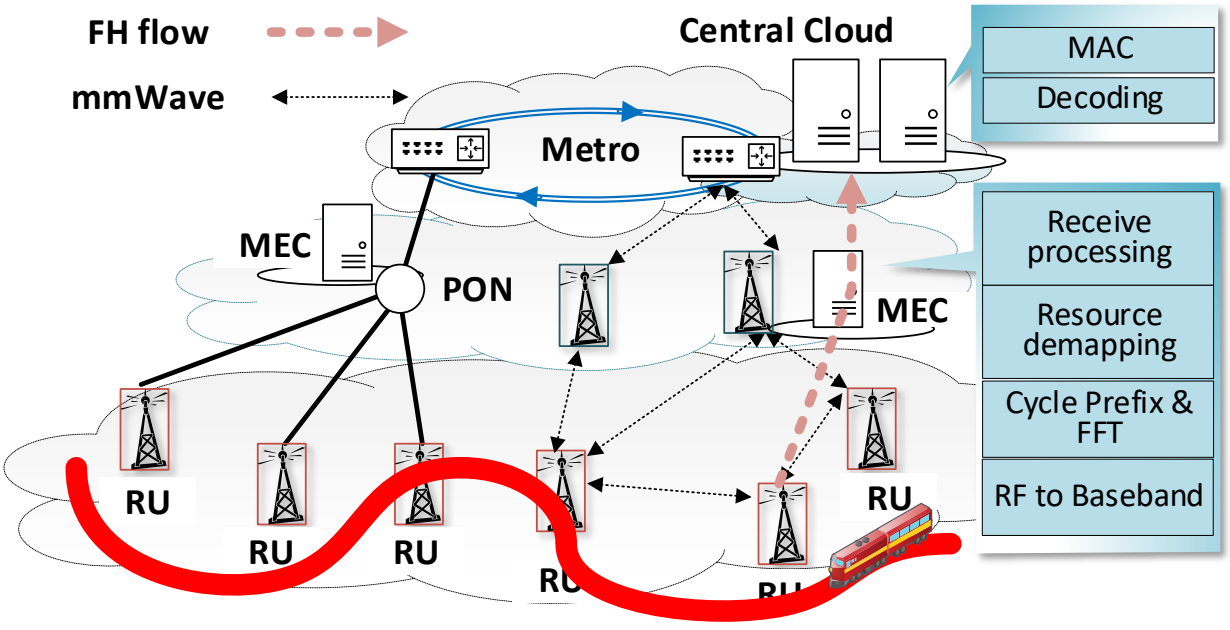

Figure 32: MEC-assisted 5G network supporting railway services. Functions up to "Receive Processing" are handled by MEC servers and the remaining by the Central Cloud, releasing network resources at the core.

In D2.3, a multi-stage framework is developed where during Stage 1 ($t = 1$) of the optimisation process, the first set of functions of all fronthaul flows in the service chain (i.e., functions with processing requirements Σ_{r1}) are assigned at servers $s \in S^1$. This is achieved by minimising the total compute and network resource power consumption, approximated through the following cost function:

$$f_1(\mathbf{x_1},\mathbf{z_1}) = \sum_{s\in S^1} \mathcal{E}_{S^1}\left(\sum_{r\in\mathcal{R}} x_{rs1}\,\Sigma_{r1}\right) + \sum_{e\in E} \mathcal{E}_e\left(\sum_{r\in\mathcal{R},s\in S^1,p\in P_{rs}} \delta_{rpe}\,z_{rp1}\right)$$

Eq. 6

Table 9 Parameters and Variables used in the Optimization framework

Symbol	Description
N	Set of Nodes in the 5G network
E	Set of Links
$\mathcal{R}$	Set of Remote Units (RUs)
T	Set of stages of the optimization problem $T = \{1,2\}$
S^t	Set of servers used at stage $t, t \in T$
P_{rs}	Set of candidate paths interconnecting RU $r \in \mathcal{R}$ with server $s \in S$
$P_{rss'}$	Set of candidate paths interconnecting server $s \in S^1$ hosting the lower layer functions of RU $r \in \mathcal{R}$ with server $s' \in S^2$ hosting the upper layer functions.
Σ_{r1}	Processing requirements of the lower layer functions of the BBU chain of RU $r \in \mathcal{R}$
Σ_{r2}	Processing requirements of the upper layer functions of the BBU chain of RU $r \in \mathcal{R}$
$h_{\Sigma_{r1}}$	Transport network bandwidth requirements of function Σ_{r1} for RU $r \in \mathcal{R}$
$h_{\Sigma_{r2}}$	Transport network bandwidth requirements of function Σ_{r2} for RU $r \in \mathcal{R}$
C_s	Total processing capacity of server s.
C_{st}	Available processing capacity of server s at stage $t, t \in T$.
C_{et}	Available capacity of link $e \in E$ at stage $t, t \in T$
δ_{rpe}	Binary coefficient indicating whether link e belongs to path $p \in P_{rs}$ realizing transport network demands of RU r or not
D_r	Delay threshold for RU r.
D_{rst}	Processing time of BBU functions of RU r at server s and stage t.
D_{rpt}	Propagation delay of FH flow originating from RU r across path p at stage t.
$\mathbf{H}_t$	Matrix with elements h_{rt}
$\mathbf{C}_{et}$	Matrix with elements C_{et}
$\mathbf{D}_r$	Matrix with elements D_r
$\mathbf{C}_s$	Matrix with elements C_s

In Eq. 6, the summation $\sum_{r\in\mathcal{R}} x_{rs1}\,\Sigma_{r1}$ captures the total processing load of all Σ_{r1} functions processed at server s, x_{rs1} is a binary decision variable indicating whether function Σ_{r1} of RU $r \in \mathcal{R}$ is processed at server s or not, $\mathbf{x}_1$ is a vector containing all first stage decision variables x_{rs1} and $\mathcal{E}_s$ is the power consumption model of server s. $\mathcal{E}_e$ is the power consumption model for links e. Network-related costs capture the costs of creating flows with rate, $h_{\Sigma_{r1}}$, transmitting the lower BBU functions Σ_{r1} from RU r, to the MEC. P_{rs} denotes the set of candidate paths interconnecting RU r with a server $s \in S^1$ and δ_{rpe} is a binary coefficient indicating whether link e belongs to path p realising transport network demands of RU r or not. Now let z_{rp1} be a variable indicating the network capacity allocated to path $p \in P_{rs1}$ for flow r and $h_{\Sigma_{r1}}$ the transport network bandwidth requirements of function Σ_{r1}. $h_{\Sigma_{r1}}$ can be directly estimated using the analysis descibed in [29]. Note that the second part of the objective function Eq.6 captures all network load that is transferred through link e. The notation used in the formulation is summarised in Table 9.

During Stage 1 of the optimisation process, the objective function should be minimised subject to a set of network and processing demand constraints described through the following set of equations:

$$\sum_{s\in S^1} x_{rs1} = 1, \qquad \forall\, r \in \mathcal{R} \tag{7}$$

$$\sum_{r\in\mathcal{R}} x_{rs1}\Sigma_{r1} \le C_{s1}, \qquad \forall\, s \in S^1 \tag{8}$$

$$\sum_{s\in S^1}\sum_{p\in P_{rs}} x_{rs1} z_{rp} = h_{\Sigma_{r1}}, \forall\, r \in \mathcal{R} \tag{9}$$

$$\sum_{r\in\mathcal{R}}\sum_{s\in S^1}\sum_{p\in P_{rs}} \delta_{rpe} z_{rp1} \le C_{e1}, \forall\, e \in E \tag{10}$$

Constraint (7) limits the number of servers where Σ_{r1}-type of functions can be processed to one, (8) indicates that the total number of tasks that can be assigned to server $s, s \in S^1$ cannot exceed its available processing capacity C_{s1} at stage 1, while equations (9) - (10) introduce network demand and capacity constraints, respectively. In (10), C_{e1} is the available capacity of network link e at stage 1. After the solution of the first stage optimisation problem, the remaining server and network capacity that can be used for the subsequent functions in the chain will be equal to:

$$\boldsymbol{C_s - \sum_{r\in\mathcal{R}} x_{rs1}\Sigma_{r1} = C_{s2}} \tag{11}$$

$$C_e - \sum_{r\in\mathcal{R}}\sum_{s\in S^1}\sum_{p\in P_{rs}} \delta_{rpe} z_{rp1} = C_{e2} \tag{12}$$

In Stage 2, the second set of functions of the FH service chain (Σ_{r2}) are forwarded to server $s \in S^2$ for processing. Now, let x_{rs2} be the second stage binary decision variables taking value equal to 1 if functions Σ_{r2} of RU $r \in \mathcal{R}$ are processed at server $s \in S^2$, 0 otherwise. Connectivity between servers $s \in S^1$ hosting Σ_{r1} of RU r and servers $s' \in S^2$ hosting Σ_{r2} is provided through a set of candidate paths $P_{rss'}$. The decision variables of the second stage optimisation problem that are responsible to forward and allocate the second set of functions of the FH service chain to the optimal servers for processing, depend on the results of the first stage problem. Typical example incudes the set of path $P_{rss'}$ that can be used to forward the output of the first function in the chain to the subsequent one (i.e., Σ_{r1} to Σ_{r2}). This set

depends on the decisions taken by the first stage problem regarding the servers where Σ_{r1} functions can be placed. Other examples include the available capacity at the servers and network links. All this unknown information is revealed gradually as we proceed deeper in the processing of the service chain. The optimal compute and optical network resource assignment problem in 5G environments can be solved through the minimisation of the following nested cost function:

$$\min_{\mathbf{x}_1 \in \mathcal{X}_1} f_1(\mathbf{x}_1, \mathbf{z}_1) + \mathbb{E}\left[\inf_{\mathbf{x}_2 \in \mathcal{X}_2} f_2(\mathbf{x}_{2,} \mathbf{z}_2)\right] \quad \text{(Eq. 13)}$$

where extending (5.1)

$$f_t(\mathbf{x}_t, \mathbf{z}_t) = \sum_{s \in S^t} \mathcal{E}_{S^t}\left(\sum_{r \in R} x_{rst} \Sigma_{rt}\right) + \sum_{e \in E} \mathcal{E}_e \left(\sum_{r \in \mathcal{R}, s \in S^t, p \in P_{rs}} \delta_{rpe} z_{rpt}\right) \quad (14)$$

The multi-stage linear programming model described through (1)-(9) can be decomposed into a Master Problem (MP) and a sub-problem (SP) and solved using BD [30].

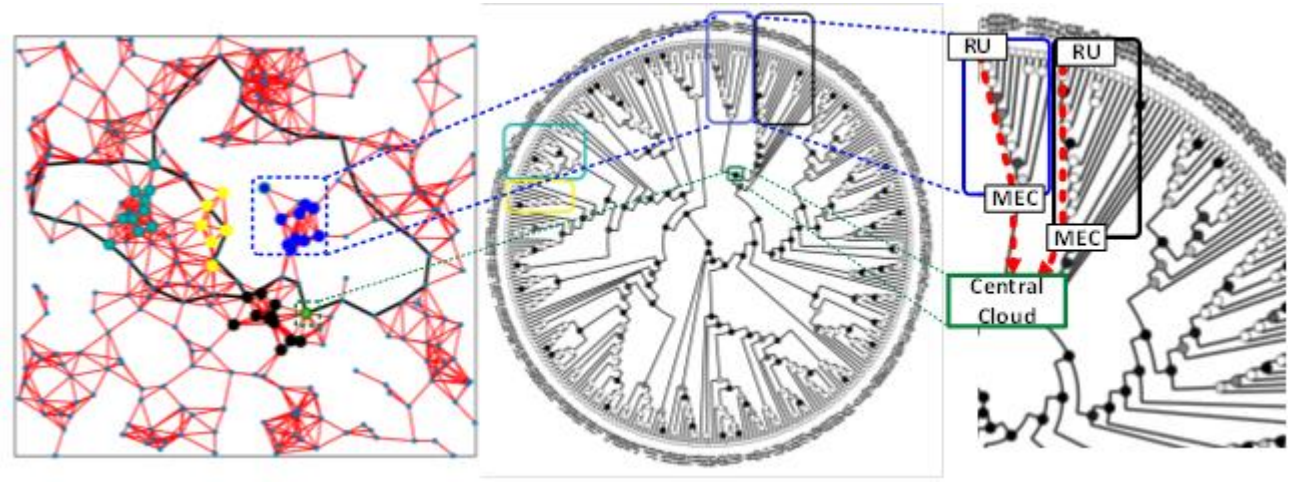

a) *b)* *c)*

Figure 33: a) Network with 300 RUs. Black lines indicate optical and red lines wireless links, b) HRG graph of the random topology in (a), c) vBBU SC in the HRG domain: RUs forward their low-level BBU functions to the MEC and then to the central cloud.

2.3.1 Accelerating Convergence Using HRG theory

The BD-based algorithm successfully solve the service provisioning problem in MEC-assisted 5G environments. However, its computational complexity is still significant as the number of parameters involved in the process increase exponentially with the size of the network making it unsuitable for large optimisation scenarios. In response to this we propose a decomposition technique based on HRGs that reduces the computational complexity of the SC process and accelerates the convergence process. Through HRG, the network graph over which the optimisation is applied can be simplified reducing the number of variables included in the optimisation model. However, a prerequisite for the successful implementation of HRG is the development of algorithms that can detect, in a cost-effective manner, a dendrogram that reflects with high probability the generic topological properties of 5G networks. This hierarchical structure can simplify the SC embedding process as it exposes to the ML-ILP problem a limited set of well-defined candidate paths that can support these flows. To apply HRG-theory the following steps are adopted:

Step 1: 5G topology decomposition using HRG

5G networks comprise access networks domains with densely interconnected devices (i.e., V2V, IoT etc) and transport optical networks sparsely interconnected with optical network nodes. HRGs capture these properties through parameter, $p_n, n \in N$ indicating the interconnection probability of any two nodes in the network. p_n takes high values in densely interconnected network (i.e. an RU servicing multiple users) and low values for optical nodes with limited connectivity. Assuming that e_n is used to denote the number of links interconnected to node n, C_n the total capacity of the node, and R_n, L_n the number of links of all nodes in the subtrees that are right and left, respectively, of node n, then, the likelihood of an HRG graph G^* is given by [31]

$$L(G^*,p_n) = \prod_{n\in G^*} p_n^{e_n/C_n}(1-p_n)^{L_n R_n - e_n/C_n} \quad \text{Eq. 15}$$

Equation (10) indicates that the connection probability of two nodes in the HRG increases with e_n/C_n. For higher values of e_n, the probability a randomly selected node to be attached to n increases. Similarly, the probability that a randomly selected RU is directly attached to an optical transport node is very low and reduces with $L_n R_n$. As $L_n R_n$ increases, the number of elements that are low in the hierarchy increase. It can be easily shown that (5.10) is maximised at

$$p_n^* = \frac{E_n}{C_n L_n R_n} \quad \text{Eq.16}$$

taking values equal to

$$L(G^*,p_n) = \prod_{n\in G} p_n^{*p_n^*}(1-p_n^*)^{C_n L_n R_n} \quad \text{Eq.17}$$

or in log scale

$$\log L(G^*,p_n) = -\sum_{n\in D} C_n L_n R_n \, \mathcal{H}_n(p_n^*) \quad \text{Eq.2-18}$$

where the $\mathcal{H}_n(p_n^*)$ function denotes the Shannon entropy.

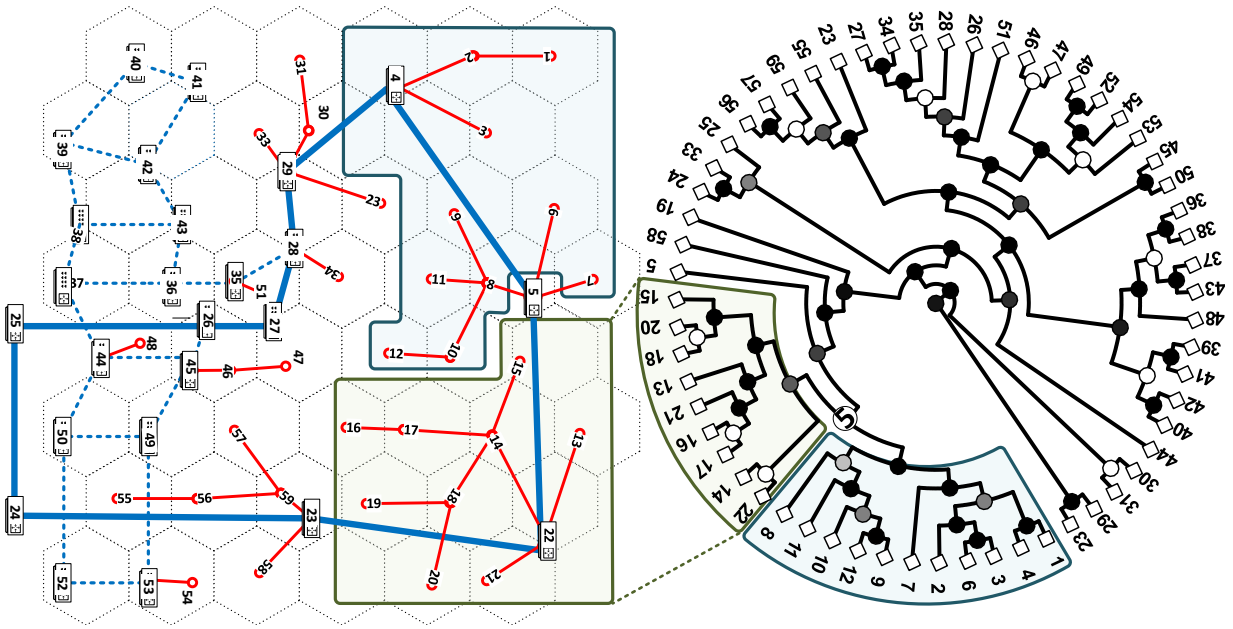

Figure 34 a) Bristol Is Open (BIO) Converged 5G Network, b) Hierarchical Random Graph (HRG) of the BIO Infrastructure.

Step 2: Optimal Fitting of the HRG to the 5G network

Once the likelihood of the possible HRGs has been determined, a sampling technique based on the Markov Chain Monte Carlo (MCMC) approach can be applied. MCMC samples the candidate HRGs proportionally to their likelihood and identifies the HRG with the maximum $L(D, p_n)$ value [31]. The maximum likelihood HRG fits the real world 5G graph with high accuracy. An example of this process for a 300 node network (**Figure 33**a)) is shown in **Figure 33**b. Once fitted, the optical transport nodes appear high in the hierarchy of the generated HRG (close to the centre). On the other hand, RUs are low in the hierarchy and are embedded at the edge of the disk (**Figure 33** c).

Step 3: Optimal Service Chaining in the HRG space

After decomposing the 5G network into a hierarchical graph, a solution for the SC problem in MEC - assisted 5G environments can be obtained. The ML-ILP problem described in Section II can be easily solved in the HRG space as the number of candidate paths that interconnect RUs with servers $s \in S$ that support processing of the requested SCs has been drastically reduced. A graphical representation of this benefit is shown in **Figure 33** c. It is observed that employing this methodology, central clouds servers which are directly attached to the core have been placed close to the root of the HRG whereas MEC servers have been embedded low in the hierarchy providing an intuitive solution to the problem. During this step, the BD algorithm described in Sec. III is executed over the simplified graph and the optimal allocation strategies are obtained.

Step 4: Service re-provisioning

HRGs are updated frequently to better fit the topological changes of the 5G network (i.e. link failures, beam steering, mobility, insufficient capacity etc). Given that these topological changes are observed mostly at the edge, the likelihood of the updated 5G graph is very similar to the original one. Therefore, during the re-provisioning phase, MCMC samples only a small subset of graphs with likelihood values close to those of the original graph. Once the updated graph has been determined, Step 3 is executed.

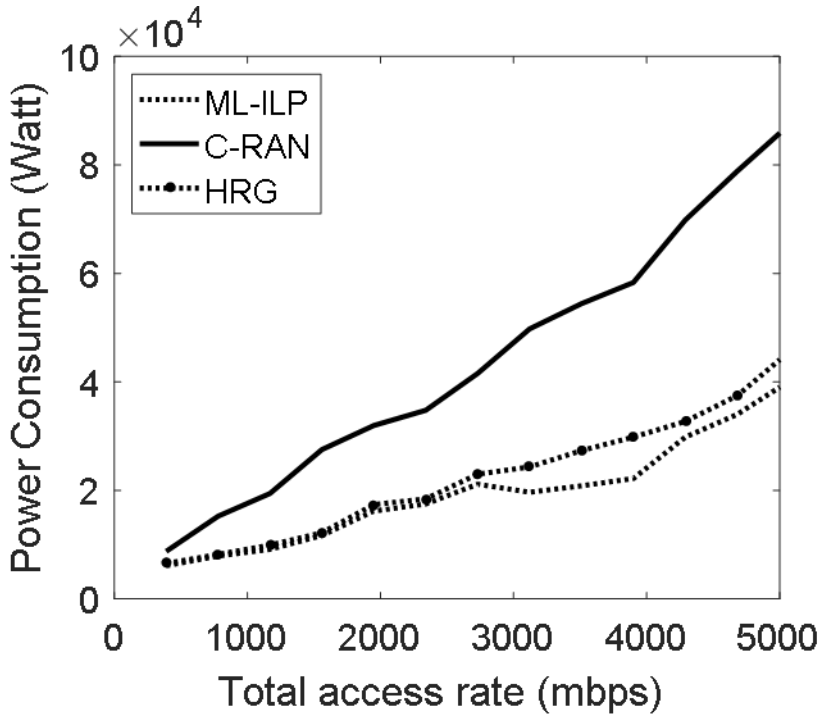

Figure 35: Comparison between C-RAN, ML-ILP and the HRG schemes for the BIO topology.

2.3.2 Numerical Results

We evaluate the performance of the proposed optimisation framework under various topologies (including the Bristol is Open (BIO) topology) for the scenario where RUs offload their signal processing functions to the MEC-assisted 5G Network. For the BIO topology we consider a set of 48 RUs evenly distributed across a 10x10 km2 area. RUs are backhauled through microwave point-to-point links and a dynamic frame based optical network solution [1]. This solution deploys a single fibre per link, 4 wavelengths of 10Gbps each per fibre and minimum bandwidth granularity of 100Mbps. Power consumption figures for the optical network can be found in [1]. The bandwidth of the microwave transceivers considered is 2Gbps and their associated power consumption is 45W. We assume the realistic traffic statistics reported in [33]. For BBU processing, two types of servers have been considered: a) small scale MEC servers close to the RUs and, b) central cloud servers hosted by large scale DCs. MEC servers have an average cost equal to 2Watts/GOPS while the processing cost for the central cloud servers is 1.6Watts/GOPS [29]. We also consider that MEC servers are placed in all optical network edge nodes whereas central cloud servers are placed in nodes 4, 22, 26 and 42

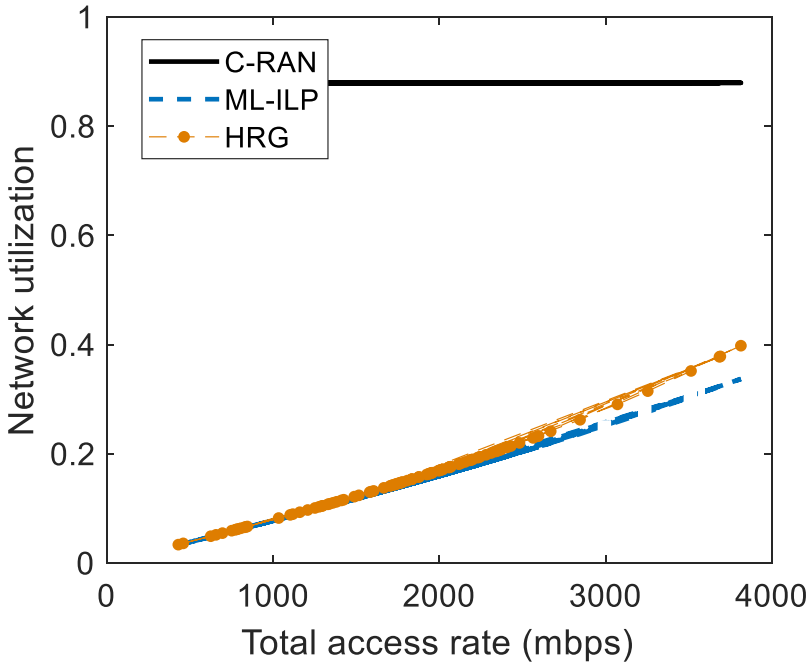

Figure 36: Comparison between C-RAN, ML-ILP and the HRG schemes for the BIO topology in terms of network utilisation.

We initially compare the proposed ML-ILP scheme with the traditional C-RAN approach where all tasks are processed by fixed BBUs placed in the central cloud, with and without the adoption of HRG. Sizing of BBUs in this case is performed under maximum traffic demands. In **Figure 35** it is shown that the HRG-based optimisation scheme outperforms C-RAN in terms of power consumption and achieves very close performance to the optimal ML-ILP approach. In C-RAN all BBU functions are offloaded to the central cloud having significant FH network requirements and, therefore, increased power consumption. Through the introduction of the proposed scheme and the processing of some functions in MEC, FH network requirements are drastically reduced leading to lower network utilisation (**Figure 36**) and reduced power consumption level. We also observe that the introduction of the HRG approach introduces minimal performance degradation compared to the optimal solution of the ML-ILP approach without the HRG simplification. As previously mentioned, HRG reduces the number of the available paths interconnecting the RUs with the compute nodes leading in some cases to sub-optimal solutions. However, compared to the benefits obtained from the reduction of the computational complexity this impact is negligible.

Figure 37 shows the impact of the number of samples taken during the MCMC process to identify the graph that reflects with high probability the properties of the 5G topology. As expected, for higher number of tree samples, the optimality gap of the solution obtained adopting HRG is reduced as the probability to detect a hierarchical graph with higher likelihood increases. The optimality gap also increases with the size of the 5G network topology. Therefore, for larger 5G network topologies a higher number of samples should be taken to achieve the same optimality gap. At this point it should be mentioned that the HRG detection process can be carried out offline (or in parallel to the ML-ILP problem) without affecting the speed of convergence of the SC allocation process.

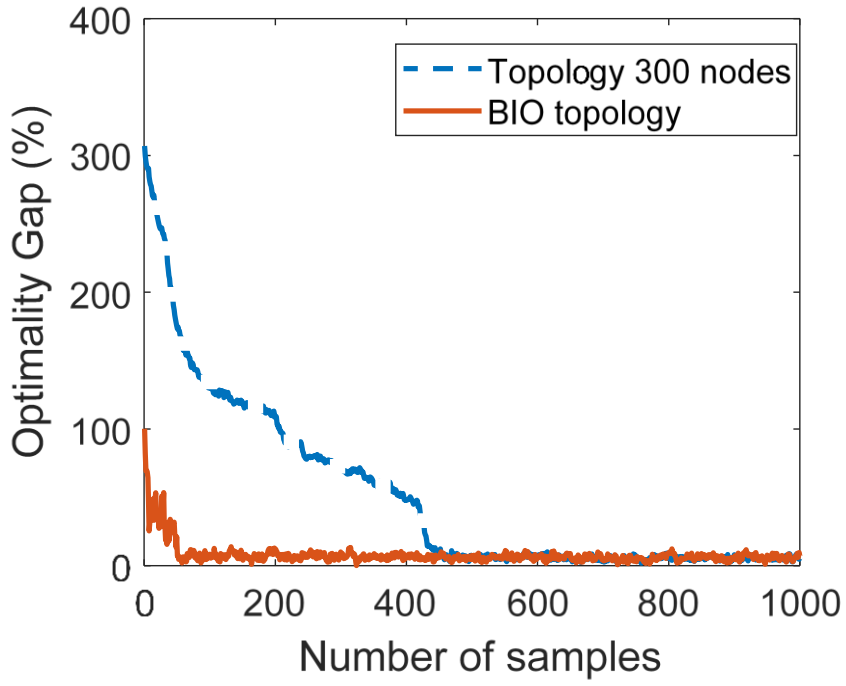

Figure 37: Optimality gap as a function of the number of HRG samples, c) Number of paths used in the ML-ILP and the HRG.

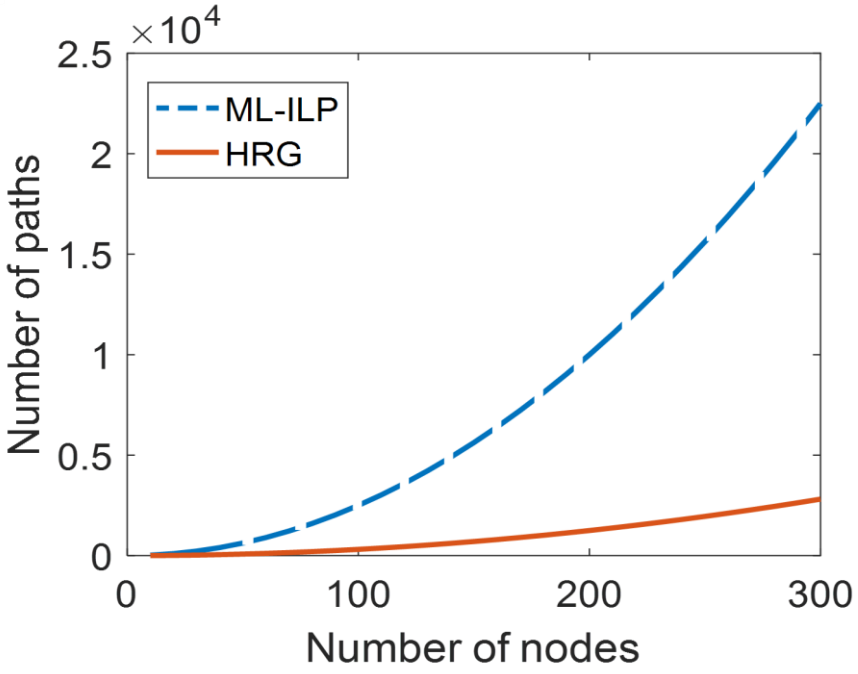

Figure 38: Number of paths used in the ML-ILP and the HRG.

From **Figure 38** it is observed that that with the adoption of HRG the complexity of the BBU function allocation is reduced. This is due to that using HRG the number of candidate paths, and consequently the number of variables, that are used to interconnect the RUs with the compute resources are minimised. This has a direct benefit on the reduction of the time required to solve the optimisation problem. The total execution time for the HRG scheme for up to 300 nodes is less than 20sec for whereas for the ML-ILP scheme the same value reaches 600 sec.

2.4 5G Network Design with Reduced Computational Complexity Using AI Techniques

The concept of Mobile Edge Cloud (MEC) has been proposed as a key enabling technology that can be used to address the strict latency and processing requirements of 5G services [101]. Through the placement of servers with moderate storage and processing power at the edge of the Radio Access Network (RAN) and in close proximity to the mobile subscribers [102], the need for longer transport distances can be reduced leading to lower end-to-end latencies. This can improve end-users experience and enable the provisioning of a wide set of delay sensitive services including, positioning, connected and automated driving, augmented reality, video analytics etc.

MEC can also assist RANs to extend their network coverage and enhance connectivity in areas where macro cell coverage is limited or not available. This concept, for example, can be realised through in-cabin/in-vehicle or even backpack installation of low-cost Remote Units (RUs) which can be coupled with softwarised implementations of the LTE protocol stack running on local MEC servers. C-RAN can address effectively the limitations of traditional RAN, reducing the cost and offering increased the scalability and flexibility. However, C-RAN requires very large transmission bandwidth and imposes strict latency and synchronisation constraints. The functional split concept allows separating the signal processing functions into individual functional blocks that can be dealt with in the form of a function chain where each function can be processed independently as long as the chain order is maintained. This approach allows to handle lower layer functions locally and offload higher layer functions remotely to the RU at a Central Unit (CU). In case that this allocation of local and remote functions is performed dynamically in a flexible fashion the approach is referred to as flexible functional split.

In 5G infrastructures transport networks can be supported through integrated optical and wireless network domains offering converged backhauling and fronthauling functionalities [90]. This approach can offer high capacity transport networks interconnecting RUs with compute resources where softwarised versions of the RAN protocol stack are executed. This is enabled by a control plane that manages and optimises the operation of a large number of highly heterogeneous network and compute elements, taking decisions related to: i) optimal embedding of service requests and creation of service chains over the converged network resources [105], [106], ii) optimal infrastructure slicing across heterogeneous network domains [107], iii) optimal sharing of common resources in support of both telecommunication and vertical industry services [108], iv) optimal fronthaul deployment strategies including optimal placing of central units with respect to remote units, functional split selection etc. [109], [110]. These problems are traditionally addressed by centralised control and orchestration platforms using a large variety of mathematical modelling frameworks, based on integer linear [111] and non-linear [101] programming, stochastic linear and non-linear formulations [112] etc.

Although these approaches can be effectively used to optimise the operational points of the whole infrastructure, they are unsuitable for real time network deployments due to their increased computational complexity and slow convergence time. The problem is further exaggerated under scenarios considering highly varying 5G topologies. A typical example is shown in Figure 1 where the introduction of short lived mobile base stations (such as LTE gNBs used for emergency or transportation services) may negatively affect the performance of the whole system.

A suitable approach to enable optimal real time decision making in 5G environments is envisioned to take advantage of low computational complexity online tools based on Neural Networks (NNs) [113] exploiting optimal solutions available through offline tools based on Integer Linear Programming (ILP) . The offline ILP planning models can be used to create a set containing the optimal design policies for converged 5G network environments. NNs can then use the output of these models for design and training purposes. Once the optimal NN structures have been identified, they can be used by the centralised controller or the MEC server to forecast in real time the optimal operational parameters of the 5G network.

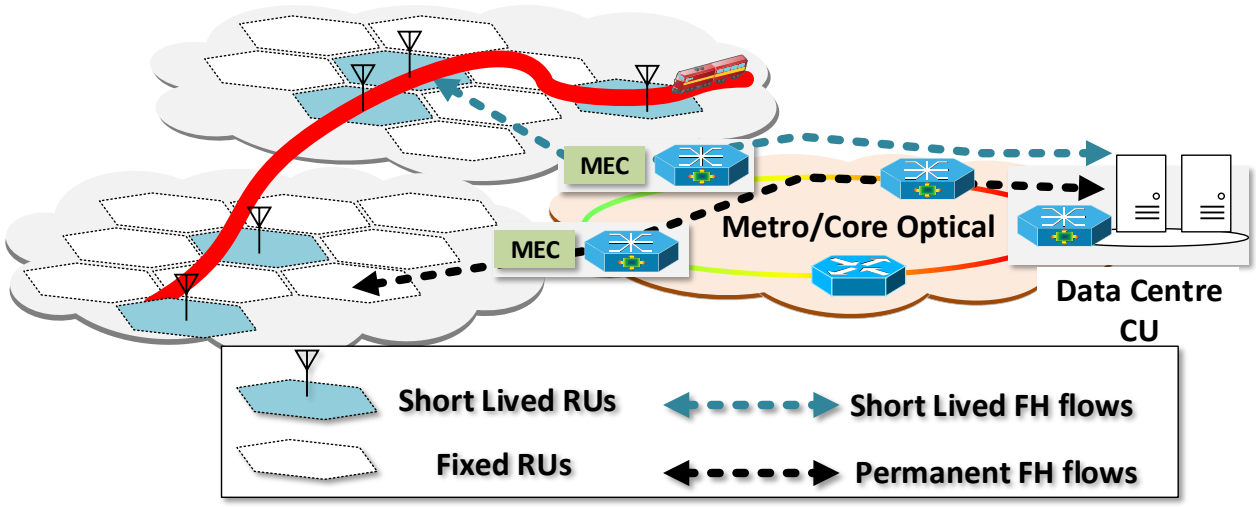

Figure 39: Varying 5G network topology with short lived/permanently operating RUs.

Preliminary results in this direction indicate that NNs can be effectively used to predict the optimal operational conditions of the 5G network that match the solutions obtained through the ILP models. However, this approach suffers from the increased computational complexity required to identify the optical NN architecture for every 5G network component (i.e. optical fibre, RUs, etc). This problem, also known as NN hyperparameter optimisation, is hard since the number of parameters that can be selected when building a NN-based mode is extremely high. Acceleration of the NN hyper-parameter tuning process has been extensively studied in the literature and several solutions have been proposed [113], [118]. These include, exhaustive search for NN structure combinations (number of neuros, hidden layers, epochs etc) with the objective to minimise the root-mean-squared-error (RMSE) [113].

In IN2DREAMS, we have proposed an alternative approach to the optimal NN hyperparameter selection problem adopting clustering techniques. Taking advantage of the correlation that exists between input traffic statistics, network topologies and routing decisions in optical clouds, a hierarchical clustering model is proposed that groups devices with similar hyperparameters. This enables the on the fly identification of the optimal NN structure for the devices encompassing the 5G network taking into account actual input traffic statistics. This approach is crucial for real time optimisation solutions and enables the NN model selection to become more flexible and re-constructible.

2.4.1 Problem Description

We consider the generic case of a converged 5G infrastructure interconnecting a set $\mathcal{R}$ of remote units (RUs) with a set $\mathcal{S}$ of S Central Units (CUs). $\mathcal{R}$ comprises a subset $\mathcal{R}_F$ of permanently installed (fixed) RUs and a subset $\mathcal{R}_{SL}$ of short-lived RUs (i.e., mobile gNBs in transportation environments or gNB offering

services in a train crossing a specific area etc) with $\mathcal{R} = \mathcal{R}_F \cup \mathcal{R}_{SL}$ In this problem setting, the accurate number of RUs and, subsequently, the source-destination (RU-CU interconnections) FH pairs is not known in advance as the number and type of short lived RUs may greatly variate over time. A graphical representation of this concept is shown in **Figure 39** where an integrating wireless access and optical transport network together with compute elements in support of FH flows for both short-lived and permanently operating RUs is illustrated.

To solve the service provisioning under uncertain source demands, a two-stage stochastic optimisation model can be formulated, with the first-stage capturing the deterministic demands generated by $\mathcal{R}_F$ and the second-stage the uncertainty introduced by $\mathcal{R}_{SL}$ In a generic form, this problem will be solved minimising the following cost function:

$$\min_{\mathbf{x}_1 \in \mathcal{X}_1} f_1(\mathbf{x}_1) + \mathbb{E}\left[\inf_{\mathbf{x}_2 \in \mathcal{X}_2} Q(\mathbf{x}_2, \omega)\right] \quad \text{Eq. 19}$$

with

$$f_1(\mathbf{x}_1) = \sum_{s \in S} \sum_{r \in \mathcal{R}_F} c_s x_{rs} + \sum_{e \in E} \sum_{r \in \mathcal{R}_F} c_e x_{re} \quad \text{Eq. 20}$$

$$Q(\mathbf{x}_2, \omega) = \sum_{s \in S} \sum_{r \in \mathcal{R}_{SL}^{\omega}} c_s x_{rs}^{\omega} + \sum_{e \in E} \sum_{r \in \mathcal{R}_{SL}^{\omega}} c_e x_{re}^{\omega} \quad \text{Eq. 21}$$

In the first stage optimisation function (Eq. 20), x_{rs} denotes the resources used at server s for the processing of the FH flows originating from RU $r \in \mathcal{R}_F$ while x_{re} is the network capacity used at link $e \in \mathcal{E}$ by the FH flows originating from RU $r \in \mathcal{R}_F$. The first stage problem is solved subject to a set of constraints $\mathcal{X}_1$ indicating that i) the total number of BBUs that can be assigned to server s cannot exceed its available processing capacity, ii) sufficient network and compute resources are allocated for the provisioning of FH flows and, iii) FH flows do not violate network capacity and latency constraints. In the second stage problem, the remaining network and compute capacity is allocated at the short-lived RUs with the objective to minimise cost function (Eq. 21) under a possible scenario ω. In equation (Eq. 21), x_{rs}^{ω} and x_{re}^{ω} indicate the compute and network resources allocated for the provisioning of a FH flow under a possible scenario where RU $r \in \mathcal{R}_{SL}^{\omega}$ is active. This scenario appears with a probability $p_{\omega} > 0$. The second stage problem is solved under a set of constraints $\mathcal{X}_2$ that take into account the remaining capacity from the first stage problem. This type of problems is solved using Stochastic Linear Programming (SLP) [101]. Therefore, using as inputs network topology details, traffic statistics, the probability distribution that the various scenarios may appear, the location where each function/task will be processed together with the required network and compute resources can be determined.

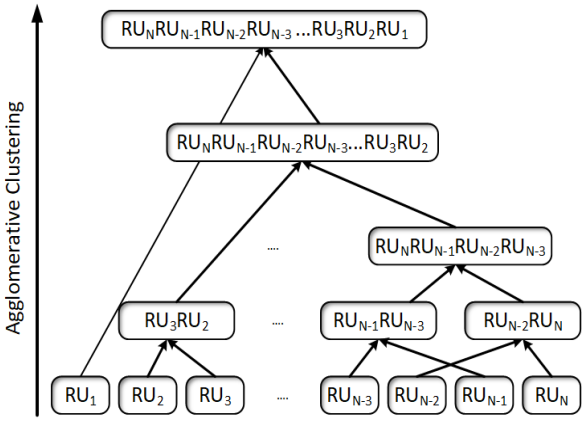

Figure 40: Dendrogram of the agglomerative clustering algorithm applied in our network elements.

The main limitation of this approach is related to the high computational complexity and the slow convergence of the SLP-based models. In response to this observation, we propose a two-stage neural network framework for real time service provisioning, extending our previous work in [113]. In, the first stage, long short-term memory (LSTM)-NNs are used for traffic forecasting while in the second multilayer perceptron (MLP)-NNs are adopted for the prediction of the optimal operational parameters of the 5G-Network [113]. This is achieved through the estimation of the optimal MLP-NN structure (number of neurons, the number of hidden layers, the batch size and the number of epochs) that can fit the solutions obtained using the offline optimisation framework. The main limitation of this approach is related to the fact that identification of the optimal hyperparameters that characterise the NN's structure is time consuming process. Therefore, for scenarios with frequent topological changes the identification of the optimal NN structure in due time is not possible.

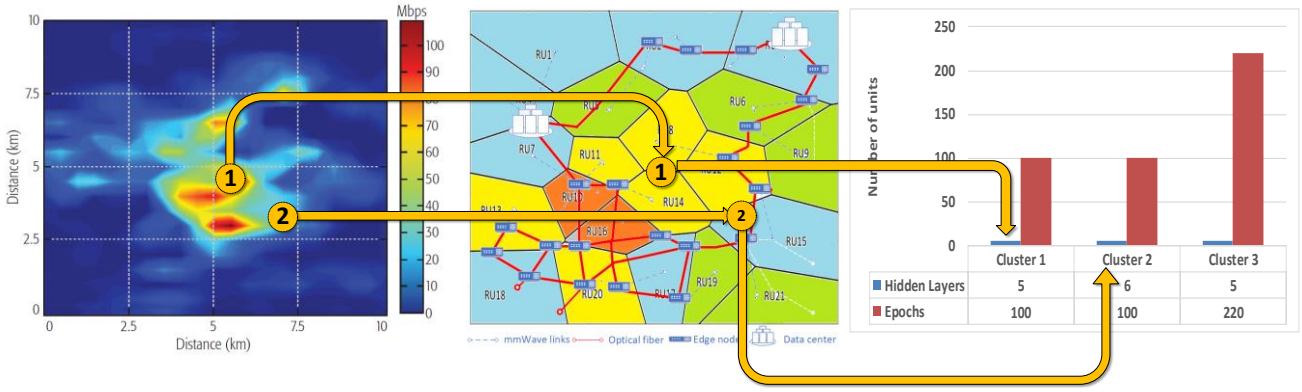

a) b) c)

Figure 41: Automated hyperparameter selection for two RUs a) wireless traffic statistics over a 10x10km access network, b) clustering of RUs based on their hyperparameters, c) lookup table for hyperparameter selection.

To simplify and accelerate the hyperparameter selection process, a clustering approach is proposed taking advantage of the inherent correlation that exists between input traffic statistics, 5G topology and routing decisions. To demonstrate the effectiveness of this approach, consider the simple case where the 5G network is altered by the arrival of two short-lived RUs, namely RU1 and RU2 shown in **Figure 41**.Once activated at the specific location, their optimal NN structure that can be used to determine the

operational parameter of interest for the upcoming time instances can be readily obtained. To achieve this, a clustering algorithm is used to group RUs with similar NN structures. When the clustering analysis is complete RUs are classified as part of one of the resulting clusters. Once RUs have been clustered, the hidden layers and epochs are selected on the fly to determine the optical the NN model structure (**Figure 41**c)). In the final step, the optimally extracted NN structure for each RU is trained using the traffic statistics that are available at the corresponding location. A detailed description of this process is provided in the following Section.

2.4.2 Real Time Optimisation For 5G

2.4.2.1 Clustering Preliminaries

Cluster analysis is a machine learning method for identifying homogeneous groups of objects, known as clusters, based on a measure of similarity. Objects belonging to the same cluster are similar to each other, but are very dissimilar to objects belonging to different clusters. Each object can be graphically represented as a point in a n-dimensional space, where n is the number of features that characterise the object. Clustering analysis is an exploratory analysis, since many parameters of the final clustering analysis have to be investigated. Particularly, the metric which measures the correlation of objects has to be selected, while the clustering algorithm that will be used and the number of different clusters have to be determined. Most methods calculate measures of similarity or dissimilarity by estimating the distance between pairs of objects. The distance between more similar objects is small, whereas the distance between dissimilar objects is large [114]. The most convenient metric for object's similarity is the Euclidean distance. There are several clustering algorithms. These algorithms can be classified in hierarchical and partitioning methods [115]. The clustering method used in this study is the hierarchical clustering and in particular the agglomerative technique. The most popular agglomerative clustering algorithms are the single linkage, the complete linkage, the average linkage and the Ward's algorithm which are differentiated according to the way that calculate the distance between the clusters. In the present study after we have implemented a trial and error process, we select the Ward's method. This algorithm calculates the total sum of squares of the distances within each cluster and aims to minimise them. These sum of squares within the cluster are known as square error sums (ESS) and their formula is:

$$ESS = \sum_{i=i}^{n} {x_i}^2 - \frac{1}{n}\left(\sum_{i=1}^{n} x_i\right)^2$$

$$ESS_{(M\ groups)} = \sum_{j=1}^{j=M} ESS_j$$

where the x_i is the score of the individual i^{th} [116].

Initially, the number of clusters is equal to the number of objects as each object represents an individual cluster. At first the most similar objects are merged to establish a new cluster. Then another pair of objects is merged and linked to a higher level of the hierarchy. In this way a tree-like structure is constructed, each level of which is composed of a different number of clusters. In the higher levels the dissimilarity between the merged clusters is increased. Finally, since similarity decreases, all the sub-clusters are merged in a single cluster at the top of the hierarchy. This process can be visualised with a dendrogram as shown in **Figure 40**.

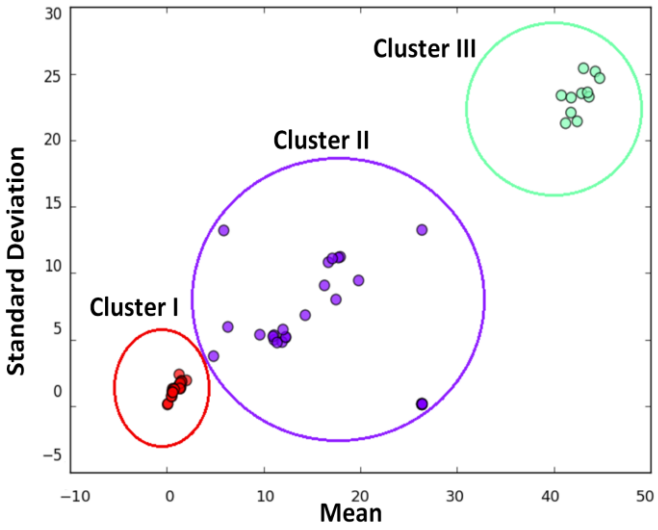

Figure 42 Clustering model results.

2.4.2.2 Hyper-parameter Optimisation using the Agglomerative Clustering Algorithm

In [113] we proposed a LSTM-NN to forecast the input traffic at each RU and we implemented an exhaustive search in order to find the optimal LSTM's structure. This work is concentrates on identifying the parameters of LSTM-NN for each RU without having to implement an exhaustive search suffering high complexity that makes it impractical for real time network configurations. Therefore, we propose to construct another model to search the NN's hyperparameters.

Table 10: Agglomerative Clustering Algorithm

Step 1: Begin with N clusters, each one composed of a single RU and a symmetric table of distances between the RUs.
Step 2: Search in the table of distances, the pair of clusters-RUs with the highest similarity, which means the smallest distance.
Step 3: If the most similar clusters are RUi and RUj., merge the clusters RUi and RUj and create a new cluster C1, that comprises the RUi and RUj objects.
Step 4: Recalculate the table of distances by removing the rows and columns related with the clusters RUi and RUj and adding a new row and column that contain the distances of the new cluster C1 and the other clusters.
Step 5: Repeat N-1 times the step 2,3, and 4. Report the clusters that were merged, the levels at which this merge was occurred.

Each RU of the dataset is characterised by a set of statistical variables associated with the traffic and its distribution. This information is sufficient for a clustering model to group similar RUs in the same cluster using the algorithm summarised in Table 10. following this, each of the resulting clusters is linked with a specific LSTM configuration. So, for the RUs belonging to the same cluster, the LSTM's parameters are selected automatically. Finally, the NN-based model is trained to predict the RU's traffic in the next time period. To assign the LSTM configurations to the appropriate clusters, we introduce a threshold value to the prediction error and we try to approximate the NN hyper-parameters instead of finding the optimal one. This relaxation enables the creation of a set of suitable LSTM configurations for each RU. Similar configurations that belongs to these sets are linked with specific clusters.

2.4.2.3 Numerical Results

Topology description

In our previous study the performance of the NN-based optimisation framework was evaluated using the optical transport network topology presented in [113] over which 21 RUs are developed. Each RU serves mobile devices that generate demands according to real dataset reported in [117]. In the current study, we extend this dataset by creating more RUs with random traffic statistics based on the distributions of the real data. This extension is mandatory and efficient to produce more reliable clustering results.

RUs grouping using clusering approach

To group the most similar RUs in the same cluster the clustering algorithm described in Section III is applied to the dataset. This dataset is composed of a set of statistical parameters that describe the traffic of the RUs and provide the required information to perform the required RU comparison and clustering. These include the traffic distribution, the mean value and standard deviation. Figure 44 shows the clustering results. Based on these results three clusters are selected.

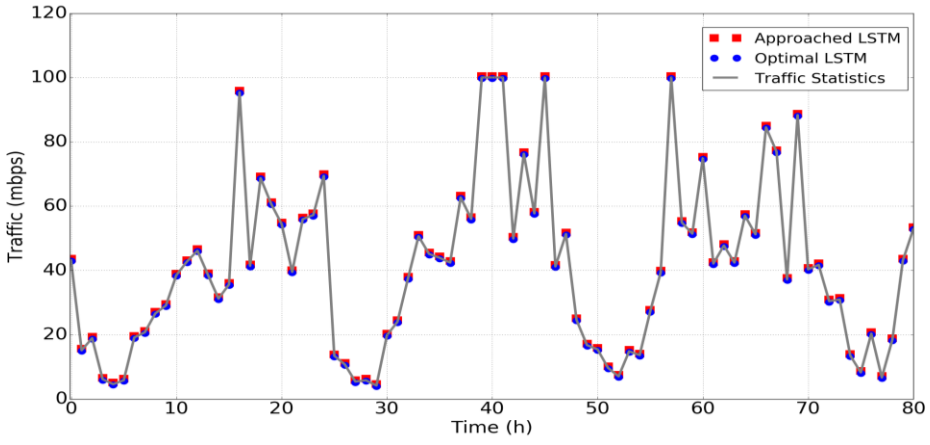

Figure 43: Traffic forecasting using LSTM as derived from the clustering approach.

b)

Figure 44: a) NN forecasting error for the two different LSTM approaches. Dashed line represents the threshold error. b) Comparison between exhaustive search and clustering approach in terms of execution time

Neural Network topology approximation

In [113] for each network element an exhaustive search described in Section II was performed to design the optimal NN architecture that predict with very high accuracy the traffic for the following time period and then the optimal policies as they have been obtained by the corresponding ILP. In the present study, this optimisation problem is relaxed by adding a higher error threshold in the range of (1.5%-5%), whereas the previously accepted error was in the range of (0.1%-3%). In addition, we introduce a clustering approach in order to reduce the execution time.

Once the clustering model has been produced, the NN hyper-parameters are selected as described above. The results that are obtained by these two different approaches must have similar performance. AA trade-off between execution time and prediction's accuracy are introduced with our clustering method. As shown in the first figure, we observe an increase on the forecasting error, which however is still below the threshold we have set. On the other hand, in the second figure, the gain in execution time is very high.

3 Control and Management of the Integrated ICT Solution

3.1 Introduction

As already discussed the proposed ICT platform (Figure 2) exhibits a large degree of heterogeneity in terms of technologies. To address the challenge of managing and operating this type of complex heterogeneous infrastructure, we propose the integration of the Software Defined Networking (SDN) and Network Function Virtualisation (NFV) approaches. In SDN, the control plane is decoupled from the data plane and is managed by a logically centralised controller that has a holistic view of the network [ETSI 2014]. In early SDN deployments the data plane implementations only supported packet forwarding related functionalities. However, the advent of new high performing technologies such as LiFi and dynamic optical railway network solutions necessitate the execution of much more complex networking functions such as scheduling, network monitoring and management, resource virtualisation, isolation etc. In response to this, SDN controlled programmable hardware infrastructures can now effectively support implementation of these functionalities using high level programming languages. At the same time, NFV enables the execution of network functions on compute resources by leveraging software virtualisation techniques [ETSI 2015]. Through joint SDN and NFV consideration, significant benefits can be achieved, associated with flexible, dynamic and efficient use of the infrastructure resources, simplification of the infrastructure and its management, increased scalability and sustainability as well as provisioning of orchestrated end-to-end services.

SDN is an emerging network architecture that aims at providing network administrators with the ability of programmable, flexible and dynamic resource management through centralised control. The fundamental concept of this architecture is the separation of the network control from the forwarding functions. The control plane is responsible for the routing of the packets and the data layer for transporting them. Unlike the traditional TCP / US architecture, where routing is in line with the static IP protocol, SDN provides the ability to use routing policies based on the requirements of each client and the needs of the network. Networks become programmable and manageable, making the infrastructure transparent for the applications and services they offer, while facilitating the resource allocation, the scalability in distributed data centres, and the virtualisation of devices that is necessary for Cloud environments[[123]-[125].The SDN architecture is divided in three basic layers: the application layer (application plane), the control layer (control plane) and the infrastructure layer (data plane) (Figure 45).

Network applications reside in the application plane through which the network administrator can immediately communicate with the controller in order to learn the network requirements and define the required behaviour to be applied to the network. Communication between the applications and the centralised controller is performed through the NorthBound SDN Interfaces (NBIs). The NBIs provide the application-level view of the network as well as the ability to directly interfere with network requirements.

The control plane contains the centralised network controller and is responsible for setting the forwarding rules to the network devices, through the Southbound SDN interface. On a physical level, the controller can be distributed to different physical machines in order to provide scalability and optimisation of processes. However, the controller behaves as a unique logical unit, with its own operating system making uniform decisions. There are two main operations that a controller must perform. The first is to transfer the system requirements that are provided from the application plane, to the data plane. The

second is to notify the application plane for any changes to the network operation that are perceived from the data plane. It consists essentially of NorthBound Agents that contribute to the application-control plane communication, the control centre that is responsible for the decision-making processes, and the CDPI (Control to Data-Plane Interface) Drivers that are responsible for the proper communication with the data plane, by providing programmatic control of all data forwarding features, report of traffic statistics on the network, and updates to the controller in the event of a network change or problem.

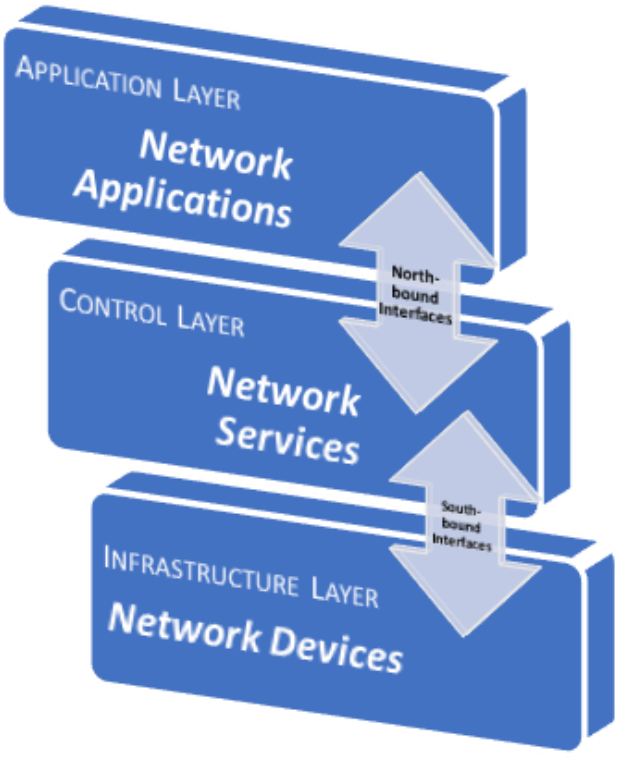

Figure 45: SDN Architecture

The infrastructure layer is a network logical entity that provides supervision and control of data forwarding and processing that take place on the network. It consists of a CDPI Agent in order to communicate with the controller and a set of devices responsible for the forwarding. The data layer - although behaving as a unified module - may be composed of distributed physical devices with shared resources, and can also work with non-SDN devices. Outside the application, control and infrastructure layer resides the Management and Admin of the SDN. Although, it is not part of the SDN architecture, it is basically the reason for the development of SDN, that is, the control that can now be applied to the networks that support SDN. Through the application layer, the administrator can update the network by defining appropriate behaviours. The communication of the applications and the administrator is accomplished with the help of the controller.

3.1.1 OpenFlow Protocol

OpenFlow is the first standard protocol for the communication of the control plane and the data plane in SDN architectures. It allows the direct access to the network devices, i.e. virtual and physical switches and routers, and the management of their data forwarding platform. OpenFlow protocol is essential for the separation of the control from network devices and its relocation to a logically distributed control

software. It is applied to both sides of the interface between the SDN control software and the network infrastructure [124].

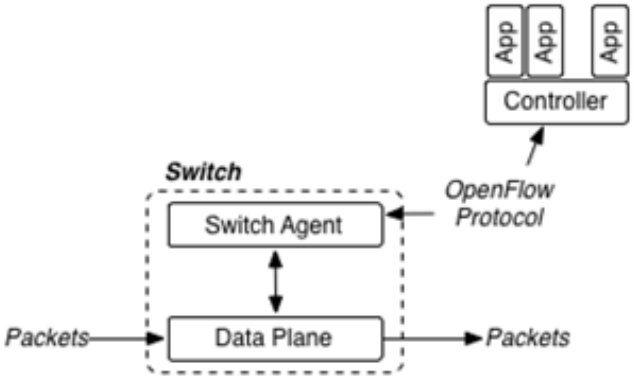

Figure 46: Architecture of OpenFlow switch [2]

OpenFlow uses the concept of flow to identify network traffic. The concept of flow is based on predefined mapping rules that can be statically or dynamically set by the controller. It also allows the administrator to specify how network traffic will be distributed according to network resources, application requirements, and routine network traffic patterns. In contrast with traditional IP networks, where in Internet routing two streams with the same start and end points will follow the same route because of the same IP addresses, in the SDN architecture two or more streams may have the same source and destination points and follow different routes with different priorities, depending on the routing policy that are assigned to.

Three kinds of messages are supported by OpenFlow: Controller-to-Switch, Asynchronous, and Symmetric. Controller-to-switch messages are originated from the Controller and enable the direct management and supervision of the state of a switch. Asynchronous messages start from the switch and aim to inform the Controller either about events that happen on the network or about changes in the state of the switch. Finally, symmetric messages originate either from the Controller or the switch and are sent without any prior request [125].

SDN that supports OpenFlow protocol can be deployed on existing networks. Networking devices can support both OpenFlow and conventional TCP / IP routing. There is the possibility of hybrid switches operating in any environment (SDN or not) or implementing centralised control over applications (network monitoring and management), so it is not necessary to replace each network device with SDN switches [125]. This is a great advantage for network providers that can be led into the SDN architecture gradually, relying on their traditional networks, turning them into SDNs.

3.1.2 *OpenFlow Switch*

The OpenFlow switch consists of two parts: the switch-agent and the data platform (Figure 2). The switch-agent communicates through the OpenFlow protocol with the controller and with the data plane through an appropriate protocol. It is responsible for translating the controller's commands into the appropriate machine language and sending them to the data platform. It also receives from the data platform any notifications and converts them into OpenFlow messages understandable by the controller and promotes them. The data platform performs the management and forwarding of the packets. Depending on the configuration, it may send packets to the switch-agent for processing. It includes flow tables and related

actions for each flow, thus the packets are forwarded according to which flow they belong to and to which flow-table action they will be matched [124].

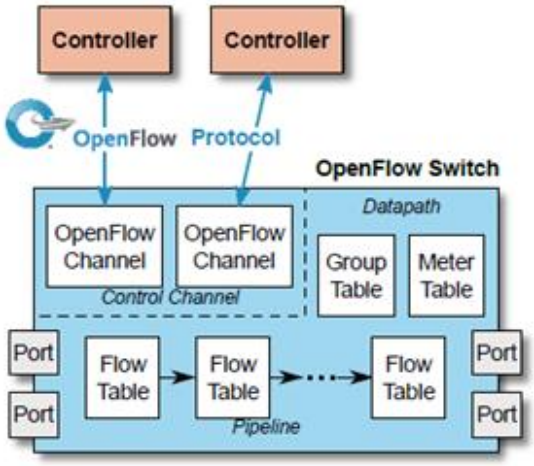

Figure 47: Main Components of an OpenFlow switch [125].

An OpenFlow switch can be any packet-forwarding device (router and switch) and consists of one or more flow-tables that are used to match and forward packets, a group table, and a secure communication channel to a Controller [125]. The Controller manages the OpenFlow switch through the channel using the OpenFlow protocol (Figure 47).With the implementation of OpenFlow, the controller can proactively or reactively add, update, and delete flow tables. Each flow table contains recordings for the flows with counters and actions for each flow. Each package entering the OpenFlow switch is contrasted with the flows of the first flow-table and continues with additional flow-tables. In the case of matching with a flow, the set of commands associated with that flow are applied, otherwise the outcome depends on the configuration of the table-miss flow. For example, the packet can be forwarded to the Controller via the OpenFlow channel, discarded, or continued in the next flow-table.

3.1.3 SDN Control

For the control of the SDN network, two controllers were tested, namely the Open Networking Operating System controller (ONOS) and the Opendaylight controller.

ONOS: ONOS was developed by the Linux Foundation community and it is an open source project on Software Defined Networking. Its code is written in JAVA language and it can be extendable. ONOS supports the OpenFlow protocol as well as other SDN architecture protocols and technologies since they can be properly configured by the administrator[126].

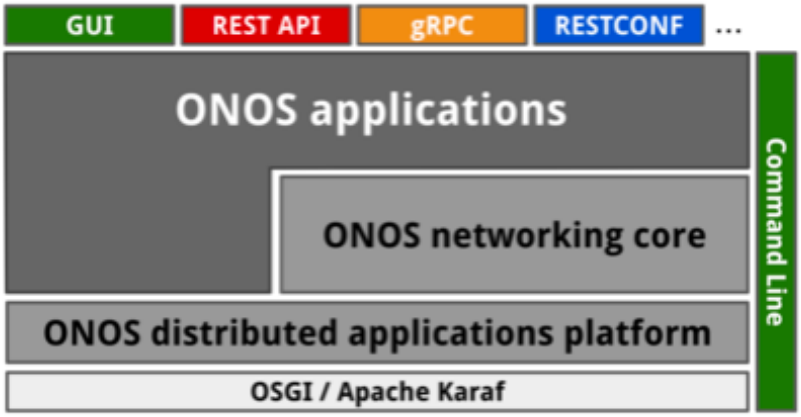

Figure 48: Architecture of ONOS Controller.

ONOS is designed to operate as a cluster of nodes that are identical in terms of their software stack and can withstand failure of individual nodes without causing disruptions in its ability to control the network operation. The architecture of ONOS controller is show in **Figure 48**. The system, that is packaged atop Apache Karaf OSGi container, provides its own set of high-level abstractions and models, apart from standard protocols and models, through which the applications can learn about the state of the network and through which they can control the flow of traffic through the network. The network graph abstraction provides information about the structure and topology of the network. The flow objective is a device-centric abstraction that allows applications to direct flow of traffic through a specific device without the need to be aware of the device table pipeline. Similarly, the intent is a network-centric abstraction that gives application programmers the ability to control network by specifying what they wish to accomplish rather than specifying how they want to accomplish it. This simplifies application development and at the same time provides the platform with added degrees of freedom to resolve what would normally be considered conflicting requests [126].

Applications can be loaded and unloaded dynamically, via REST API or GUI, and without the need to restart the cluster or its individual nodes. ONOS application management subsystem assumes the responsibility for distributing the application artifacts throughout the cluster to assure that all nodes are running the same application software. ONOS base distribution contains over 175 applications, which fall into numerous categories, e.g. traffic steering apps, device drivers, ready-to-use YANG models, utilities, monitoring apps.

The system provides REST API, CLI and an extensible, dynamic web-based GUI. gRPC interfaces for ONOS are under active development.

Opendaylight: The OpenDayLight (ODL) controller was developed by the Linux Foundation community and it is an open source project on Software Defined Networking. Its code is written in JAVA language and it can be extendable [127]. Major companies in the industry such as Cisco, Brocade, Juniper Networks, IBM, Vmware, Ericsson, Microsoft, Big Switch Networks as well as independent Open Source engineers are working to help develop the ODL project. ODL supports the OpenFlow protocol as well as other SDN architecture protocols and technologies since they can be properly configured by the administrator [128].

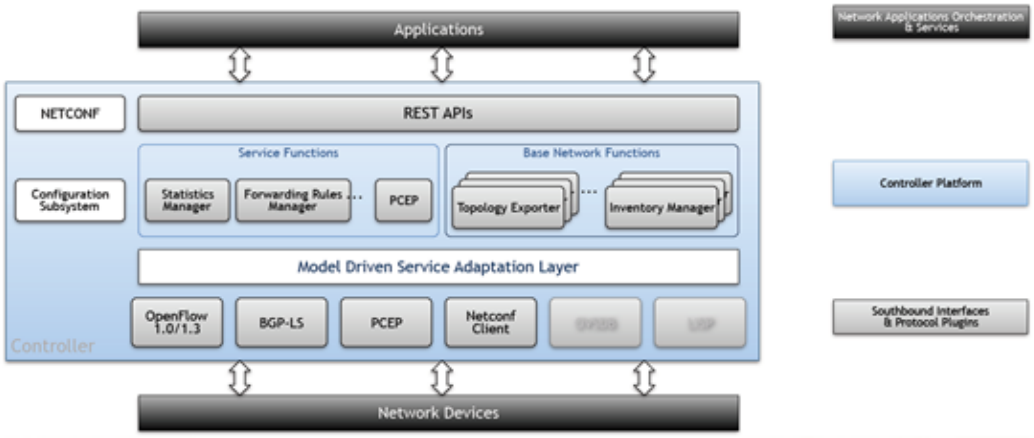

Figure 49: Architecture of OpenDayLight Controller [127].

The architecture of ODL controller is shown in Figure 49. The controller platform incorporates both Northbound and Southbound interface. The Northbound interface provides services to the controller as well as a set of REST API applications that can be used to manage and configure the network infrastructure. Access to the Northbound interface of the controller is possible after authentication and licensing of the user. REST (Representational State Transfer) is an architectural design used in web applications (WEB development). Systems designed in REST architecture have good performance, reliability and scalability in terms of the number of users they can gradually support. RESTful systems typically communicate through the HTTP protocol through the GET, PUT, POST, DELETE methods commonly used by the browser to retrieve and send data to remote servers [129]. Outside of the browser, the communication with RESTful systems can be accomplished via a terminal and in particular via the curl bash command, along with the appropriate arguments (username, code, URI). Curl can send any required text in json or xml format. The information returned by the system is also in json or xml format.

The Southbound interface implements protocols for managing and controlling the underlying network infrastructure. Several extensions are being implemented either to support network protocols or to directly communicate with the hardware. The most prominent protocols implemented are OpenFlow, NetConf, SNMP, OVSDB. The controller platform communicates with the network using the Southbound interface and provides basic network services through a set of functions described below [130]:

- Host Tracker: It saves information about system terminals (MAC addresses, IP, switch type, port number) and provides an API to retrieve information about them. It can work in a static or dynamic way. Statically, the Host Tracker database is manually handled through Northbound APIs. Dynamically Host Tracker uses the ARP protocol to detect information.
- L2 Switch: Upon the arrival of a packet, this function learns the MAC address of the source. If the destination is known, it transfers the packet to the destination, otherwise it sends a broadcast message (i.e. a message to all devices) to all external network ports.
- OpenFlow Forwarding Rules Manager: It manages basic forwarding rules, resolves any conflict between these rules and validates them. Furthermore, it communicates with Southbound extensions and loads the OpenFlow rules to the switches.

- OpenFlow Statistic Manager: It implements the statistics collection by sending statistics requests to all active nodes of the network and storing their responses to the operational store. It also returns information to the Northbound API for the following:
  - node-connector (the port of the connected switch)
  - flow
  - meter
  - table
  - group statistics
- OpenFlow Switch Manager: It provides information about the nodes (switches) of the network as well as the ports to which they are connected. As long as the controller discovers new network elements, their information is stored in the Switch Manager data tree. The Northbound API can be used to retrieve this information.
- Topology Processing: It saves and handles information about the network devices. When the controller starts, the Topology Manager creates the central node of the topology. Then it is informed regularly of the topology and of any alarms or changes on this tree.
- In ODL, the integration of Southbound and Northbound APIs with the data structures used in various controller components is provided through the Model Driven Service Abstraction Layer (MD-SAL). In MD-SAL, any data associated with the operation state of the network is stored in a Document Object Model (DOM), known as a data tree. There are two kinds of data trees in the ODL controller:
- Configuration: It is used to store information that will not be deleted after the controller is restarted. In addition, configurations that are sent to the controller via the REST API are also stored in the configuration tree.
- Operational: Here the controller stores temporary information that arise while performing processes on the network, as well as information that are discovered from the Configuration data field.

3.2 Implementation

3.2.1 Infrastructure Layer

The switch that was chosen for testing and implementation purposes is the Hewlett Packard Enterprise Aruba 2930F layer 3 switch. This multi-port switch can offer low latency for high-speed networking. It also supports Power over Ethernet technologies and full network management capabilities. The Aruba-OS wired switches are 802.1Q VLAN-enabled. A group of networked ports assigned to a VLAN form a broadcast domain configured on the switch. On a given switch, packets are bridged between source and destination ports that belong to the same VLAN. A switch port can be dedicated to only one VLAN (untagged) or be part of more than one VLANs (tagged). The switch can be managed remotely by configuring an IP address and a sub-net mask. Once the switch is connected to the network, features like performance optimisation, traffic control, network security etc., can be accessed through a more commodious way, by a remote telnet session or through the switch's Web browser interface [131].

- *Network Configuration*

Originally, the switch has one VLAN, the DEFAULT-VLAN that is assigned to all ports. In order to configure the switch with an IP address, a management VLAN should be created. In the Command Line Interface (CLI), the following scripts can be used create a management VLAN with a specific IP:

```
Aruba-Switch(config)# vlan 111 ip address [ip-address] [mask-length]
Aruba-Switch(config)# oobm disable
Aruba-Switch(config)# management-vlan 111
Aruba-Switch(config)# vlan 111 untagged [range of ports]
```

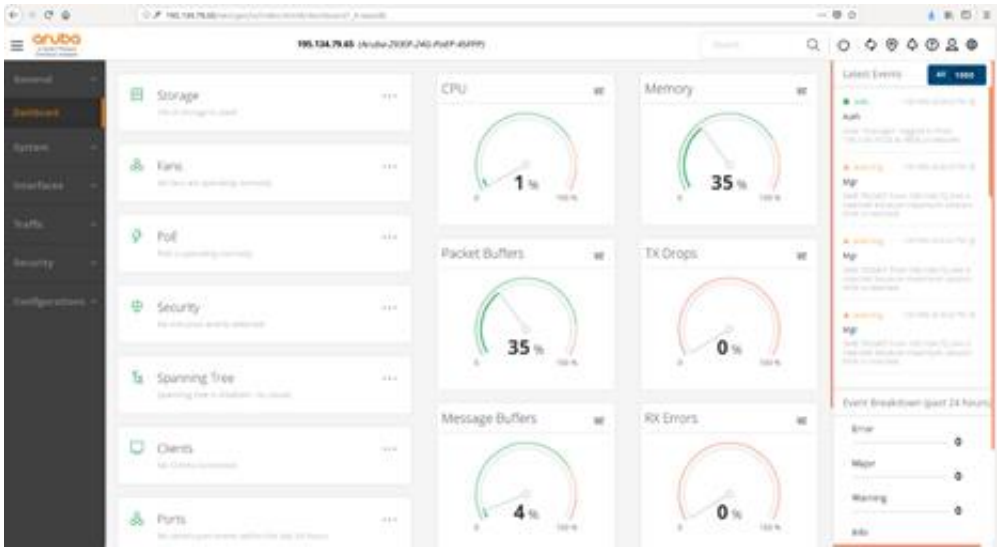

Figure 50: Web interface of Aruba switch 2930F-24G-PoEP-4SFPP.

The switch can be managed remotely through the web interface (Figure 50), or the CLI by the devices that are connected to VLAN 111.

Openflow Configuration

The Aruba switch also complies with the SDN architecture and the Openflow Switch Specification. OpenFlow implementation can be used to separate OpenFlow traffic and non-OpenFlow traffic with OpenFlow instances. Traffic within an OpenFlow instance does not influence or degrade non-OpenFlow traffic. OpenFlow configuration commands are applied per-instance. The communication channel between the OpenFlow Controller and the OpenFlow switch traverses the control-plane to communicate data and rules about how OpenFlow instances should operate. The OpenFlow instances/ VLANs are the data-plane, which is where the OpenFlow rules are applied. Control-plane traffic is configured through a separate channel in order not to traverse the data-plane and avoid data-plane outages or other issues.

An OpenFlow instance can either be in the Virtualisation or Aggregation Mode (Figure 51).

- Virtualisation mode allows non-OpenFlow VLANs and VLANs that belong to OpenFlow instances to be configured on the switch. Each OpenFlow instance is independent and has its own OpenFlow configuration and OpenFlow controller connection. An OpenFlow instance in virtualisation mode must have a VLAN associated as a member VLAN. In In2Dreams this functionality is critical as it allows multiplexing of traffic coming from conventional devices with OpenFlow enabled traffic.
- In Aggregation mode, all VLANs in the switch are part of an OpenFlow instance. The exception is the management VLAN and a VLAN that communicates to the controller. The OpenFlow controller manages all the switching and routing for the switch. [10]

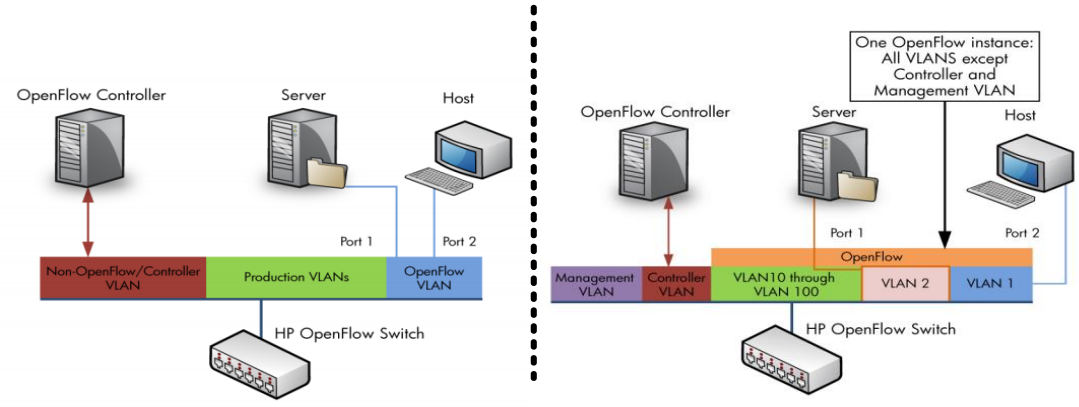

Figure 51: Virtualisation mode vs Aggregation mode of an OpenFlow instance in Aruba switch [131]

Therefore, for this implementation the virtualisation mode has been considered. The openflow controller can be configured using the following commands

```
Aruba-Switch(config)# openflow controller-id [id] ip [IP address] port
[tcp-port] controller-interface vlan [vlan-id]
```

The commands below enter the OpenFlow configuration and create an openflow instance associated with the created controller

```
Aruba-Switch(config)# openflow        /* Enters the openflow configuration*/

Aruba-Switch(openflow)# instance [name] /* Creates an openflow instance */

Aruba-Switch(ins-[name])# member vlan [id] /* SDN controlled VLAN */

Aruba-Switch(ins-[name])# controller-id [id] / * SDN controller*/
```

By default, the instance is configured to use the standard-match pipeline model. The standard-match pipeline model enables an instance to advertise its policy-engine and software tables. The ip-control pipeline model enables an OpenFlow version 1.3 instance to advertise its IP control table along with policy-engine and software tables. The custom pipeline model enables an OpenFlow controller to customise an OpenFlow pipeline model for OpenFlow version 1.3 instance. The default custom pipeline consists of three Hash tables and one TCAM table, as shown in Figure 52.

```
Aruba-Switch(ins-[name])# pipeline-model [standard-match or ip-control or
custom] /* Configure an OpenFlow instance pipeline model*/
```

Standard Match	
Flow Table	**Table Number**
Start	0
Policy Table	100
S/W Table 1	200
S/W Table 2	201
S/W Table 3	202
S/W Table 4	203

Figure 52: Table number configuration on standard-match pipeline model.

```
Aruba-Switch(ins-[name])# table-num [policy-table or sw-table-#] [0-254]
/*Configure table number for flow tables */
```

hardware and software by default.

3.2.2 APPLICATIONS

3.2.2.1 Creating intents using ONOS controller

ONOS provides an interactive GUI with the ability to see the network topology and change its configuration. An example is shown in the following figure:

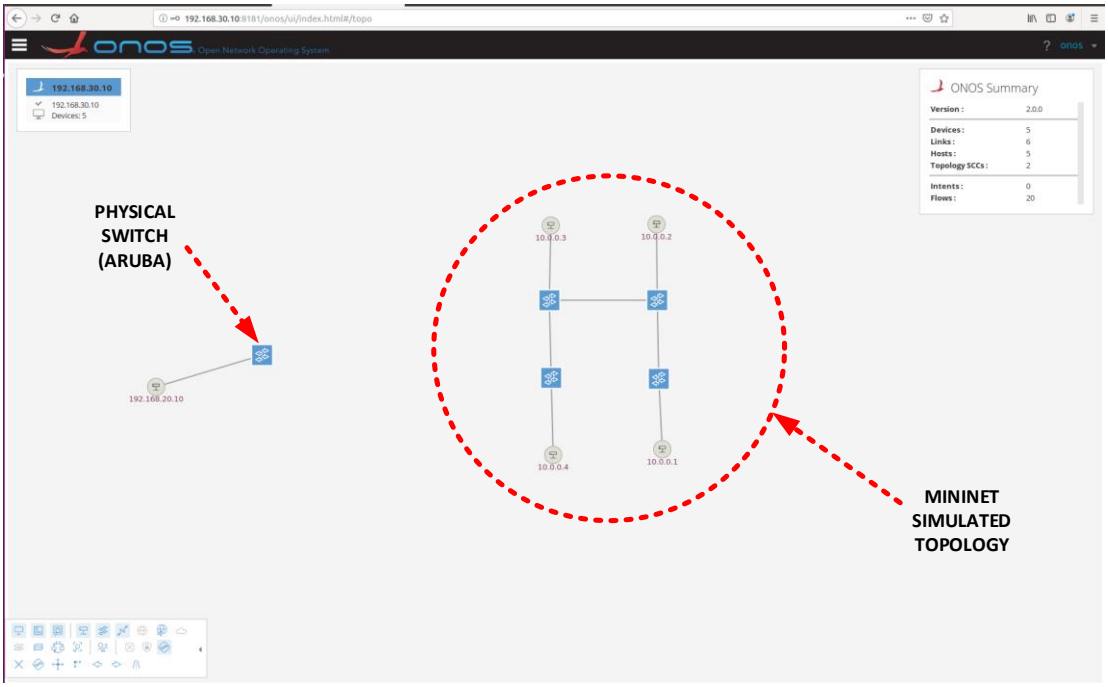

Figure 53: Graphical display of network topology in ONOS GUI

Through ONOS, devices, links and the servers can be directly managed. In addition to this, flows associated with specific services and priorities can be instantiated.

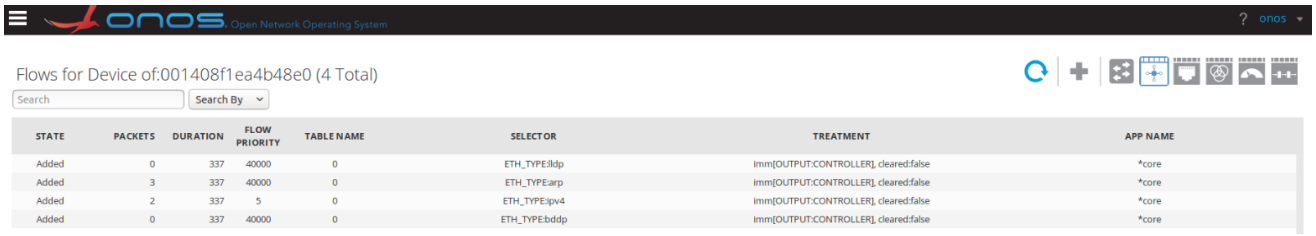

Figure 54: Flows installed in Aruba switch

During the initialisation period no forwarding-traffic flows are added to the switch from the controller, meaning that the communication between the hosts in the network is unfeasible. There are two ways of acquiring a basic L2 functionality. The first is a simple reactive forwarding provided by ONOS. When activated, it is installs forwarding flows on demand. The second way is the use of intents.

```
onos@root > flows -s
deviceId=of:0000000000000001, flowRuleCount=4
    ADDED, bytes=46148, packets=332, table=0, priority=40000, selector=[ETH_TYPE:bddp], treatment=[immediate=[OUTPUT:CONTROLLER], clearDeferred]
    ADDED, bytes=46148, packets=332, table=0, priority=40000, selector=[ETH_TYPE:lldp], treatment=[immediate=[OUTPUT:CONTROLLER], clearDeferred]
    ADDED, bytes=630, packets=15, table=0, priority=40000, selector=[ETH_TYPE:arp], treatment=[immediate=[OUTPUT:CONTROLLER], clearDeferred]
    ADDED, bytes=588, packets=6, table=0, priority=5, selector=[ETH_TYPE:ipv4], treatment=[immediate=[OUTPUT:CONTROLLER], clearDeferred]
deviceId=of:0000000000000002, flowRuleCount=4
    ADDED, bytes=91740, packets=660, table=0, priority=40000, selector=[ETH_TYPE:lldp], treatment=[immediate=[OUTPUT:CONTROLLER], clearDeferred]
    ADDED, bytes=882, packets=21, table=0, priority=40000, selector=[ETH_TYPE:arp], treatment=[immediate=[OUTPUT:CONTROLLER], clearDeferred]
    ADDED, bytes=91740, packets=660, table=0, priority=40000, selector=[ETH_TYPE:bddp], treatment=[immediate=[OUTPUT:CONTROLLER], clearDeferred]
    ADDED, bytes=980, packets=10, table=0, priority=5, selector=[ETH_TYPE:ipv4], treatment=[immediate=[OUTPUT:CONTROLLER], clearDeferred]
deviceId=of:0000000000000003, flowRuleCount=4
    ADDED, bytes=92157, packets=663, table=0, priority=40000, selector=[ETH_TYPE:bddp], treatment=[immediate=[OUTPUT:CONTROLLER], clearDeferred]
    ADDED, bytes=92157, packets=663, table=0, priority=40000, selector=[ETH_TYPE:lldp], treatment=[immediate=[OUTPUT:CONTROLLER], clearDeferred]
    ADDED, bytes=882, packets=21, table=0, priority=40000, selector=[ETH_TYPE:arp], treatment=[immediate=[OUTPUT:CONTROLLER], clearDeferred]
    ADDED, bytes=980, packets=10, table=0, priority=5, selector=[ETH_TYPE:ipv4], treatment=[immediate=[OUTPUT:CONTROLLER], clearDeferred]
deviceId=of:0000000000000004, flowRuleCount=4
    ADDED, bytes=630, packets=15, table=0, priority=40000, selector=[ETH_TYPE:arp], treatment=[immediate=[OUTPUT:CONTROLLER], clearDeferred]
    ADDED, bytes=45870, packets=330, table=0, priority=40000, selector=[ETH_TYPE:lldp], treatment=[immediate=[OUTPUT:CONTROLLER], clearDeferred]
    ADDED, bytes=45870, packets=330, table=0, priority=40000, selector=[ETH_TYPE:bddp], treatment=[immediate=[OUTPUT:CONTROLLER], clearDeferred]
    ADDED, bytes=588, packets=6, table=0, priority=5, selector=[ETH_TYPE:ipv4], treatment=[immediate=[OUTPUT:CONTROLLER], clearDeferred]
deviceId=of:001408f1ea4b48e0, flowRuleCount=4
    ADDED, bytes=0, packets=0, table=0, priority=40000, selector=[ETH_TYPE:lldp], treatment=[immediate=[OUTPUT:CONTROLLER]]
    ADDED, bytes=0, packets=3, table=0, priority=40000, selector=[ETH_TYPE:arp], treatment=[immediate=[OUTPUT:CONTROLLER]]
    ADDED, bytes=0, packets=0, table=0, priority=40000, selector=[ETH_TYPE:bddp], treatment=[immediate=[OUTPUT:CONTROLLER]]
    ADDED, bytes=0, packets=2, table=0, priority=5, selector=[ETH_TYPE:ipv4], treatment=[immediate=[OUTPUT:CONTROLLER]]
onos@root >
```

Figure 55: Installed flows

The Intent Framework is a subsystem that allows applications to specify their network control desires in form of policy rather than mechanism. The ONOS core accepts the intent specifications and translates them, via intent compilation, into installable intents, which are essentially actionable operations on the network environment. These actions are carried out by the *intent* installation process, which results in some changes to the environment, such as tunnel links being provisioned, flow rules being installed on a switch, or optical lambdas (wavelengths) being reserved. The intents can be installed using either the CLI or the GUI [133][134]. An example is shown in Figure 56 where a connection between the source and destination nodes can be instantiated. The associated flows are shown in Figure 57

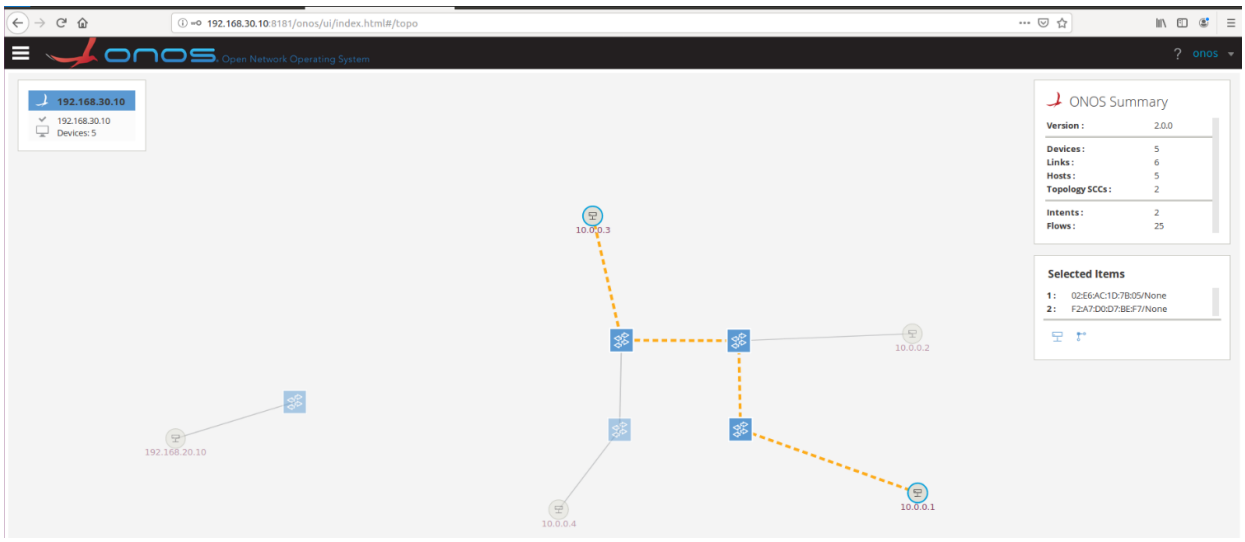

Figure 56: Creation of an intent through the ONOS GUI.

Figure 57: Installed flows from ONOS intent framework.

3.2.2.2 Implementing quality of service (QoS) using Opendaylight controller

Quality of service using Openflow meters

A meter is a switch element which measures and controls the ingress rate of packets which is the rate of packets prior to the output. Meters have been introduced in OpenFlow protocol in version 1.3 as an optional feature. Meters are created and managed by OpenFlow protocol in meter table on the switch and attached directly to the flows. A meter has a component called meter band which specifies the rate at which meter is applied. A meter can have one or more-meter bands but only a single band is applied for a flow at a time based on the measured packets rate. A flow which is mapped to a meter, directs packets to the meter which measures the rate of the packets and activates appropriate meter band if the measured rate of packets go beyond the rate defined in meter band [137]. Typical metrics that are used by Openflow to ensure QoS include:

- *Meter identifier*: a 32 bit unsigned integer uniquely identifying the meter.
- *Meter bands*: an unordered list of meter bands, where each meter band specifies the rate of the band and the way to process the packet.
- *Counters*: updated when packets are processed by a meter.

Each meter may have one or more meter bands. Each band specifies the rate at which the band applies and the way packets should be processed. Packet are processed by a single meter band based on the current measured meter rate, the meter applies the meter band with the highest configured rate that is lower than the current measured rate. If the current rate is lower than any specified meter band rate, no meter band is applied. Each meter band is identified by its rate and contains [125]:

- *Band type: defines how packet are processed*
- *Rate: used by the meter to select the meter band, defines the lowest rate at which the band can apply*
- *Counters: updated when packets are processed by a meter band*
- *Type specific arguments: some band types have optional arguments.*

A basic configuration is to limit the bandwidth of a flow. A typical example is shown in the following script limiting the flow rate for a specific connection below 50Mbps. The created flow is shown in Figure 58.

```
{
    "meter": [
        {
            "flags": "meter-kbps",
            "meter-id": "1",
            "barrier": "true",
            "meter-name": "testmeter",
            "meter-band-headers": {
                "meter-band-header": [
                    {
                        "band-id": "0",
                        "meter-band-types": {
                            "flags": "ofpmbt-drop"
                        },
                        "band-rate": "50000",
                        "band-burst-size": "0",
                        "drop-rate": "50000",
                        "drop-burst-size": "0"
                    }
                ]
            }
        }
    ]
}
```

```
Aruba-2930F-24G-PoEP-4SFPP(openflow)# show openflow ins 3 meters

 OpenFlow Instance Meters

 Meter ID              : 1
 Flow Count            : 1
 Input Packet Count    : 842706
 Input Byte Count      : 69425564
 Duration              : 181227

                           Precedence Packet/Byte
 Band Type Rate            Level      Count
 --------- --------------- ---------- ------------------------
 Drop      50000 kbps      N/A        11428896
```

Figure 58: Installed meter in Aruba switch

The iperf program can validate that indeed, we restricted the bandwidth of the specific flow below 50MB, as show in Figure 59.

```
^Cstack@Fourier-consysnetlab:~$ iperf -s
------------------------------------------------------------
Server listening on TCP port 5001
TCP window size: 85.3 KByte (default)
------------------------------------------------------------
[  4] local 192.168.50.10 port 5001 connected with 192.168.50.20 port 38484
[ ID] Interval       Transfer     Bandwidth
[  4]  0.0-10.0 sec  1.09 GBytes   938 Mbits/sec
```

a)

```
^C^Cstack@Fourier-consysnetlab:~$ iperf -s
------------------------------------------------------------
Server listening on TCP port 5001
TCP window size: 85.3 KByte (default)
------------------------------------------------------------
[  4] local 192.168.50.10 port 5001 connected with 192.168.50.20 port 38646
[ ID] Interval       Transfer     Bandwidth
[  4]  0.0-10.1 sec  53.2 MBytes  44.4 Mbits/sec
```

b)

Figure 59: Available bandwidth a) before and b) after implementing QoS

3.3 Control plane scalability/stability analysis

5G aims at incorporating many technologies, under the same infrastructure (FH/BH network). Efficient management and operation of such a heterogeneous infrastructure can be achieved applying novel network designs that are aligned with the SDN open reference architecture. The controller is in charge of populating the forwarding table of the switch. The communication between the two entities is carried out through a secure channel. This centralised structure makes the controller able to perform network management functions, while allowing easy modification of the network behaviour through the centralised control layer. However, in such infrastructures the end to end latency is augmented. Considering that latency is critical to many network applications, a subject of current research is the size of the SDN network (controller placement problem) in order to be able to cope with the timing requirements of network services and applications.

In IN2DREAMS, we propose a next generation network solution that includes: a) the concept of Flexible Functional Split (FFS) between a set of servers that can offer a range of processing capabilities and can be geographically distributed across the network infrastructure, b) the employment of the MEC architecture in the form of specific purpose low processing power servers embedded in the wireless access network (also known as cloudlets) and c) a FH/BH transport network with SDN control, connecting the MEC domains with medium to large-scale DCs hosting general purpose servers placed at the optical access and metro domains. In this environment, the controller placement problem is investigated, under the scope of the stability of the whole system. To address this issue, we propose a novel mathematical model based on Evolutionary Game Theory (EGT) that allows network operators to dynamically adjust their FH split options with the objective to minimise their total operational expenditures. The stability of the proposed scheme depends on network latency, thus a metric for sizing the SDN FH/BH network is proposed.

3.3.1 Evolutionary Game Theory: Basic Concepts

Evolutionary Game Theory (EGT) studies the interactions of non-cooperative players that play repeatedly strategic games [60]. Contrary to classic Game Theory that examines the behaviour of rational players,

EGT focuses on how the strategies can "survive" through evolution and how they help the players who choose them to "strengthen" and better meet their needs.

Evolutionary processes are described by three main components: the population, the game and the dynamical model that describe the processes. The most common dynamics is called the Replicator Equation (RE) and can be expressed as:

$$\dot{x}_i(t) = x_i(t)\left(F_i(\boldsymbol{x}(t)) - \bar{F}(\boldsymbol{x}(t))\right), \qquad i \in S \qquad \text{Eq. 5-1}$$

where S is the set of strategies that are available to the population, $\boldsymbol{x}(t) = [\, x_1(t)\ \ x_2(t) \dots\ \ x_i(t) \dots\,]^{T}$ is the population state at time t with $x_i(t)$ symbolising the proportion of the population that uses strategy i at time t, and $F_i(\boldsymbol{x}(t))$, $\bar{F}(\boldsymbol{x}(t))$ are the expected payoff of strategy i and the mean payoff respectively [60]. According to this equation the percentage growth rate $\dot{x}_i/x_i$ of the strategies that are currently used is equal to the excess of the current payoff versus the average population's payoff. This means that strategies employed at present will be spread or eliminated depending on whether their payoff is better or worse than the average.

In the above, the interaction between individuals is assumed to be instant and their results immediate. However, this is not the case in most realistic scenarios. In communication networks especially, the impact of an action may be belated, due to network latency. Thus, it is more realistic to consider a system where the strategies evolve considering the payoff values perceived in a past moment. The adjusted RE is given below [61] [62]:

$$\dot{x}(t) = x_i(t) \cdot \left(f_i(\boldsymbol{x}(t-\tau)) - \sum_{i \in S} x_j(t) \cdot f_j(\boldsymbol{x}(t-\tau)) \right) \qquad \text{Eq. 3-2}$$

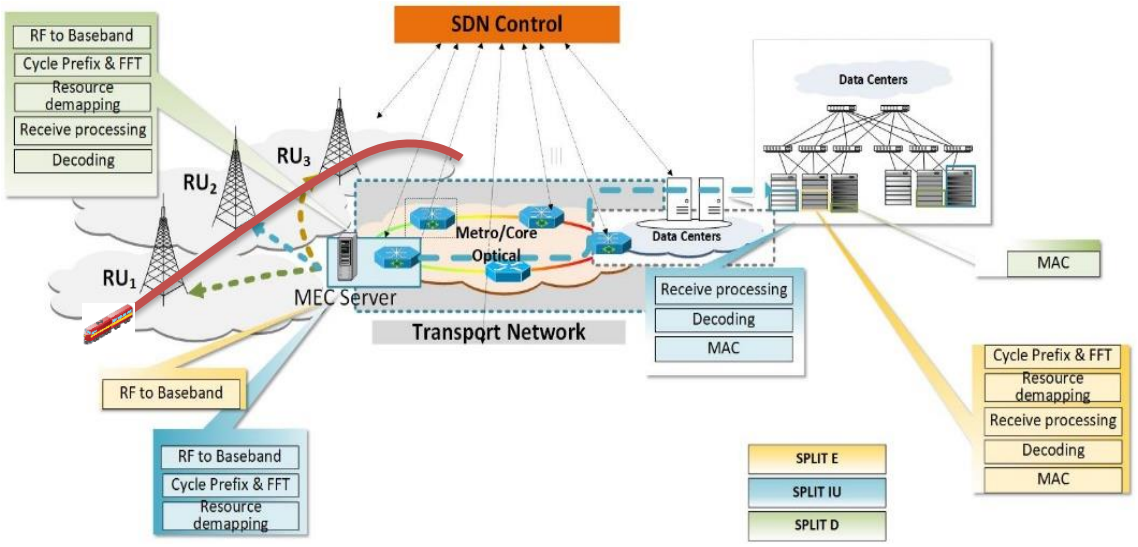

Figure 60: Network architecture. In the MEC, a decision about which functions should be processed locally is made for each RU. The remaining set of functions for each RU are transferred through a common network infrastructure with centralised control to a DC for further processing.

We consider the 5G network topology shown in **Figure 60**. In this scenario, the RUs are installed at the trackside, managed and operated by coexisting Mobile Network Operators (MNOs). The RUs share a set of computational resources that are located both at the edge of the access network (in a MEC server) and at the metro/core network (in the Cloud). The interconnection between the MEC server and the central cloud servers is carried out by an SDN- controlled optical FH/BH transport network.

The MNOs can decide where to perform the processing of the low layer functions of the LTE protocol stack. According to the eCPRI specification, three possible functional splits can be identified [63]. In split E (split 1 for simplicity) MEC is responsible for the RF processing of the received signals and the Cloud performs the entire baseband processing. In split IU (split 2), MEC handles the per cell processing (RF processing, cyclic prefix (CP) elimination, frequency domain transformation (FFT) and resource demapping), while the remaining functions are performed at the Cloud (Equalisation, IDFT, QAM, multi-antenna processing, Forward Error Correction (FEC), higher level operations (MAC, RLC, PDCP). Finally, in split D (split 3) the entire lower layer function chain is performed at the MEC server, and the higher lever functions in the Cloud. One can conclude that as the split is placed lower in the 5G protocol stack, the required transport capacity increases [64].

Each RU periodically selects one of the three possible functional splits with probability x_i, $i = 1,..,3$. The decisions are sent to the SDN controller, who is responsible for the application of the policies. We consider the scenario in which all the necessary resources are available. When the policies have been applied, the payoffs are calculated and the RUs are reviewing their split option strategy. Specifically, if a better (lower) payoff is observed, then the probability of an RU to select the specific split option increases (decreases). The new policies are sent to the controller and the same procedure is repeated. The time between each repetition is referred to as revision time. To address this scenario, EGT can provide a suitable optimisation framework that can be used to support energy-aware FH service provisioning over a common infrastructure.

Denote as $\boldsymbol{x}(t) = [\, x_1(t)\ \ x_2(t)\ \ x_3(t)]\ ^T$ the state vector of the RU, where $x_i(t)$ refers to the RU's probability of choosing split i. If the RU revises its strategy with a time rate $r_i(\boldsymbol{x})$, the change of the proportion of the probabilities is described by the following dynamical equation:

$$\dot{x}_i(t) = \sum_{j \in S} x_j(t) r_j(\boldsymbol{x}(t)) p_j^i(\boldsymbol{x}(t)) - \sum_{j \in S} x_i(t) r_i(\boldsymbol{x}(t)) p_i^j(\boldsymbol{x}(t)) \qquad \text{Eq. 3-3}$$

where S is the set of strategies that consists of the three possible splits and $p_i^j(\boldsymbol{x})$ is the rule of change in the probability of choosing split i when the RU changes from split i to split j and can be expressed as:

$$p_i^j(\boldsymbol{x}(t)) = \begin{cases} x_j(t)(u(j,t) - u(i,t)) & j \neq i \\ 1 - \sum_{j \neq i} x_j(t)(u(j,t) - u(i,t)) & otherwise \end{cases} \qquad \text{Eq. 3-4}$$

with $u(i,t)$ symbolising the payoff of split i at time t. Making the assumption that all time rates are constantly equal to one $(r_i(\boldsymbol{x}) \equiv 1 \frac{revion}{time\ unit})$, the following differential equation yields:

$$\dot{x}_i(t) = x_i(t) \left[u(i,t) - \sum_{j \in S} x_j(t) u(j,t) \right] \qquad \text{Eq. 3-5}$$

which satisfies the replicator dynamics model.

3.3.2 Payoff Function

The objective of the MNOs is to minimise their own service power consumption requirements and, hence, the service operational costs. Thus, the payoff function per operator is formed by summing up the power consumption of the network and compute elements required to support FH services. Table 11 summarises the network and processing demands of each functional split.

Table 11 Network and Processing Demands of Each Functional Split

Split	*Network Rate*	*Processing Functions*	
		Local	*Remote*
1 (E)	$R_1 = N_o \cdot f_s \cdot N_Q \cdot N_R$	RF	FFT, RE Demapping, Rx Processing, DEC, MAC
2 (Iu)	$R_2 = N_{sc} \cdot T_s^{-1} \cdot 2 \cdot N_Q \cdot N_R \cdot \eta$	RF, FFT, RE Demapping	Rx Processing, DEC, MAC
3 (D)	$R_3 = N_{sc} \cdot T_s^{-1} \cdot \eta \cdot S$	RF, FFT, RE Demapping, Rx Processing, DEC	MAC

For this problem setting, the payoff of an RU operated by an MNO that chooses split i against another RU operated by a different MNO who chooses split j is described by the payoff matrix $\boldsymbol{A}$, with elements $a_{ij} = -\left(P_{PROCESSING\,ij} + P_{NET\,ij}\right) + b, \quad i,j \in S$ where $P_{PROCESSING}$ and $P_{NET_{ij}}$ refer to the total compute and network energy consumption respectively, when split i competes with split j and b is a positive constant that guarantees the robustness of the system. Technical parameters like the oversampling factor (N_o),

the sampling frequency (f_s), the quantisation bits per I/Q (N_Q), the number of receiving antennas (N_R), the number of subcarriers used (N_{sc}), the percentage of used resource elements (η), and the spectral efficiency (S) affect the required capacity and the power consumption of each processing function [64], [65].

Due to the nature of the SDN transport network, the payoff values are provided to the MNOs through the SDN controller. It is evident, that this kind of procedure indicates that the strategies will evolve based on information related to a past moment. This will be reflected to the expected payoff of the strategies. Network delay is mainly composed of propagation, serialisation, switching/routing and queuing delay. Although propagation and switching/routing delays are constant, the rest are highly affected by the network traffic. Due to this, we expect that network delay is a random variable that is characterised by a probability density function. Specifically, if the payoff is received not instantly, but after a random delay τ, with probability distribution $P(t)$ the expected payoff of an RU using strategy i as well as the average payoff are determined by [66]:

$$u(i,t) = \int_0^\infty P(\tau)(\boldsymbol{A}\boldsymbol{x}(t-\tau))_i \, \bar{u} = \sum_{j \in S} x_j(t) u(j,t)$$

3.3.3 Stability Analysis

Since the above system of equations cannot be easily solved by analytical methods it is important to examine its qualitive behaviour without actually solving it. We concentrate on finding the stability of a solution exploiting the Lyapunov stability theorem. This method is based on the expansion of the right part of the dynamical system as a Taylor series about an equilibrium point $\boldsymbol{x}^0$. If the initial condition $\boldsymbol{x}(0) = \boldsymbol{x}_0$ is close enough to $\boldsymbol{x}^0$, then $\boldsymbol{x}$ will be a small perturbation for some time interval extending from zero. Thus, it is acceptable to neglect the higher-order terms, and approximate the nonlinear system by the linear system:

$$\dot{\boldsymbol{x}}(t) = \boldsymbol{J_o}\boldsymbol{x}(t) + \boldsymbol{J_1}\boldsymbol{x}(t-\tau) \qquad \text{Eq. 3-6}$$

where $\boldsymbol{J}_o \in \mathbb{R}^{2x2}$ and $\boldsymbol{J}_1 \in \mathbb{R}^{2x2}$ are respectively, the Jacobian matrix, and the delayed Jacobian matrix evaluated at equilibrium at $\boldsymbol{x^0}$.

The stability of the system requires that all roots of its characteristic equation have a negative real part. The system admits to seven equilibrium points: three corner points, one interior and three corner side points. The linearisation about each of the three corner critical points produces an ordinary differential equation that is independent of the delayed variables as in the non-delayed three strategies game.

At the interior critical point all the payoffs are equal. The differential system that emerges depends only on the delayed variables, thus one should anticipate that the distributed delay will affect its stability. The characteristic equation is formed as:

$$u^2 + E \cdot u + F = 0, \qquad u = \frac{\lambda}{Q} \qquad \text{Eq. 3-7}$$

The last three critical points are equilibriums where only two of the three strategies survive (corner side points). Their characteristic equation can be written as $(\lambda - l_1) \cdot (\lambda - l_2 Q) = 0$ where the parameters λ_1 and λ_2 depend on the corner side equilibrium point. As we can conclude from the above, our analysis can

be restricted for finding the solution of the equation $\lambda - C\int_0^\infty P(\tau)e^{-\lambda\tau} = 0$. This equation is the characteristic equation of the linear differential equation $\dot{x}(t) = C\int_0^\infty x(t-\tau)f(t)d\tau$.

From [67] we derive the following necessary and sufficient condition for the asymptotic stability of the equilibriums:

Proposition: If $C < 0$ and the expected value (E) of the delay's probability density satisfies the condition $E(\tau) < \frac{\pi}{\gamma\cdot|C|}$, where $\gamma = 2$ when the pdf is symmetrical, or else $\gamma = \sup\{\gamma|\cos w = 1 - \frac{\gamma w}{\pi}, w > 0\}$, then the equilibrium point is stable (the proof can be found in [67]). Last but not least, as far as the variance of the distribution is concerned, the stability of the system increases as the variance grows [67].

3.3.4 SDN Controller Placement

It is well known that the SDN controller is responsible for collecting and providing to the MNOs of the RUs the required information from all controlled devices. The maximum delay corresponds to the delay of the most distant node to the controller path plus the delay of the controller-MEC path. Thus, assuming that each controlled device may host a MEC, the stability of the system is achieved only when the round-trip time (RRT) of the controller's path to the most remote device is less than $\frac{\pi}{\gamma\cdot|C|}$. Based on this limit, we propose a heuristic algorithm that tries to identify the minimum number and associated position of SDN controllers with the aim to guarantee the stability of the 5G infrastructure. This is performed with low computational complexity.

At first, the heuristic algorithm finds the maximum network radius, which is the number of hops of the longest end-to-end path. Then, for each node it calculates the maximum RRT to all the other nodes inside the network radius. If the result of all nodes is a number higher than $\frac{\pi}{\gamma\cdot|C|}$, the network radius is reduced by one, and the same procedure is repeated, until a case is found where the RRT from a node to all other nodes within the network radius. The nodes that meet this requirement, are marked as possible controller candidates. From this set, the algorithm chooses as the first controller the one that is connected to the largest number of devices within the network radius. These devices and the first controller are removed from the network, and the whole procedure is repeated for the downscaled network. The algorithm ends when the downscaled network has no network nodes.

3.3.5 Results and Discussion

In order to see the effectiveness of our model we considered the network of Figure 61 with the system parameters shown in Table 12. The cost ratio (remote/central processing) was assumed to be equal to two. Furthermore, the relationship of the transport network's energy consumption with the required capacity for the support of the FH services was assumed to be nonlinear, since the non-linear model is best to describe the technology advancements in terms of energy efficiency of network devices

Table 12 Parameters of the system configuration

Symbol	Quantity	Value
B	bandwidth	20 MHz
Ant	number of the rx antennas	2
M	modulation	6 bits/symbol
R	coding rate	1/2
dt	time-domain duty-cycling	100%
f_s	sampling frequency	30.72 MHz
N_o	oversampling factor	2
N_{sc}	number of used subcarriers	1200
T_s	symbol duration	66.6 μs
N_Q	quantisation bits per I/Q	10
S	spectral efficiency	3 bit/cu
η	assumed RB utilisation	70%

The stability analysis indicates that the equilibrium point in such a scenario is $x_1^* = 0.2957$, $x_2^* = 0.7043$, $x_3^* = 0$. This means that in the non-delayed system the optimal split choice is split 2. However, as it was stated previously the SDN transport network introduces additional delay to the system. This delay can be divided to two main components, namely the processing delay of the SDN controller and the transport delay.

The SDN controller chosen for the implementation is the ODL controller, which is a scalable controller infrastructure that supports SDN implementations in modern heterogeneous networks of different vendors [70]. For measuring the processing delay of the ODL controller, we developed an application that communicates externally with the controller. For evaluations, a linear network topology with Out of Band control plane was emulated in Mininet, a tool that can emulate and perform the functions of network devices in a single physical host or virtual machine (VM) [71]. Both Mininet and ODL controller were implemented on the same machine (Intel® Core™ i5-7400U CPU @ 3.00 GHz (4 cores)) to overcome the Ethernet interface speed limitations. 7.7 GB of memory was available. The system was running Ubuntu 16.04 LTS-64 bit. The application implements at first step a mechanism for collecting data on the network topology and at second step a mechanism for sending echo messages to all switches simultaneously, and measuring the maximum time elapsed for receiving a reply. The time response of ODL is measured by averaging the results of a hundred number of tests, in order to achieve higher accuracy. The results showed an exponential relation between the controller's processing delay and the network devices.

As far as the transport delay is concerned, we used monthly delay measurements extracted from GRNET [19], in order to find the dependence of the end to end transport delay on the end to end hops. Our analysis concluded that this relationship can be well approximated with a linear function. Furthermore, the best pdf that fitted the end to end delay was the generalised t-student distribution [73].

Taking these into consideration, we expect that the total induced SDN network's delay will be a random variable that is characterised by the generalised t-student distribution, with expected value that depends on the size of the transport network and the hops between two network nodes. Thus, the upper delay limit for our example is given by $E_{max} = 1.6449$ time units.

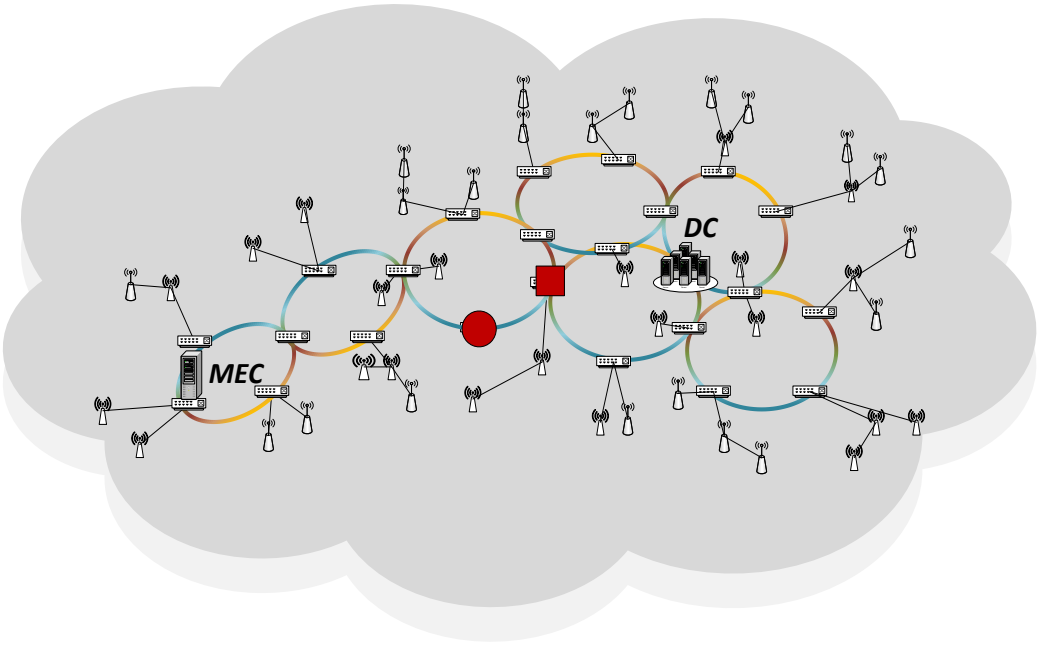

Figure 61 Assumed FH/BH transport network. The red circle represents the position of the SDN controller, after the implementation of the heuristic algorithm described in section 3.3. The red square represents the optimal position estimated according to the average propagation latency -case.

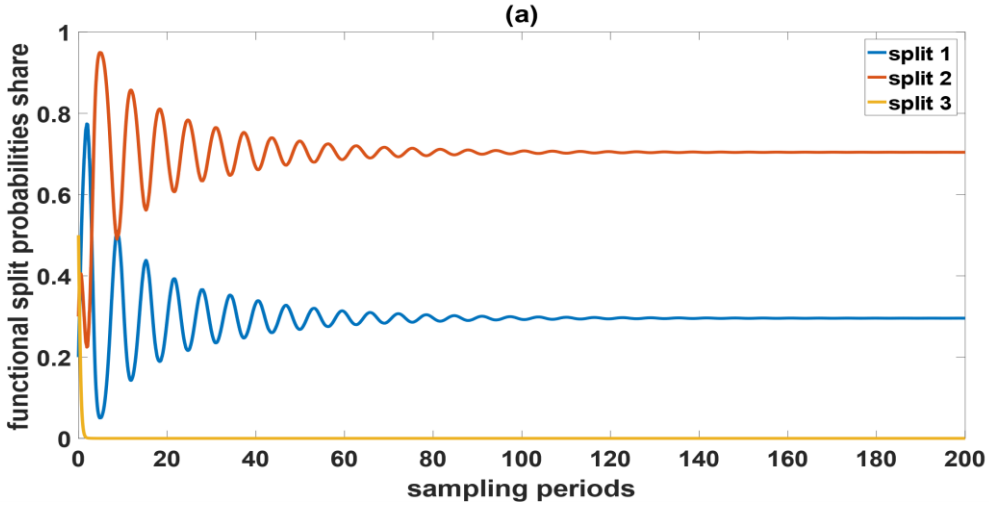

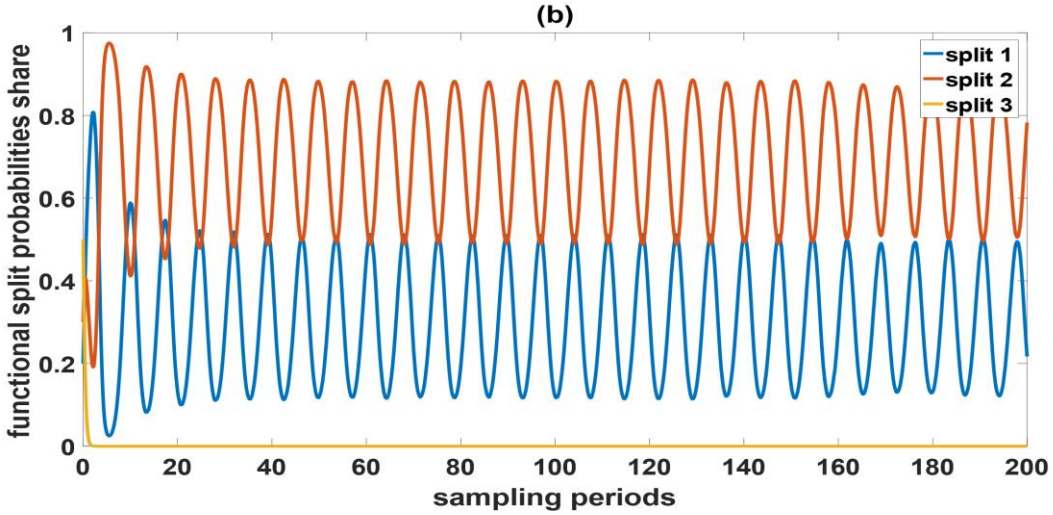

Figure 62 Evolution of the probabilities of the three split options, with the parameters described in Table II, when: (a) the controller is placed in the proposed location (red circle in Figure 2) by the heuristic, b) the controller is placed in the proposed location (red square in Figure 2) of the average propagation latency-case described in [58]

The assumed FH/BH transport network's topology for our example is depicted in Figure 61. The figure also shows the possible controller placements after implementing the heuristic algorithm described in the previous section. In order to test the validity of the heuristic, we investigate the evolution of strategies in two cases: 1) when the controller is placed in one of the proposed locations by the heuristic, 2) when the controller is placed in the location identified by the average propagation latency optimisation technique described in [58]. **Figure 62** illustrates the evolution of split option selection probability under the proposed EGT based approach and the average latency minimisation scheme described above. As can be seen in the former case (**Figure 62** a) after few sampling periods the scheme converges to a mixed solution where all antennas operate under a single split option mode that will be either split 1 or split 2. However, in the second case, the placement of the SDN controller at a node that does not satisfy the stability threshold leading to an unstable operational mode for the 5G network. The reason behind this is that the increased control plane delay in this case introduces inaccurate information of the network status at the controller. Therefore, decision making is performed with outdated information that leads to an oscillation around the optimal operating point preventing it from converging to a stable solution.

4 End-to-end Demonstration

4.1 Testbed introduction

The overall IN2DREAMS solution has been tested in a realistic environment at UNIVBRIS testbed facilities. This test network enables network slicing as a service, as required by various stakeholders as the Network Operation use case. Using 5G network concepts we deliver several services based on different network slices operating concurrently. In one slice, we deliver services for the Enhanced Mobile Broadband use case; while in another network slice, we deliver high and/or low throughputs, demanding Ultra Low Latency Reliable Services as in the Critical Communications use case. Also, several virtual networks can be grouped for different business demands and serve many devices forming the Massive Internet of Things use case.

The University of Bristol's Smart Internet Lab 5G Testbed comprises multiple levels of research ready SDN switches connecting diverse layers of access technologies, to high performance cloud compute resources via an innovate exchange and orchestration mechanism. The focus for this test network is to enable experimentation in network service virtualisation and innovative network function testing with access agnostic connectivity to end users.

Permanently installed in Millennium Square and the Smart Internet Lab are five heterogeneous, 5G ready wireless access technologies connected via dedicated, high capacity optical fibres, Edgecore and Corsa SDN switches and mmWave radio. A dedicated out of band management network provides flexibility of configuration and control of all active devices in the network. Control of network architecture is made available to NetOS, an intelligent SDN controller.

The cloud infrastructure at the Smart Internet Lab is built on OpenStack with a virtualised Evolved Packet Core (EPC) from Nokia. This allows virtual network functions to be deployed as a mobile edge computing service close to the edge of the network providing performance enhancements to the user.

Connectivity to additional 5G testbeds is provided through the 5G UK Exchange, a novel architecture for orchestration of virtual network functions and SDN configuration. This exchange resides in a neutral datacentre with 10Gbit connectivity through JANET to connected partners. The purpose of the 5G UK Exchange allows researchers to dynamically provision both virtual and physical network functions in each testbed from a catalogue of available services. This will allow end-to-end 5G research to take place across the globe.

4.1.1 University of Bristol, Smart Internet Lab's 5G Test Network Capability

The University of Bristol testbed showcases and facilitates research on the following technology capabilities.

- Multi-vendor SDN enabled packet switched network
  - Corsa switch (Corsa DP2100)
  - Edgecore switch (Edgecore AS4610 series)
- SDN enabled optical (Fibre) switched network
  - Polatis Series 6000 Optical Circuit Switch
- Multi-vendor Wi-Fi
  - SDN enabled Ruckus Wi-Fi (T710 and R720)

- Nokia Wi-Fi (AC400)

- Nokia 4G and 5G NR
  - 4G EPC & LTE-A (Dual FDD licensed bands for 1800MHz and 2600MHz; with 15MHz T&D licence)
  - 5G Core & 5G NR Massive MiMO (TDD band 42 at 3.5GHz; with 20MHz T&D licence)
  - 28Ghz fixed-wireless access demonstrator for two-weeks exhibition
- Self-organising multipoint-to-multipoint wireless mesh network
  - CCS MetNet. A 26GHz with 112MHz T&D licence providing 1.2Gbps throughput
- Massive MIMO NR radio demonstrator
  - National Instruments (NI) Massive MIMO demonstrator 128 antenna base station
  - 12 client UE devices (TDD band 42 at 3.5GHz with 20MHz bandwidth)
- LiFi Access point
  - pureLiFi LiFi access points supporting 43Mbps
- Cloud and NFV hosting
  - Nokia Multi-access Edge Computing and Nokia Cloudband for network slicing and virtualisation
  - Opensource MANO (OSM) datacentre release THREE
  - Openstack Pike VIM datacenter for MEC VNF hosting, built upon
  - 11x Dell PowerEdge T630 compute servers with GPU support; 700+ vCPU cores, 1TB+ RAM and 100TB of HDD storage.
- Inter-island Interconnectivity
  - 10Gbit/s Ethernet VPLS NetPath+ from JISC to each exchange Island
  - Dedicated secure hosting of the 5G UK Exchange in Virtus Datacentre
  - Corsa DP2200 SDN Switch provided inter-island connectivity via OpenFlow 1.3
- Advanced fibre optics FPGA convergence of all network technologies enabling considerable flexibility, scalability and programmability of the front/back-haul, to provide experimentation with
  - Elastic Bandwidth-Variable Transponders
  - Programmable Optical White-box
  - Bandwidth-Variable Wavelength Selective Switches (BV-WSS)

4.1.2 Testbed architecture

The University of Bristol Smart Internet Lab 5G testbed is a multi-site solution connected through a 10km fibre ring with several active switching nodes. The core network is located at the High-Performance Network (HPN) research group laboratory at the University of Bristol with access technologies located in Millennium Square for outdoor coverage and We The Curious science museum for indoor coverage.

4.1.2.1 Wireless Access Technologies

Figure 63 presents the high-level architecture of the University of Bristol testbed. The design of this architecture may be described in four distinct technical areas:

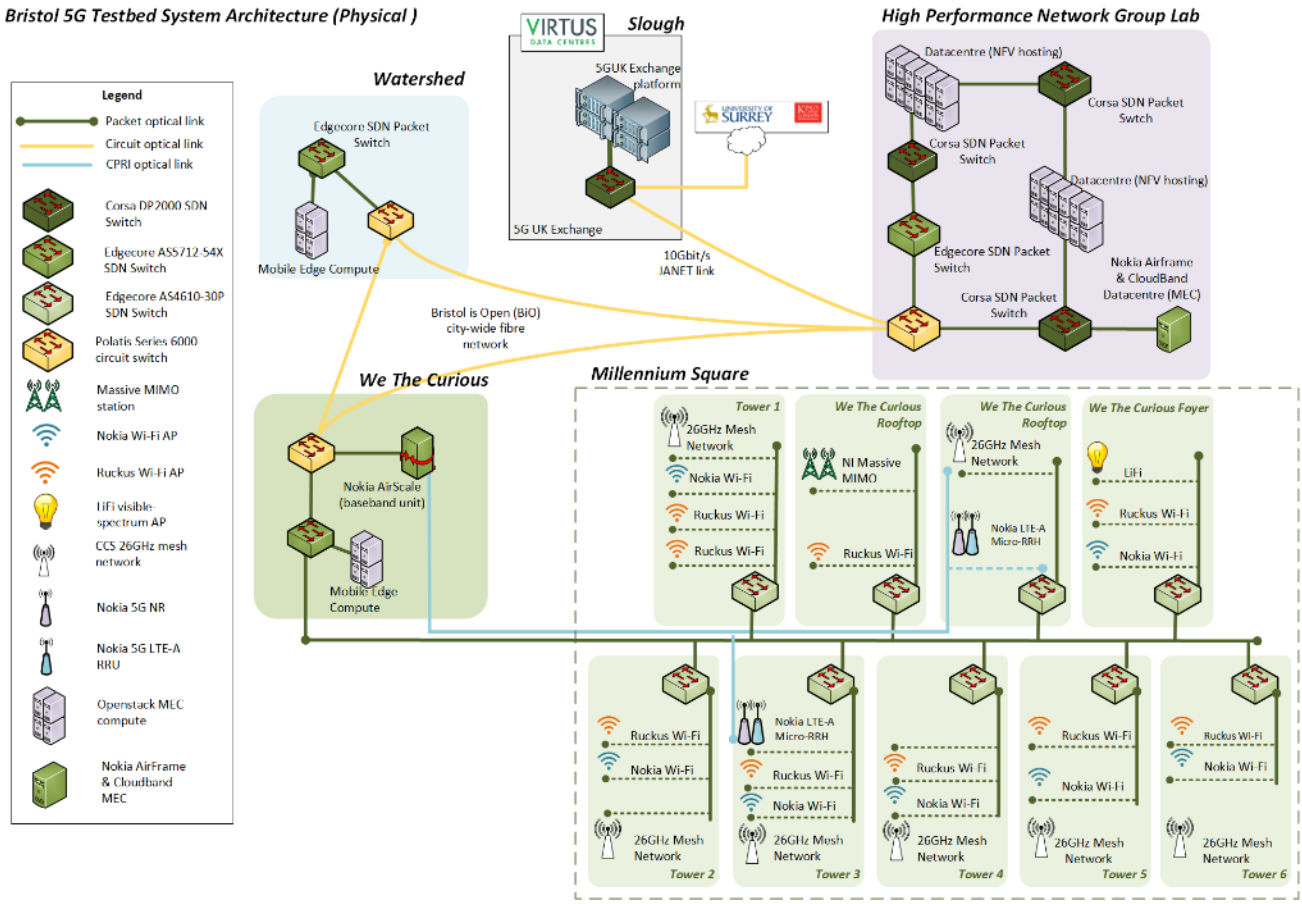

Figure 63: University of Bristol top level system architecture

Figure 64 shows a geographical representation of the multiple access technologies deployed within Millennium Square and We The Curious, a science museum in the centre of Bristol. Connectivity terminates via fibre optic at distinct points in the square with onward links through the use of fixed wireless access mmWave radios. To allow for future expansion, termination locations have been over engineered with enough installed fibre and power capacity to allow the next generation of 5G connectivity. Space and power for mobile edge computing (MEC) has been provisioned at key locations around Millennium Square to allow the deployment of virtual network functions (VNF) and low latency real-time application processing close to the end user.

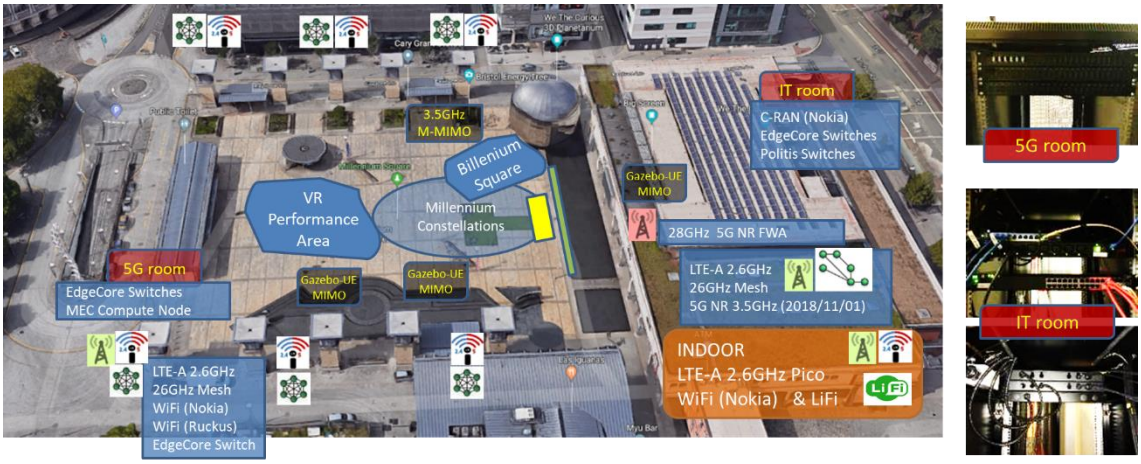

Figure 64: Location of the Access Points at Millennium Square and We the Curious science museum.

Figure 65: Nokia AirScale RRH & Antenna

Figure 66: Wi-Fi APs in Millennium Square

Figure 67: CSS Metnet

This testbed has combined wireless access technologies from multiple vendors across four 5G pioneer radio bands into a dynamic and flexible architecture allowing for future reconfiguration and experimentation with innovative radio architectures and waveforms. Connectivity is provided through the following solutions:

1. To provide a grounding for Nokia's upcoming 5G NR product, Nokia have delivered and demonstrated their most advanced 4G LTE-A product, which was used in all the public demonstrators during the Layered Realities weekend. This LTE-A solution delivers a 15MHz 4x4 MIMO radio access network to our experimenters and has been tested at reliably delivering 100Mbit/s download (30Mbit/s upload) from our NFV datacentre through the Millennium Square (based on given licenced spectrum and user profile configured in the EPC).
   Ongoing developments include a 5G NR Massive MIMO (TDD band 42 at 3.5GHz), which will deliver even greater network throughput rates and bandwidth sharing functionality. Figure 65 shows the split baseband radio architecture provided by Nokia to support future migration to 5G NR through software upgrades to the System Module and replacement of the remote radio head (RRH). Two RRHs are installed in Millennium Square allowing experimentation and testing of 4G technologies with a robust roadmap to 5G.
2. To facilitate truly ubiquitous wireless connectivity for new and legacy devices, Wi-Fi networks can be provisioned using eight multi-vendor 2.4GHz and 5GHz access point (AP) deployments. The APs supplied by Nokia (shown top in Figure 66) integrate with the Nokia FlexiZone controller allowing for seamless handover between LTE and Wi-Fi, a key concept in 5G RAN design.
   The APs provided by Ruckus (shown middle in Figure 66) are 802.11ac Wave 2 devices utilising 4x4 MIMO with BeamFlex+ technology for adaptive beam steering and over 1Gbps data rate per user. All Ruckus APs are controlled via an integrated SmartZone access point controller, hosted in the cloud infrastructure detailed below. This AP controller provides a North Bound interface allowing direct access by the NetOS SDN controller. This architecture facilitates network-slicing through optical, electrical and radio technologies via on-demand SSID creation.
   Wi-Fi featured heavily throughout the Layered Realities weekend as a demonstration of network segmentation and as the primary radio access network for two of the public demonstrations.

3. The Layered Realities 5G showcase weekend demonstrated the proof of concept prototype for 5G NR Fixed Wireless Access solution providing high capacity link between the balcony and the marquee in the Millennium square. (see Figure 68). The solution encompassed an EPC emulator, the Nokia AirScale baseband on the AirFrame blade connected over CPRI interface to the antenna, which is a 16×16, 256 element unit. The Intel 5G MTP test UE was in the marquee. The system deployed 2 component carrier aggregation based on the available license, for a total of 200MHz channel bandwidth. This demonstrated throughput of 680Mbps observed within the marquee.

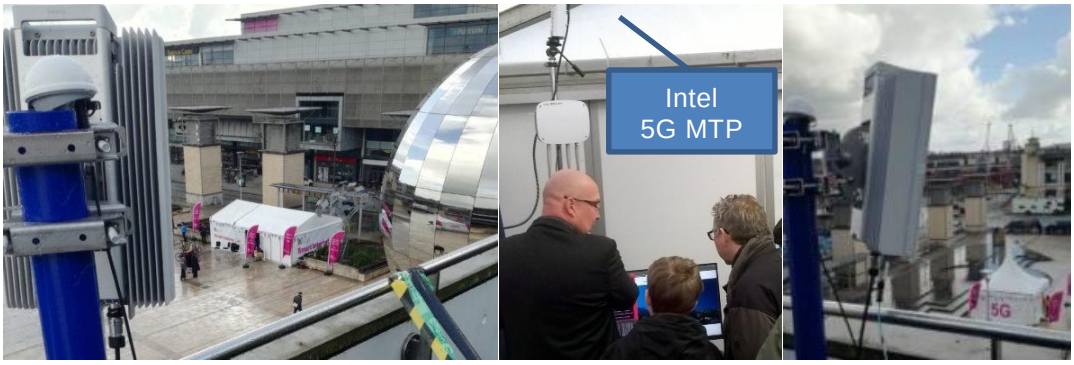

Figure 68 5GNR 28GHz Proof of Concept

4. mmWave communications are an important part of the 5G standardisation process. To showcase this technology in the University of Bristol, Smart Internet Lab 5G testbed, commercial devices provided by CCS were deployed in the network. The CCS Metnet nodes operate at 26GHz and form a self-organising mesh network for fixed wireless access with gigabit connectivity.

   Seven Metnet nodes are deployed in the testbed, connected to the Edgecore SDN switches. This architecture allows dynamic configuration of connectivity, either providing Wi-Fi backhaul over the mmWave mesh network or through the installed fibre network to the NFV cloud datacentre. With no radio planning, the CCS network is able to autonomously organise itself into a high-performance distribution and access network, demonstrating its ability to provide low-configuration last-mile access in a congested environment.

   The Metnet nodes are managed and configured via an element management system (EMS) allowing allocation of bandwidth to specific high demand nodes or viewing of the current mesh topology. The CCS EMS resides in the cloud infrastructure at the University of Bristol and is accessible from the testbed's management network.

5. The LTE-A network provided the 4G air interface using 15MHz bandwidth from BT in 2.6GHz spectrum and provided device connectivity for various demonstrations during the public demonstration. For validation we tested this network for throughput using a video on demand 5G network slice service towards a mix of 4G terminals receiving high definition video clips from the network simultaneously. This is shown in Figure 69 where one laptop with a 4G dongle and 5 x Samsung S8 handsets received HD video on demand simultaneously. Figure 69 shows different tests and capture of the information from the BTS or EPC management system.

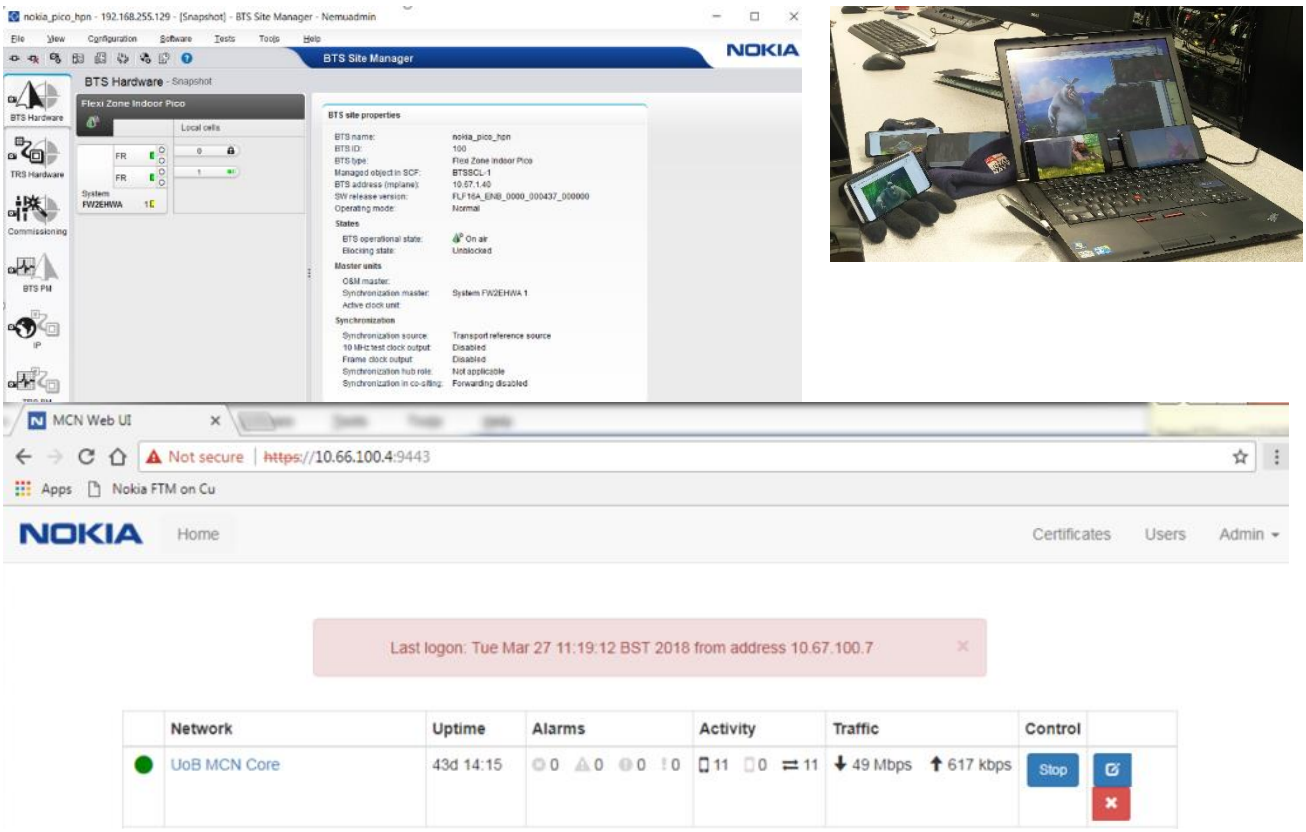

Figure 69: LTE-A service test validation

6. In collaboration with National Instruments (NI) and University of Bristol's Communication Systems and Networks (CSN) research group, the future 5G air interface technology Massive MIMO has been integrated with the 5G testbed. This system comprises a 128 antenna base station and 12 client devices. Operating in the pioneer band of 3.51GHz TDD, simultaneous transmission to all clients in 20MHz bandwidth yields over 80bits/second/hertz spectral efficiency (see Figure 70).

Figure 70: Massive MIMO test network at the Smart Internet Lab

Figure 71: LiFi client dongle

7. To showcase the 5G principle of access-agnosticism with novel access modes, the pureLiFi AP has been integrated with the core and distribution network of the testbed. Inside the public foyer of the We The Curious museum, an exhibit has been revealed to the public demonstrating the behaviour of a network stream encoded in visible light, and the effects of blocking it with curtains. The architecture of a LiFi network is similar to Wi-Fi whereby access points communicate with clients within visible range. For LiFi, an AP resembles a ceiling light (and its

secondary purpose is lighting) whilst a client is embedded within a USB dongle, creating a network bridge for any USB host (Figure 71). Multiple LiFi APs are controlled via an EMS residing in the University of Bristol cloud infrastructure. This entity controls all APs within the network including those based in We The Curious and the University of Bristol.

4.1.2.2 Network Connectivity

The University of Bristol's testbed has been futureproofed by delivering a wholly-uncontended, privately managed fibre network in the Millennium Square public space. The testbed's optical-connectivity asset is comprised of a hub-and-spoke network of 96F single-mode fibre cables installed at each radio test tower, terminated at a central distribution node inside the We The Curious museum.

Figure 72: Termination of single optical spoke in distribution node

Being wholly owned and managed by the Smart Internet Lab, this optical connectivity asset can expand to support dozens of optical applications per radio test tower, each delivering up to 40Gbit/s uncontested throughput rates with current transceivers. This futureproofing means the testbed will be ready for whatever bandwidth and latency requirements may need to be tested and experimented upon for years to come.

To connect the multiple urban testbed locations around Bristol, Bristol Is Open has provided access to their city-wide single-mode optical fibre network. This allows the island to quickly scale-out potential deployments to include additional locations, such as the SS Great Britain and M-Shed tourist hubs. The entire datapath network within the island is switched via a distribution network of Edgecore 4610P and 5610-52X SDN switches to provide full network slicing and segmentation via a centralised NetOS SDN controller.

4.1.2.3 Cloud and NFV Hosting

A primary consideration when selecting a cloud environment for NFV hosting and orchestration was to deliver a heterogeneous datacentre of multi-vendor assets. To this end the University of Bristol has implemented both an Opensource MANO (OSM) datacentre, a Nokia MEC platform and Nokia Cloudband solution.

The OSM datacentre employs an Openstack Pike Virtualised Infrastructure Manager (VIM) for orchestration, hosting and storage of VNFs as either KVM virtual machines, or LXC containers. To integrate a network service's VNF, Openstack Neutron provider networks, Open Daylight and NetOS SDN

controllers are used. Zeetta Networks' NetOS has allowed the testbed to extend VNFs to terminations such as Physical Network Function endpoints (e.g. Wi-Fi SSIDs). This NFV cloud solution was used in the March Layered Realities public demonstration to host network functions enjoyed by the public. This NFV cloud is built upon industry standard and popular technologies such as KVM virtualisation. The Openstack cloud environment adopted by our Opensource MANO solution made use of SR-IOV passthrough techniques to give direct access to time-slices of valuable hardware (e.g. network interface cards). The VNFs were configured during instantiation using Cloud-Init scripts.

Figure 73: Bristol 5GUK Dream Team at the OSM datacentre launch

Nokia's LTE-A solution and planned 5G NR extensions, include a MEC platform that allows the deployment and integration of virtualised cloud applications directly within the Evolved Packet Core of the network. This allows the direct connection of novel network applications at the S1 interface of the LTE-A network, eliminating almost all network-path latency from the user's application experience. The Nokia MEC is based on established industry standard virtualisation technologies already familiar to researchers and enterprises. We expect the uptake of this MEC to be as quick as the familiarisation of our OSM cloud. Lastly, Nokia's competitor to the OSM NFV setup Cloudband is finalising its deployment inside our testbed network. Cloudband is an ETSI MANO compatible NFV solution based on Openstack-orchestrated KVM virtualisation, and Nokia Nuage SDN networking of VNFs. The finalised deployment of this platform will open to research some of Nokia's most advanced network virtualisation technologies such as distributed.

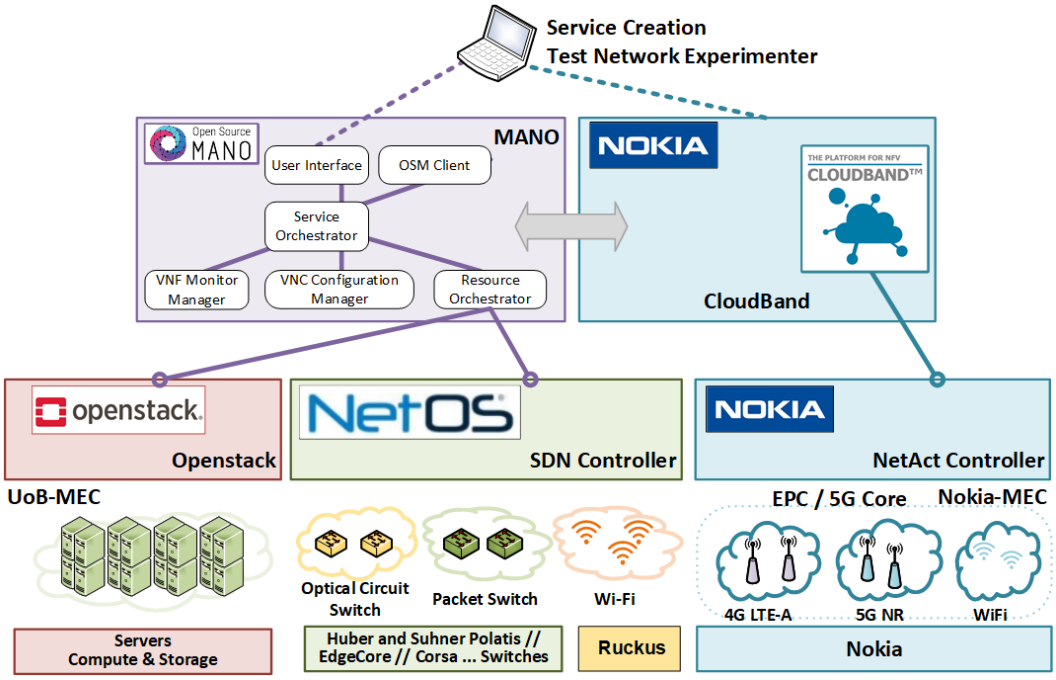

Figure 74: Bristol's Island Control and Management Network

5 Conclusions

The present deliverable proposes a communication platform based on wireless (LTE, Wi-Fi and LiFi, mmWave, FSO) and wireline technologies (optical electrical) for the provisioning of services in railway environments. The overall solution is managed through an architectural framework inspired by the ETSI NFV/SDN reference model principles. This framework enables control and management of this highly heterogeneous environment and facilitates end-to-end service orchestration with guaranteed Quality of Service.

The performance of the individual technologies that has been developed or extended throughout the project including the FSO links, the optical network and the associated interfaces are investigated using theoretical models, simulations and field trial validations. The overall solution has been integrated in the 5G UNIVBRIS testbed.

6 References

[1] Y. Hasegawa, "A Transmission Control Protocol for Free-Space Optical Communications," *GLOBECOM 2017 - 2017 IEEE Global Communications Conference*, Singapore, 2017, pp. 1-7. doi: 10.1109/GLOCOM.2017.8255094

[2] http://lightpointe.com

[3] https://mrvfso.com

[4] Varotsos, G.K.; Nistazakis, H.E.; Stassinakis, A.N.; Volos, C.K.; Christofilakis, V.; Tombras, G.S. Mixed Topology of DF Relayed Terrestrial Optical Wireless Links with Generalized Pointing Errors over Turbulence Channels. *Technologies* 2018, *6*, 121. https://doi.org/10.3390/technologies6040121

[5] G. K. Varotsos, H. E. Nistazakis, A. N. Stassinakis, G. S. Tombras, V. Christofilakis and C. K. Volos, "Outage performance of mixed, parallel and serial DF relayed FSO links over weak turbulence channels with nonzero boresight pointing errors," *2018 7th International Conference on Modern Circuits and Systems Technologies (MOCAST)*, Thessaloniki, 2018, pp. 1-4. doi: 10.1109/MOCAST.2018.8376648

[6] Androutsos, N.A.; Nistazakis, H.E.; Stassinakis, A.N.; Sandalidis, H.G.; Tombras, G.S. Performance of SIMO FSO Links over Mixture Composite Irradiance Channels. *Appl. Sci.* 2019, *9*, 2072. https://doi.org/10.3390/app9102072

[7] Androutsos, N.A.; Nistazakis, H.E.; Khalid, H.; Muhammad, S.S.; Tombras, G.S. Serial DF Relayed FSO Links over Mixture Gamma Turbulence Channels and Nonzero Boresight Spatial Jitter. *Computation* 2019, *7*, 34. https://doi.org/10.3390/computation7030034

[8] M. P. Ninos, H. E. Nistazakis, A. N. Stassinakis, G. S. Tombras, V. Christofilakis and A. D. Tsigopoulos, "CDMA radio on FSO links over gamma turbulence channels with nonzero boresight pointing errors," *2018 7th International Conference on Modern Circuits and Systems Technologies (MOCAST)*, Thessaloniki, 2018, pp. 1-4.doi: 10.1109/MOCAST.2018.8376650

[9] M. P. Ninos, H. E. Nistazakis, H. G. Sandalidis and G. S. Tombras, "CDMA RoFSO Links With Nonzero Boresight Pointing Errors Over M Turbulence Channels," in IEEE Photonics Journal, vol. 10, no. 5, pp. 1-12, Oct. 2018, Art no. 7906312. doi: 10.1109/JPHOT.2018.2856369

[10] D. Manousou, A. Stassinakis, E. Syskakis, H. Nistazakis, G. Tombras, C. Volos and A. Tsigopoulos, (2018). Estimation of the influence of Vanadium dioxide optical filters at the performance of visible light communication systems. 1-4. 10.1109/MOCAST.2018.8376653.

[11] L. Wangwei, Z. Gaoling, S. Bin, L. Jin, Z. Xinwen, H. Gaorong, "Preparation and thermochromic properties of sol-gel-derived Zr-doped VO2 films. Surface and Coatings Technology", Vol. 320, 10.1016/j.surfcoat.2016.12.070, 2016.

[12] J. Du, Y. Gao, H. Luo, Z. Zhang, L. Kang, Z. Chen, "Formation and metal-to-insulator transition properties of VO 2–ZrV 2O 7 composite films by polymer-assisted deposition", Solar Energy Materials and Solar Cells - SOLAR ENERG MATER SOLAR CELLS, Vol. 95, pp. 1604-1609, DOI: 10.1016/j.solmat.2011.01.009, 2011.

[13] Manousou, D.K.; Stassinakis, A.N.; Syskakis, E.; Nistazakis, H.E.; Gardelis, S.; Tombras, G.S. Experimental Implementation and Theoretical Investigation of a Vanadium Dioxide Optical Filter for Bit Error Rate Enhancement of Enhanced Space Shift Keying Visible Light Communication Systems. *Computation* 2019, *7*, 30. https://doi.org/10.3390/computation7020030

[14] H. Kotake, S. Haruyama, M. Nakagawa and K. Seki, "BER Characteristic of Ground-to-Train Communication System Using Free-Space Optics Technology," *2007 9th International Conference on Transparent Optical Networks*, Rome, 2007, pp. 165-169. doi: 10.1109/ICTON.2007.4296271

[15] Paudel, Rupak, Le Minh, Hoa, Ghassemlooy, Zabih, Iaz, M. and Rajbhandari, Sujan (2010) *High speed train communications systems using free space optics.* In: IET Railway Young Professionals Best Paper Competition, 5 October 2010, The Medical Society, London, UK.

[16] R. Paudel, X. Tang and Z. Ghassemlooy, "Laboratory demonstration of FSO ground-to-train communications with multiple base stations," *2016 10th International Symposium on Communication Systems, Networks and Digital Signal Processing (CSNDSP)*, Prague, 2016, pp. 1-6.

[17] M. A. Esmail, A. Ragheb, H. Fathallah and M. Alouini, "Experimental demonstration of outdoor 2.2 Tbps super-channel FSO transmission system," *2016 IEEE International Conference on Communications Workshops (ICC)*, Kuala Lumpur, 2016, pp. 169-174. doi: 10.1109/ICCW.2016.7503783

[18] N. Cvijetic, D. Qian, J. Yu, Y. Huang and T. Wang, "100 Gb/s per-channel free-space optical transmission with coherent detection and MIMO processing," *2009 35th European Conference on Optical Communication*, Vienna, 2009, pp. 1-2.

[19] M. A. Esmail, H. Fathallah and M. Alouini, "An Experimental Study of FSO Link Performance in Desert Environment," in *IEEE Communications Letters*, vol. 20, no. 9, pp. 1888-1891, Sept. 2016. doi: 10.1109/LCOMM.2016.2586043

[20] M. A. Esmail, H. Fathallah and M. Alouini, "Outdoor FSO Communications Under Fog: Attenuation Modeling and Performance Evaluation," in *IEEE Photonics Journal*, vol. 8, no. 4, pp. 1-22, Aug. 2016, Art no. 7905622. doi: 10.1109/JPHOT.2016.2592705

[21] Bourazani D., Stassinakis A.N., Nistazakis H.E., Varotsos G.K., Tsigopoulos A.D., Tombras G.S. "Experimental Accuracy Investigation for Irradiance Fluctulations of FSO links Modeled by Gamma Distribution". 8th IC-SCCE. 2018.

[22] Khalid, H.; Muhammad, S.S.; Nistazakis, H.E.; Tombras, G.S. Performance Analysis of Hard-Switching Based Hybrid FSO/RF System over Turbulence Channels. *Computation* 2019, *7*, 28. https://doi.org/10.3390/computation7020028

[23] G. D. Roumelas, H. E. Nistazakis, A. N. Stassinakis, G. S. Tombras and C. K. Volos, "Triple Hybrid Terresstrial FSO/RF/MMW System with Receiver's Diversity," *2019 8th International Conference on Modern Circuits and Systems Technologies (MOCAST)*, Thessaloniki, Greece, 2019, pp. 1-4. doi: 10.1109/MOCAST.2019.8741540

[24] A.N Stassinakis, H.E. Nistazakis, G.K. Varotsos, G.S. Tombras, "Performance of underwater wireless optical link under weak turbulence and pointing errors using heterodyne QAM technique", 23rd Conference on Optical Network Design and Modelling (ONDM) 2019.

[25] Roumelas, G.D.; Nistazakis, H.E.; Stassinakis, A.N.; Volos, C.K.; Tsigopoulos, A.D. Underwater Optical Wireless Communications with Chromatic Dispersion and Time Jitter. *Computation* 2019, *7*, 35. https://doi.org/10.3390/computation7030035

[26] G. K. Varotsos, H. E. Nistazakis, G. S. Tombras, K. Aidinis, F. Jaber and K. K. Mujeeb Rahman, "On the use of Diversity in Transdermal Optical Wireless Links with Nonzero Boresight Pointing Errors for Outage Performance Estimation," *2019 8th International Conference on Modern Circuits and Systems Technologies (MOCAST)*, Thessaloniki, Greece, 2019, pp. 1-4. doi: 10.1109/MOCAST.2019.8741807

[27] Varotsos, G.K.; Nistazakis, H.E.; Aidinis, K.; Jaber, F.; Rahman, K.M. Transdermal Optical Wireless Links with Multiple Receivers in the Presence of Skin-Induced Attenuation and Pointing Errors. *Computation* 2019, *7*, 33. https://doi.org/10.3390/computation7030033

[28] A. Tzanakaki et al., "Wireless-Optical Network Convergence: Enabling the 5G Architecture to Support Operational and End-User Services," *IEEE Communications Magazine*, vol. 55, no. 10, pp. 184-192, Oct. 2017.

[29] N. Gkatzios, M. Anastasopoulos, A. Tzanakaki and D. Simeonidou, "Compute Resource Disaggregation: An Enabler for Efficient 5G RAN Softwarisation," *2018 European Conference on Networks and Communications (EuCNC)*, Ljubljana, Slovenia, 2018, pp. 1-5.

[30] A.M. Geoffrion. Generalized Benders decomposition. *Journal of Optimization Theory and Applications*, Vol. 10, No. 4. pp. 237–260, 1972.

[31] A. Clauset et al., Hierarchical structure and the prediction of missing links in networks, Nature 453, 98–101, 2008

[32] N. Gkatzios, M. Anastasopoulos, A. Tzanakaki and D. Simeonidou, "Compute Resource Disaggregation: An Enabler for Efficient 5G RAN Softwarisation," *2018 European Conference on Networks and Communications (EuCNC)*, Ljubljana, Slovenia, 2018, pp. 1-5.
[33] X. Chen et al., "Analyzing and modeling spatio-temporal dependence of cellular traffic at city scale," *in Proc. of IEEE International Conference on Communications* (ICC), 2015.
[34] A. Tzanakaki *et al*., "5G infrastructures supporting end-user and operational services: The 5G-XHaul architectural perspective," *IEEE ICC*, 2016.
[35] M. Ruffini, Multi-Dimensional Convergence in Future 5G Networks. IEEE/OSA JLT, Vol. 35, No. 3, March 2017.
[36] B. Khorsandi, F. Tonini, C. Raffaelli, "Design methodologies and algorithms for survivable C-RAN," *ONDM* 2018, pp. 106-111.
[37] B. M. Khorsandi, C. Raffaelli, M. Fiorani, L. Wosinska and P. Monti, "Survivable BBU Hotel placement in a C-RAN with an Optical WDM Transport," *DRCN 2017* 2017, pp. 1-6.
[38] M. Shehata, O. Ayoub, F. Musumeci and M. Tornatore, "Survivable BBU Placement for C-RAN over Optical Aggregation Networks," *2018 20th ICTON*, Bucharest, 2018, pp. 1-4.
[39] S. Mohamed et al., "Resilient BBU placement in 5G C-RAN over optical aggregation networks", Photonic Network Commin., Jan. 2019
[40] E. Wong, E. Grigoreva, L. Wosinska and C. M. Machuca, "Enhancing the survivability and power savings of 5G transport networks based on DWDM rings," in *IEEE/OSA Journal of Optical Communications and Networking*, vol. 9, no. 9, pp. D74-D85, Sept. 2017.
[41] C. Colman-Meixner, G. B. Figueiredo, M. Fiorani, M. Tornatore and B. Mukherjee, "Resilient cloud network mapping with virtualized BBU placement for cloud-RAN," *in proc. of ANTS*, Bangalore, 2016,
[42] A. Tzanakaki, M. P. Anastasopoulos and D. Simeonidou, "Optical networking: An Important Enabler for 5G," *2017 European Conference on Optical Communication (ECOC)*, 2017, pp. 1-3.
[43] T. K. Dikaliotis, A. G. Dimakis, T. Ho and M. Effros, "On the delay of network coding over line networks," *IEEE ISIT* 2009, pp. 1408-1412.
[44] 5G-XHaul Project, Deliverable D2.2 " System Architecture Definition", submitted on July 1st, 2016.
[45] "IEEE Standard for a Precision Clock Synchronization Protocol for Networked Measurement and Control Systems", IEEE Std 1588-2008.
[46] Y. Yan. et al, "FPGA-based Optical Network Function Programmable Node", in Proc. OFC (2014)
[47] A.-F.Beldachi. et al, 'Experimental Demonstration of 5G Fronthaul and Backhaul Convergence based on FPGA-based Active Optical Transport'. *in proc of* ECOC 2018.
[48] http://www.ieee802.org/1/pages/tsn.html
[49] https://www.xilinx.com/products/intellectual-property/axi_10g_ethernet.html
[50] https://www.xilinx.com/support/documentation/ip_documentation/axi_10g_ethernet/v3_1/pg157-axi-10g-ethernet.pdf
[51] 5G-XHaul Project, Deliverable D3.1 " Evaluation of wireless-optical converged functionalities at UNIVBRIS testbed", June 31st, 2016
[52] N. Gkatzios, M. Anastasopoulos, A. Tzanakaki and D. Simeonidou, "Compute Resource Disaggregation: An Enabler for Efficient 5G RAN Softwarisation," *2018 European Conference on Networks and Communications (EuCNC)*, Ljubljana, Slovenia, 2018, pp. 1-5.
[53] X. Chen et al., "Analyzing and modeling spatio-temporal dependence of cellular traffic at city scale," *in Proc. of IEEE International Conference on Communications* (ICC), 2015.
[54] A. Tzanakaki et al., "Wireless-Optical Network Convergence: Enabling the 5G Architecture to Support Operational and End-User Services," in IEEE Communications Magazine, vol. 55, no. 10, pp. 184-192, Oct. 2017.
[55] M. Kamel, W. Hamouda and A. Youssef, "Ultra-Dense Networks: A Survey," in IEEE Communications Surveys & Tutorials, vol. 18, no. 4, pp. 2522-2545, Fourthquarter 2016.
[56] H. Liu, F. Eldarrat, H. Alqahtani, A. Reznik, X. de Foy and Y. Zhang, "Mobile Edge Cloud System: Architectures, Challenges, and Approaches," in IEEE Systems Journal, vol. 12, no. 3, pp. 2495-2508, Sept. 2018.
[57] Software-Defined Networking", https://www.opennetworking.org/sdn-definition/ .
[58] B. Heller, R. Sherwood and N. McKeown, "The Controller Placement Problem", in Proceedings of Hot Topics in Software Defined Networking (HotSDN), 2012.
[59] D. Hock, M. Hartmann, S. Gebert, M. Jarschel, T. Zinner and P. Tran-Gia, "Pareto-optimal resilient controller placement in SDN-based core networks," Proceedings of the 2013 25th International Teletraffic Congress (ITC), Shanghai, 2013, pp. 1-9.
[60] J. W. Weibull, "Evolutionary Game Theory", MIT Press, 1997.
[61] Tao Yi and Wang Zuwang, "Eject of Time Delay and Evolutionarily Stable Strategy", Academic Press Limited, 1997.
[62] Germán Obando et.al., "Replicator dynamics under perturbations and time delays", Springer Mathematics of Control, Signals, and Systems, Vol 28, no 3, 2016.

[63] eCPRI Specification V1.1 (2018-01-10), http://www.cpri.info/
[64] Wübben et.al., "Benefits and Impact of Cloud Computing on 5G Signal Processing", in IEEE Signal Processing Magazine, pp. 35-44, November 2014.
[65] C. Desset et.al., "Flexible power modeling of LTE base stations", in IEEE Wireless Communications and Networking Conference (WCNC), Shanghai, China, April, 2012.
[66] N. Ben-Khalifa, R. El-Azouzi and Y. Hayel, "Random time delays in evolutionary game dynamics," 2015 54th IEEE Conference on Decision and Control (CDC), Osaka, 2015, pp. 3840-3845.
[67] S. Bernard et.al., "Sufficient conditions for stability of linear differential equations with distributed delay", Discrete & Continuous Dynamical Systems -series B, vol 1, no 2, pp. 233-256, 2001.
[68] J. Baliga, R. Ayre, K. Hinton, W. V. Sorin and R. S. Tucker, "Energy Consumption in Optical IP Networks," in Journal of Lightwave Technology, vol. 27, no. 13, pp. 2391-2403, 2009.
[69] Internet2 Layer 2 services. https://www.internet2.edu/products-services/advanced-networking/layer-2-services/
[70] Platform Overview. https://www.opendaylight.org.
[71] Mininet Overview. http://mininet.org/overview/
[72] https://grnet.gr/infrastructure/network-and-topology/
[73] Student's t-distribution. https://en.wikipedia.org/wiki/Student%27s_t-distribution
[74] "5G Vision. The 5G Infrastructure Public Private Partnership: the next generation of communication networks and services.," 2015. [Online]. Available: [Online] https://5g-ppp.eu/wp-content/uploads/2015/02/5G-Vision-Brochure-v1.pdf.
[75] "GSMA Intelligence, Understanding 5G: Perspectives on future technological advancements in mobile.," Dec 2015. [Online].
[76] "3GPP Release 12. (E-UTRAN), Overall description, Stage 2 (Release 12). TS36.300, v12.6.0.".
[77] "3GPP Release 10. Architecture enhancements for non-3gpp accesses. Technical specification TS 23.402, 2012. Release 10.".
[78] "ETSI GS NFV-SWA 001 V1.1.1 (2014-12), "Network Functions Virtualisation (NFV); Virtual Network Functions Architecture"," 2014.
[79] Wang, Y., Haas, H., 2015. Dynamic Load Balancing With Handover in Hybrid Li-Fi and Wi-Fi Networks, *Journal of Lightwave Technology,* Volume: 33, Issue: 22.
[80] "CHINA mobile White paper, C-RAN: The Road Towards Green RAN," [Online]. Available: http://labs.chinamobile.com/cran/.
[81] "Meet LTE-R, the network responsible for next-generation smart trains," [Online]. Available: https://www.rcrwireless.com/20161115/fundamentals/smart-trains-lte-tag31-tag99.
[82] R. He and et. al, "High-Speed Railway Communications: from GSM-R to LTE-R," IEEE Vehicular Communications Magazine, 2016.
[83] "Connected Rail Solution Design Guide," November 2016. [Online]. Available: https://www.cisco.com/c/dam/en_us/solutions/industries/docs/cts-dg.pdf.
[84] "Cisco Wireless Controller Configuration Guide, Release 8.2," [Online]. Available: https://www.cisco.com/c/en/us/td/docs/wireless/controller/8-2/config-guide/b_cg82/b_cg82_chapter_0101101.html.
[85] Haas, H., *et. al*, 2016. "What is LiFi," *Journal of Lightwave Technology*, Volume: 34 , Issue: 6
[86] Chen, C., Basnayaka, D., Haas, H., 2016. "Downlink Performance of Optical Attocell Networks," Journal of Lightwave Technology, Volume: 34, Issue: 1
[87] Epple, B., 2007. "Performance Optimization of free space optical communication protocols based on results from FSO demonstrations," SPIE 6709, *Free-Space Laser Communications* VII, 670915.
[88] Refai, H., Sluss, J., Refai, H., 2005. "The transmission of multiple RF signals in free-space optics using wavelength division multiplexing," SPIE 5793, *Atmospheric Propagation II.*
[89] Ninos, M., *et. al.*, 2018. CDMA Radio on FSO links over Gamma Turbulence Channels with Nonzero Boresight Pointing Errors, *Int. Conf. on Modern Circuits and Systems Technolgy*, 2018.

[90] Mai, V., et. al, 2013. Performance of TCP over free-space optical atmospheric turbulence channels, *Journal of Optical Communications and Networking*, Volume: 5 , Issue: 11, pp. 1168 - 1177.

[91] Hasegawa, Y., 2017. A Transmission Control Protocol for Free-Space Optical Communications, *IEEE Global Communications*.

[92] "Huawei, Building 4G on High-Speed Railways," [Online]. Available: http://www1.huawei.com/en/static/HW-371912.pdf.

[93] Tzanakaki, A., *et.al.,* 2016. 5G infrastructures supporting end-user and operational services: The 5G-XHaul architectural perspective, *In proc. of IEEE ICC*, 2016.

[94] Sivaraman, A., 2016, Packet Transactions: High-Level Programming for Line-Rate Switches, *ACM SIGCOMM*

[95] Brebner, G., 2015. Programmable hardware for high Performance SDN, OFC

[96] "ETSI GS NFV-EVE 005 V1.1.1, Network Functions Virtualisation (NFV); Ecosystem; Report on SDN Usage in NFV Architectural Framework. 2015-12.".

[97] Jin H., *et al*, 2013, "OpenFlow-Based Flow-Level Bandwidth Provisioning for CICQ Switches, *IEEE Transaction on Computers*, vol. 62.

[98] Tzanakaki, A., et al., 2013. Virtualization of heterogeneous wireless-optical network and IT support of cloud and mobile Services, *IEEE Communications Magazine*, Volume: 51, Issue: 8.

[99] Chen X., *et al*, 2015. Analyzing and modeling spatio-temporal dependence of cellular traffic at city scale, IEEE ICC

[100] Fang, Y., Chlamtac, I., 2002. Analytical Generalized Results for Handoff Probability in Wireless Networks, *IEEE Trans Communications*, Volume: 50, Issue: 3.

[101] M. Anastasopoulos, A. Tzanakaki and D. Simeonidou, "Service Chaining in MEC – Assisted Large Scale 5G Networks," 2018 European Conference on Optical Communication (ECOC), Rome, 2018, pp. 1-3.

[102] ETSI White Paper No. 11, Mobile Edge Computing A key technology towards 5G, Sep. 2015.

[103] A. Tzanakaki et al., "5G infrastructures supporting end-user and operational services: The 5G-XHaul architectural perspective," 2016 IEEE International Conference on Communications Workshops (ICC), Kuala Lumpur, 2016, pp. 57-62.

[104] Common Public Radio Interface:eCPRI Interface Specification, D01, Aug. 2017.

[105] A. Gupta et al., |On service-chaining strategies using Virtual Network Functions in operator networks", Computer Networks, Vo. 133, 14 March 2018.

[106] 5G Vision. The 5G Infrastructure Public Private Partnership: the next generation of communication networks and services. 2015. [Online].

[107] A. Tzanakaki et al., "Wireless-Optical Network Convergence: Enabling the 5G Architecture to Support Operational and End-User Services", IEEE Commun. Mag., pp. 184 – 192, Aug. 2017.

[108] M. Anastasopoulos et al., "ICT platforms in support of future railway systems", in proc. of TRA 2018, Apr. 2018.

[109] F. Musumeci, C. Bellanzon, N. Carapellese, M. Tornatore, A. Pattavina, and S. Gosselin, "Optimal BBU Placement for 5G C-RAN Deployment Over WDM Aggregation Networks," J. Lightwave Technol. 34, 1963-1970 (2016).

[110] T. Pfeiffer, "Next generation mobile fronthaul and midhaul architectures [Invited]," in IEEE/OSA Journal of Optical Communications and Networking, vol. 7, no. 11, pp. B38-B45, November 1 2015.

[111] M. Fiorani, S. Tombaz, J. Martensson, B. Skubic, L. Wosinska and P. Monti, "Modeling energy performance of C-RAN with optical transport in 5G network scenarios," in IEEE/OSA Journal of Optical Communications and Networking, vol. 8, no. 11, pp. B21-B34, Nov. 2016.

[112] M. Anastasopoulos, A. Tzanakaki and D. Simeonidou, "Stochastic Energy Efficient Cloud Service Provisioning Deploying Renewable Energy Sources," in IEEE Journal on Selected Areas in Communications, vol. 34, no. 12, pp. 3927-3940, Dec. 2016.

[113] Antonia Pelekanou, Markos Anastasopoulos, Anna Tzanakaki, Dimitra Simeonidou, "Provisioning of 5G Services Employing Machine Learning Techniques", International Conference on Optical Network Design and Modeling, May 2018.

[114] Jure Leskovec, Anand Rajaraman, Jeffrey D. Ullman, "Mining of Massive Datasets", Cambridge University Press New York, NY, USA 2011

[115] M. Starstedt and E. Mooi, "Cluster Analysis", Springer-Verlag, Berling 2014.

[116] Joe H. Ward, Jr, "Hierarchical Grouping to Optimize an Objective Function", Journal of the American Statistical Association, vol. 58, no. 301, pp. 236-244, March 1963.

[117] X. Chen et al., "Analyzing and modeling spatio-temporal dependence of cellular traffic at city scale," in proc. of IEEE ICC, pp.3585-3591, 2015

[118] Jinn-Tsong Tsai, Jyh-Horng Chou, Tung-Kuan Liu, "Tuning the Structure and Parameters of a Neural Network by Using Hybrid Taguchi-Genetic Algorithm", IEEE Transactions on Neural Networks, vol. 17, no. 1, January 2006.

[119] H.K. Lam, S.H. Ling, F.H.F. Leung, P.K.S. Tam, "Tuning of the structure and Parameters of Neural Networks using Improves Genetic Algorithm", IEEE Transactions on Neural Networks, vol. 14, no. 1, January 2003.

[120] Dinesh P. Pitambare, "Survey on Optimization of Number of Hidden Layers in Neural Networks, International Journal of Advances Research in Computer and Communication Engineering, November 2016.

[121] Hossein Valavi, Peter J. Ramadge, "An Upper-Bound on the Required Size of a Neural Network Classifier", ICASSP, 2018.

[122] James Bergstra, Yoshua Bengio, "Random Search for Hyper-Parameter Optimization", Journal of Machine Learning Research, February 2012

[123] "Software-Defined Networking", https://www.opennetworking.org/sdn-definition/

[124] "Openflow", http://flowgrammable.org/sdn/openflow/

[125] "OpenFlow Switch Specification", Version 1.3.0 (Protocol version 0x04), Open Networking Foundation,2012

[126] "Open Network Operating System (ONOS)", https://onosproject.org

[127] "OpenDaylight", https://opendaylight.org

[128] "OpenDayLight Project", https://en.wikipedia.org/wiki/OpenDaylight_Project

[129] "REST (representational state transfer)", http://searchsoa.techtarget.com/definition/REST

[130] "OpenDayLight Wiki", https://wiki.opendaylight.org/view/Main_Page

[131] "Aruba 2930F / 2930M Management and Configuration Guide for ArubaOSSwitch 16.05",https://h20628.www2.hp.com/km-ext/kmcsdirect/emr_na-a00038765en_us-3.pdf

[132] "Aruba OpenFlow 1.3 Administrator Guide for ArubaOS-Switch 16.05", https://support.hpe.com/hpsc/doc/public/display?docId=a00038767en_us

[133] "Basic ONOS Tutorial", https://wiki.onosproject.org/display/ONOS/Basic+ONOS+Tutorial

[134] "Intent Framework", https://wiki.onosproject.org/display/ONOS/Intent+Framework

[135] "OpenDaylight OpenFlow Plugin:End to End Flows", https://wiki.opendaylight.org/view/OpenDaylight_OpenFlow_Plugin:End_to_End_Flows

[136] "L2 Switch User Guide", https://docs.opendaylight.org/en/stable-fluorine/user-guide/l2switch-user-guide.html

[137] "Using meters to implement QoS in OpenDaylight", https://www.talentica.com/blogs/using-meters-to-implement-qos-in-opendaylight/